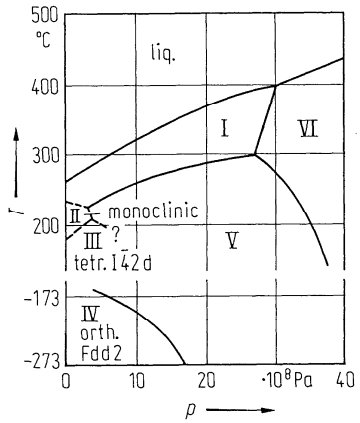

Fig. 33A-1-001. KH_2PO_4 (KDP). Phase diagram with regard to p [76Pis].

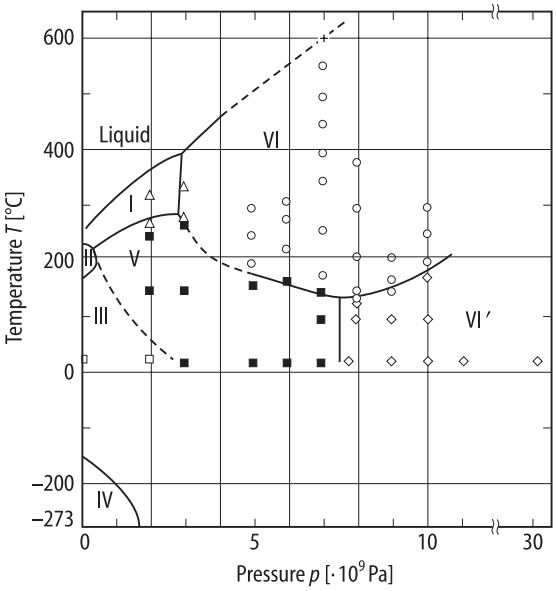

Fig. 33A-1-002. KH_2PO_4 (KDP). p–T phase diagram up to 30 GPa [95Kob]. Thick line: phase boundary determined by X-ray diffraction. Thin line: data from [70Rap]. +: melting point. Other symbols correspond to data points in every phase. The phase boundary between phases III and V is tentatively drawn based on [89End, 91Bao].

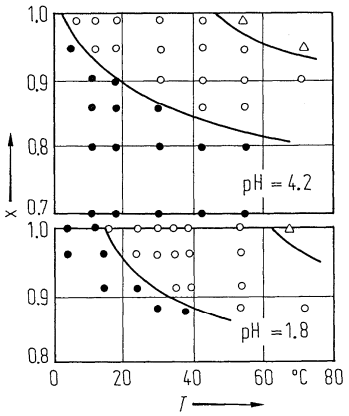

Fig. 33A-1-003. $KH_{2(1-x)}D_{2x}PO_4$. Crystallization in solutions with various x and acidity [77Str]. Full circles: tetragonal phase. Triangles: monoclinic phase. Open circles: mixture of both phases.

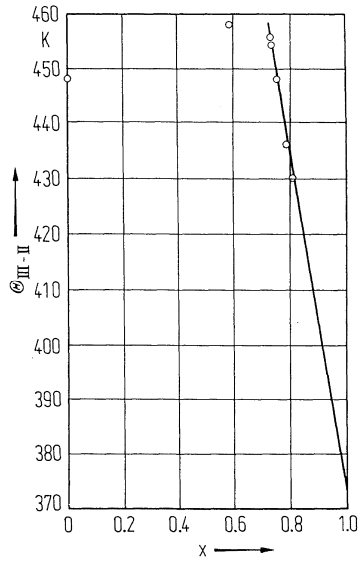

Fig. 33A-1-004. $KH_{2(1-x)}D_{2x}PO_4$. Θ_{III-II} vs. x [78Sha].

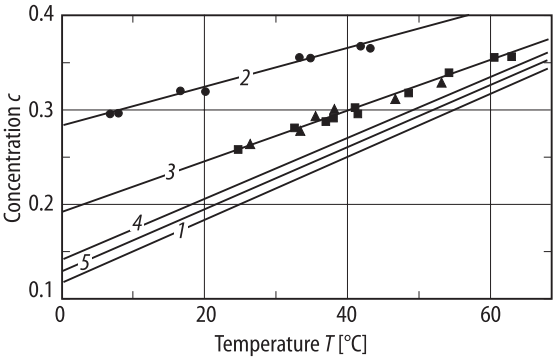

Fig. 33A-1-005. KH_2PO_4 (KDP). *c* vs. *T* [95Zai]. *c*: concentration of KDP in aqueous solution (kg/kg solution). *1*: solubility curve. *2*, *3*: metastable boundary of solutions with (full square) and without (full circle) a growing crystal, respectively, and with an empty platform (full triangle). *4*, *5*: traditional level of stability data of [83Loi] and [73Syn], respectively.

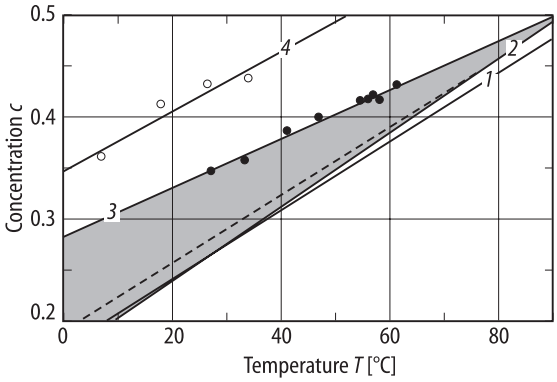

Fig. 33A-1-006. KD_2PO_4 (98% deuterated). c vs. T [95Zai]. c: concentration of DKDP in aqueous solution (kg/kg solution). *1*: monoclinic phase solubility. *2*: tetragonal phase solubility. *3*: metastable boundary with growing crystal. *4*: metastable boundary without crystal. Shaded area: tetragonal crystal growth region. Dashed line: data from [81Jia].

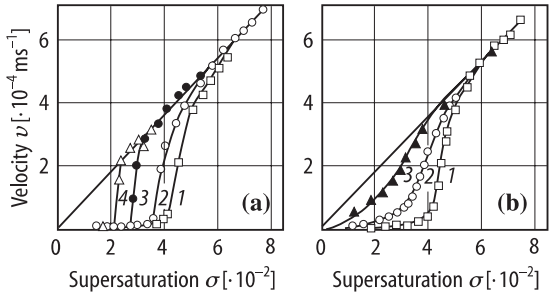

Fig. 33A-1-007. KH_2PO_4 (KDP). υ vs. σ [95Ras]. υ: step velocity on prismatic faces in solutions. σ: supersaturation, $\sigma = \ln(c/c_0)$, where c and c_0, respectively, are the actual and equilibrium concentrations of KDP in solution. (**a**) acidic condition; [pH, P_2O_5 in solvent (g/100 g of solvent)]. Curve *1*: [4.23, 0]; curve *2*: [3.45, 0.778]; curve *3*: [2.91, 5.12]; curve *4*: [2.65, 7.40]. (**b**) alkalic condition; [pH, K_2O in solvent (g/100 g of solvent)]. Curve *1*: [4.37, 0]; curve *2*: [4.9, 0.37]; curve *3*: [5.41, 1.00].

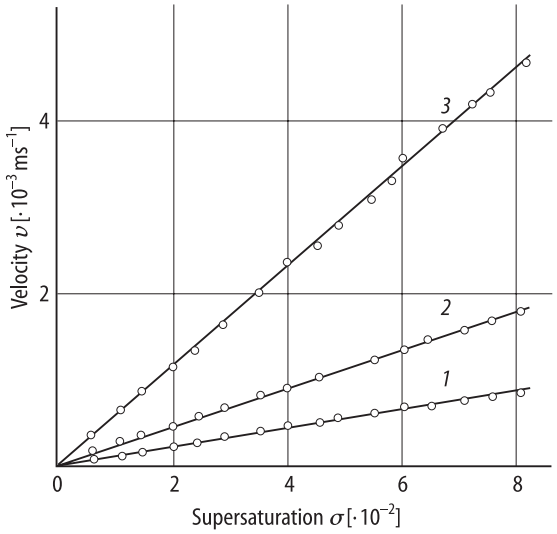

Fig. 33A-1-008. KH_2PO_4 (KDP). υ vs. σ [95Ras]. υ: bipyramidal face step velocity in solutions. σ: supersaturation, $\sigma = \ln(c/c_0)$, where c and c_0, respectively, are the actual and equilibrium concentrations of KDP in solution. Curves *1–3* correspond to different vicinal slopes. pH = 4.34.

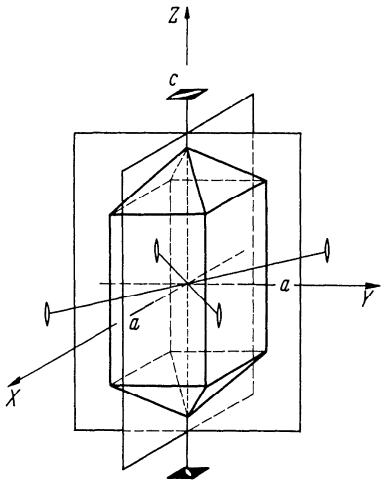

Fig. 33A-1-009. KH_2PO_4 (KDP). Crystal form and symmetry [38Bus].

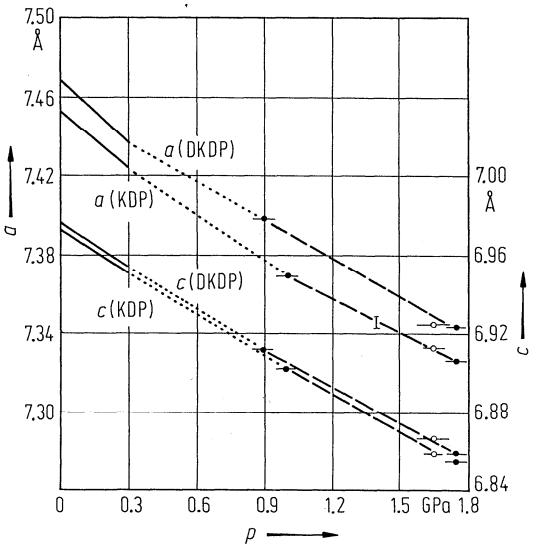

Fig. 33A-1-010. KH_2PO_4 (KDP), KD_2PO_4 (DKDP). *a*, *c* vs. *p* [82Tib]. Open circle: single crystal, full circle: powder. Full lines are results in [71Mor].

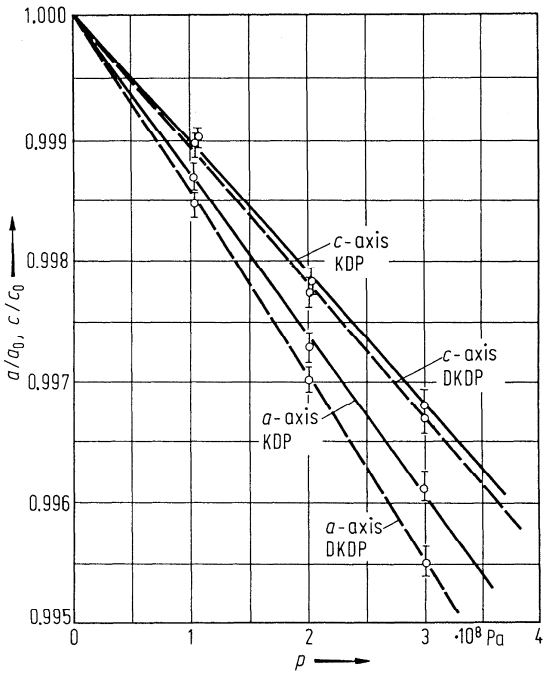

Fig. 33A-1-011. KH_2PO_4 (KDP), KD_2PO_4 (DKDP). a/a_0, c/c_0 vs. p at 295 K [71Mor]. a_0, c_0: unit cell parameters at the atmospheric pressure.

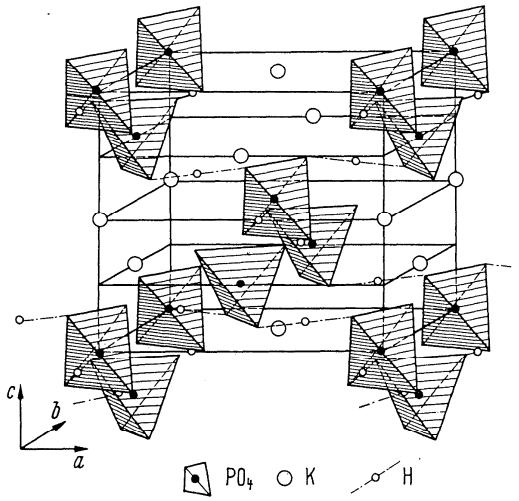

Fig. 33A-1-012. KH_2PO_4 (KDP). Structure at RT [30Wes]. Hydrogen positions are shown schematically.

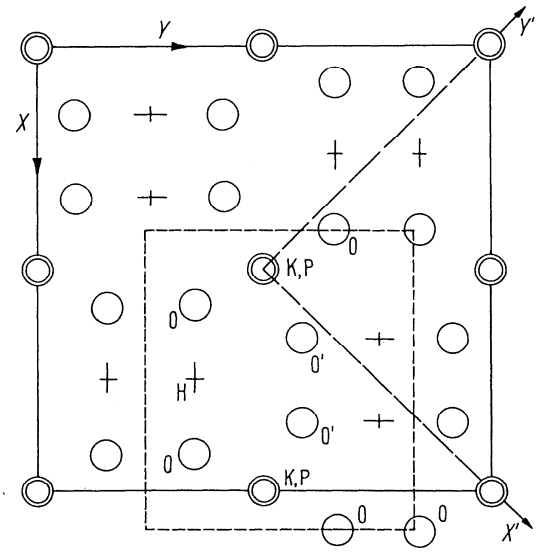

Fig. 33A-1-013. KH_2PO_4 (KDP). Projection on (001) [55Bac]. Representing the relation between a body centered ($I\bar{4}2d$) cell with *X*, *Y* axes and a face centered ($F\bar{4}d2$) cell with *X'*, *Y'* axes. The dotted lines indicate the representative portion of the unit cell shown in Fig. 33A-1-014.

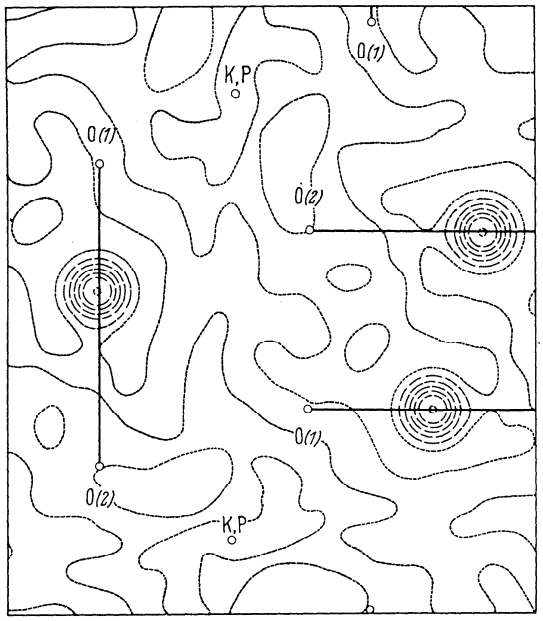

Fig. 33A-1-014. H_2PO_4 (KDP). Projection of H atoms on (001) at 77 K [55Bac]. This Fourier map corresponds to the portion surrounded by the dotted lines in Fig. 33A-1-013.

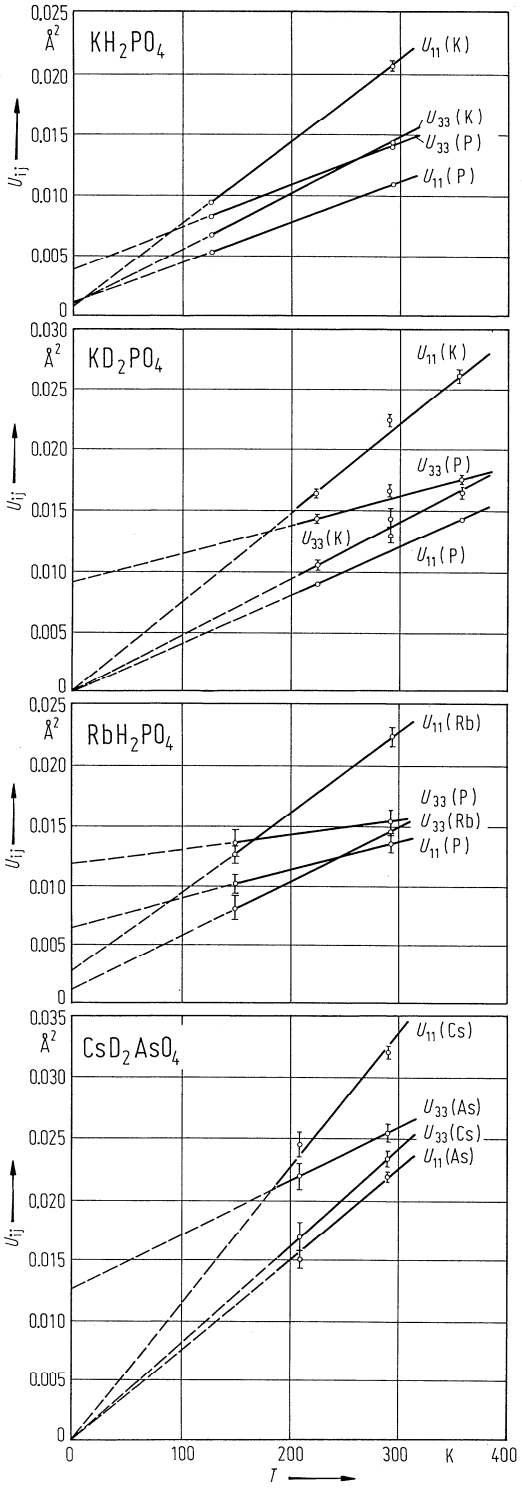

Fig. 33A-1-015. KH_2PO_4 (KDP), KD_2PO_4 (DKDP), RbH_2PO_4 (RDP), CsD_2AsO_4 (DCDA). Anisotropic temperature parameters U_{ij} vs. T [82Nel]. U_{ij} are defined by Eq. (d) in Introduction. The data of RbH_2PO_4 and CsD_2AsO_4 are from [80Ken] and [81Hay], respectively.

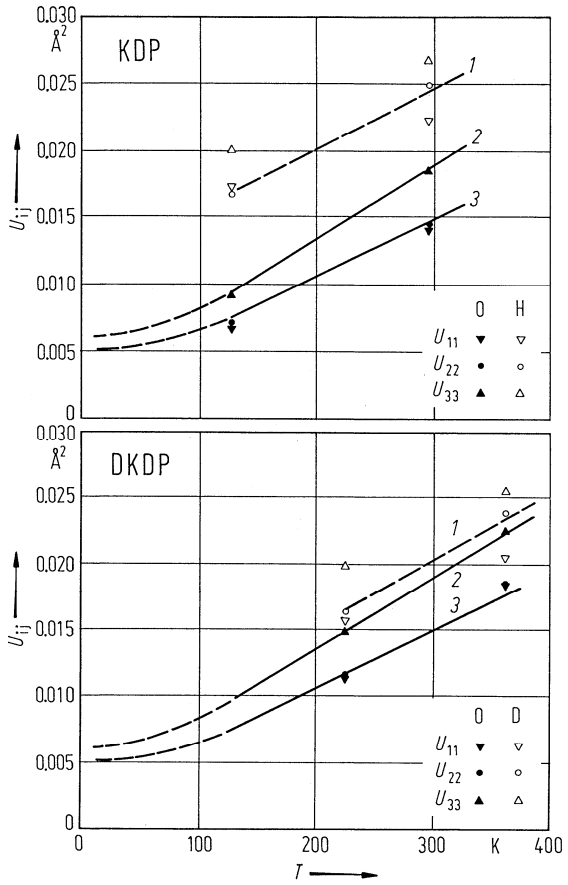

Fig. 33A-1-016. KH_2PO_4 (KDP), KD_2PO_4 (DKDP). Anisotropic temperature parameters U_{ij} vs. T of O and H/D atoms [82Nel]. U_{ij} are defined by Eq. (d) in Introduction. Curves *1*, *2* and *3* are Debye-Waller expressions for U_{22}(H/D), U_{33}(O) and $U_{11,22}$(O), respectively.

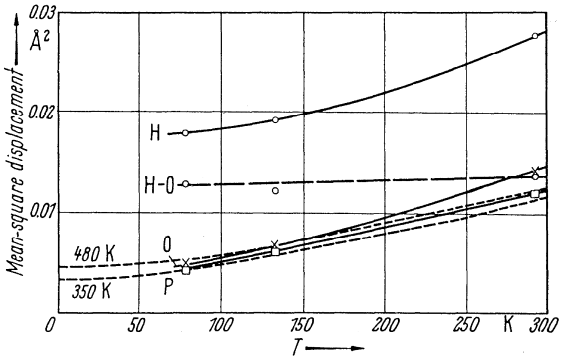

Fig. 33A-1-017. KH_2PO_4 (KDP). Mean square displacements of x, y of H, O, P atoms vs. T [55Bac]. The dotted lines show the theoretical curves for Debye temperatures of 350 K and 480 K.

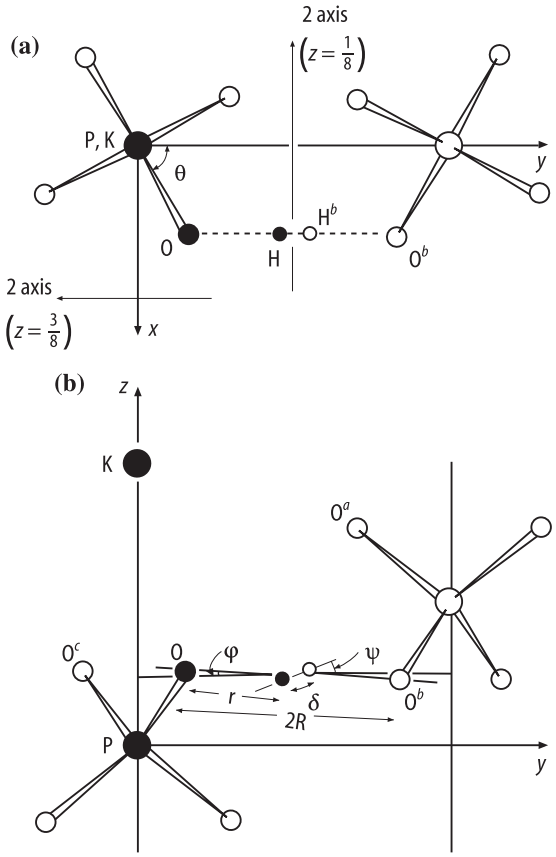

Fig. 33A-1-018. KH_2PO_4 (KDP). Tetragonal structure at 293 K [88Tun]. (**a**) projection along the *z* axis. (**b**) projection along the *x* axis. Superscripts on atom symbols correspond to the atom labelling shown in Table 33A-1-020. θ: angle between the *xy*-projection of the P–O bond and the positive *y* axis. 2*R*: distance between the O atoms of the hydrogen bond. δ: separation of the two H sites in a hydrogen bond. φ, ψ: inclinations of the O–O and H–H lines, respectively, to the *xy* plane. For clarity, the displacements of the O and H atoms from $z = 1/8$ are exaggerated by a factor of four in (**b**).

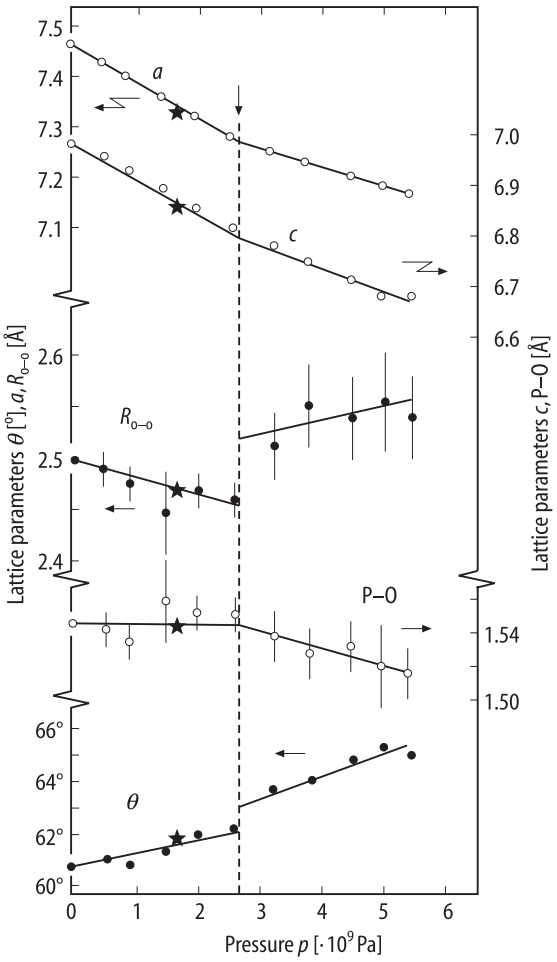

Fig. 33A-1-019. KH_2PO_4 (KDP). a, c, R_{o-o}, P–O, θ vs. p [89End]. R_{o-o}: hydrogen bond length. P–O: P–O distance in the PO_4 tetrahedron. θ: rotation angle of PO_4 tetrahedron around the 4-fold axis. Arrow and dotted line indicate pressure at which structural change can be observed. Full star: data by Tibballs [82Tib].

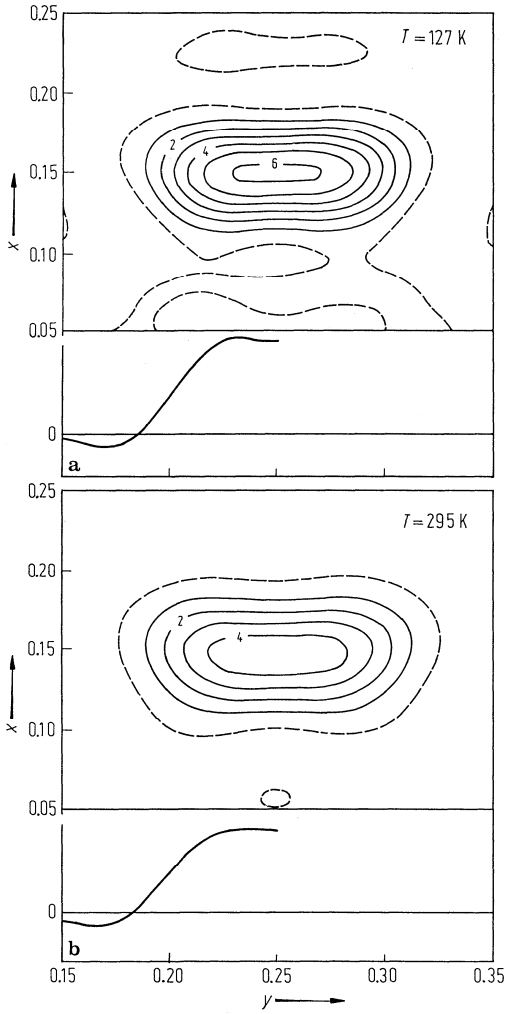

Fig. 33A-1-020. KH_2PO_4 (KDP). Proton density of the *xy* plane at 127 K (**a**) and 295 K (**b**) [82Nel]. The contours are drawn in an arbitrary scale. The lower figures show their sections along ***y*** ($y \leq 0.25$).

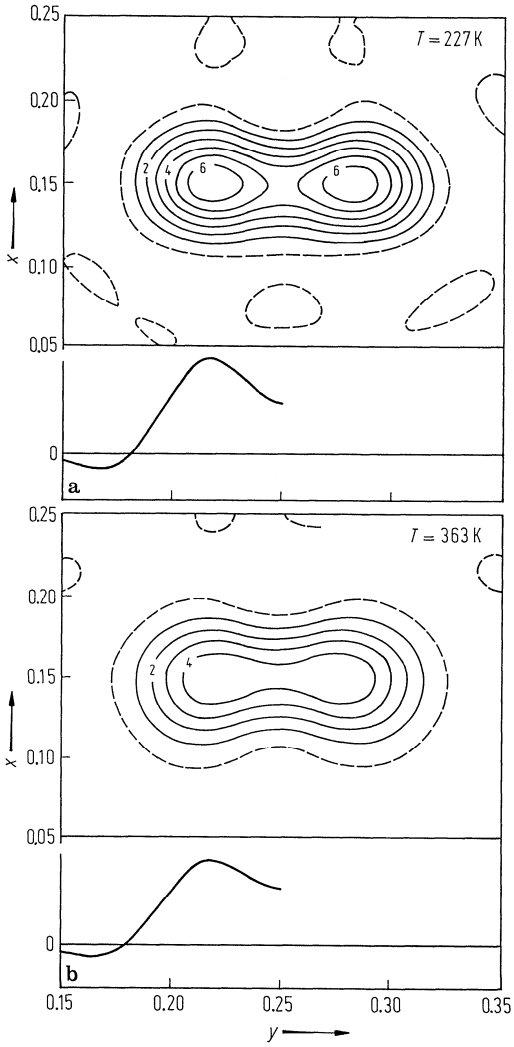

Fig. 33A-1-021. KD_2PO_4 (DKDP). Deuteron density of the *xy* plane at 227 K (**a**) and 363K (**b**) [82Nel]. The contours are drawn in an arbitrary scale. The lower figures show their sections along ***y*** ($y \leq 0.25$).

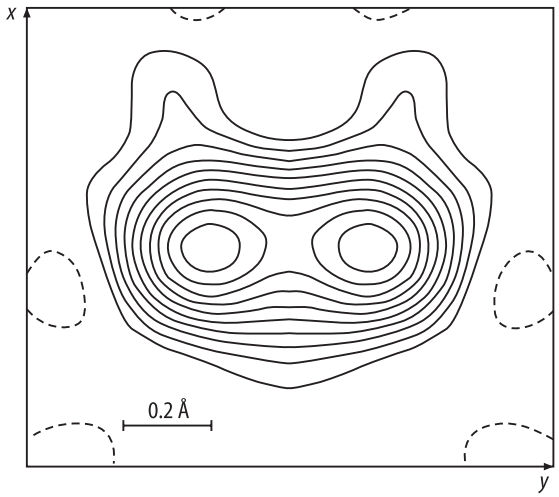

Fig. 33A-1-022. KH_2PO_4 (KDP). Proton density at Θ_f + 2 K [83Kuh]. The contours are equally spaced on an arbitrary scale.

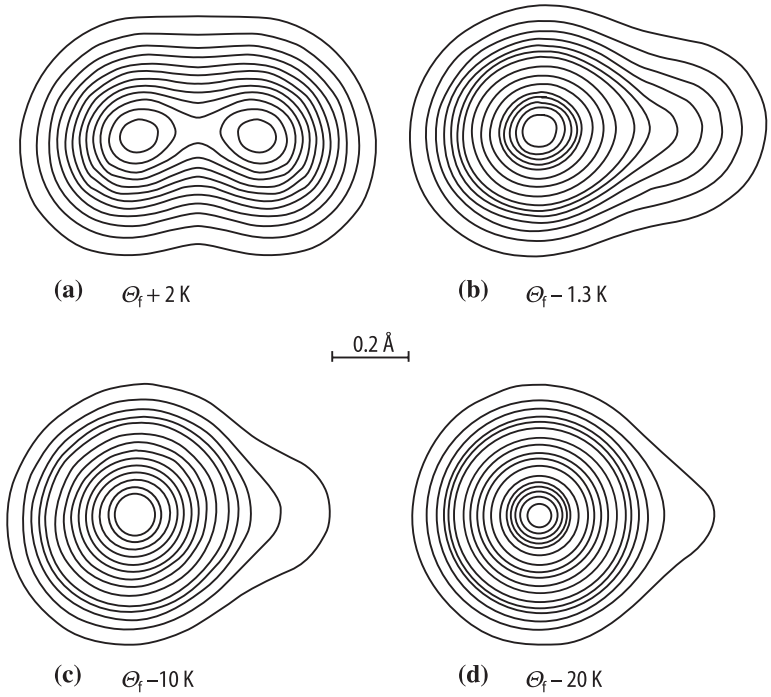

Fig. 33A-1-023. KH_2PO_4 (KDP). Sections of proton density at several temperatures [85Nel]. The sections contain the H–H joining the two proton sites and the line at constant *z* perpendicular to H–H. The contours are equally spaced on a common arbitrary scale.

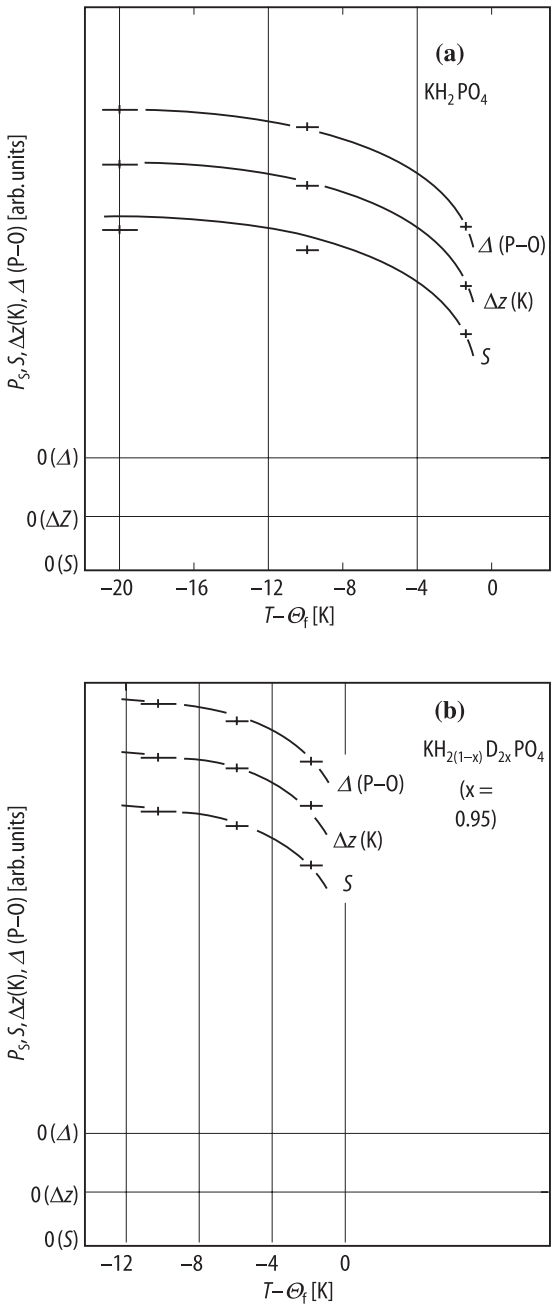

Fig. 33A-1-024. (**a**) KH_2PO_4 (KDP), (**b**) $KH_{2(1-x)}D_{2x}PO_4$ (x = 0.95). *S*, Δz(K), Δ(P–O) vs. $T - \Theta_f$ [85Nel]. *S*: degree of proton (deuteron) ordering. Δz(K): displacement of K atom along the *z* axis relative to P atom. Δ(P–O): change in P–O mean distance from the value just above Θ_f. Spontaneous polarizations P_s of KH_2PO_4 [73Sam] and $KH_{2(1-x)}D_{2x}PO_4$ [77Cha] are shown by full curves for comparison.

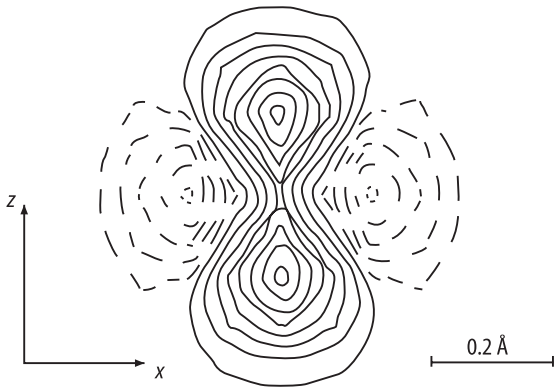

Fig. 33A-1-025. KD_2PO_4 (DKDP). Anharmonic deformation of the P atom in a (010) section [90McM2]. Full line: positive density. Dashed line: negative density.

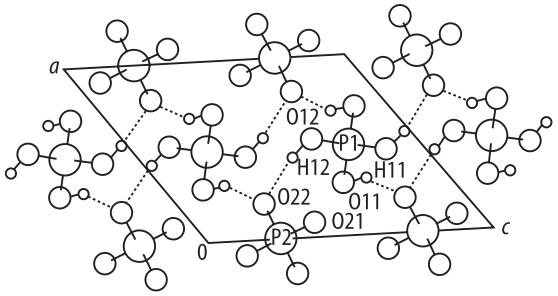

Fig. 33A-1-026. KH_2PO_4 (monoclinic). Structure projected on the (010) plane [95Mat]. T = RT. K ions are omitted. K(1) and K(2) are in the columns containing P(1) and P(2), respectively.

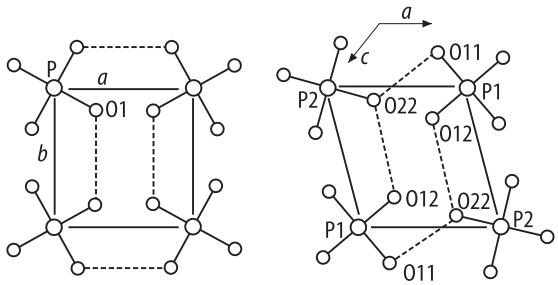

(a) **(b)**

Fig. 33A-1-027. KH_2PO_4 (monoclinic). Structures of (**a**) tetragonal crystal projected on (001) and (**b**) monoclinic crystal projected on (010) [95Mat]. K ions are omitted.

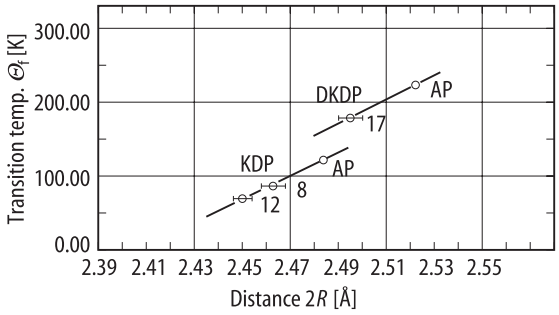

Fig. 33A-1-028. KH_2PO_4 (KDP), KD_2PO_4 (DKDP). Θ_f vs. 2R [90McM1]. 2R: distance between O atoms of the hydrogen bonds. AP: atmospheric pressure. Numerals attached to the data points are the hydrostatic pressure [in 10^8 Pa] applied.

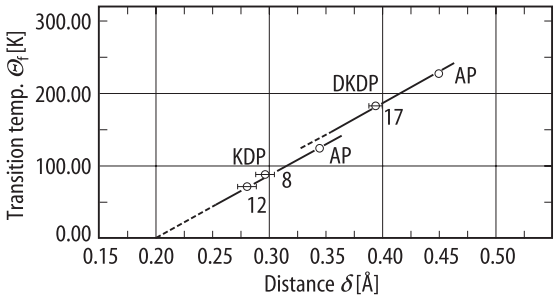

Fig. 33A-1-029. KH_2PO_4 (KDP), KD_2PO_4 (DKDP). Θ_f vs. δ [90McM1]. δ: separation of the two H sites in the hydrogen bond. AP: atmospheric pressure. Numerals attached to the data points indicate the hydrostatic pressure [in 10^8 Pa] applied.

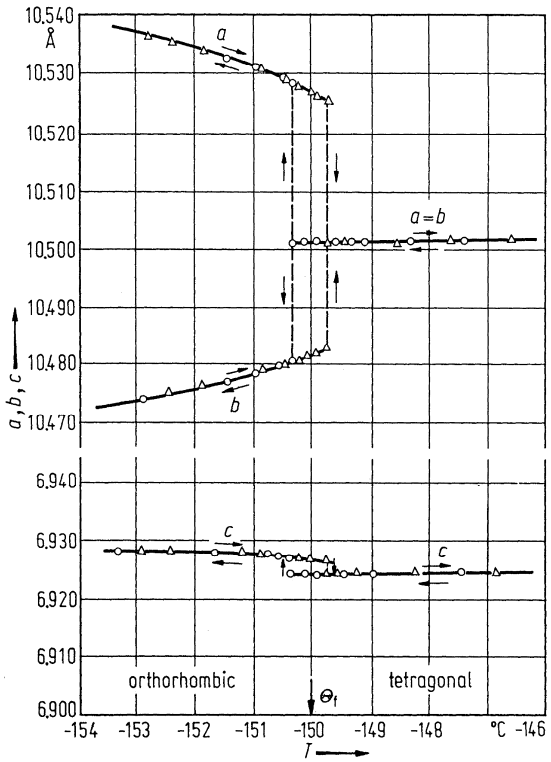

Fig. 33A-1-030. KH_2PO_4 (KDP). *a*, *b*, *c* vs. *T* in the vicinity of Θ_t [70Kob].

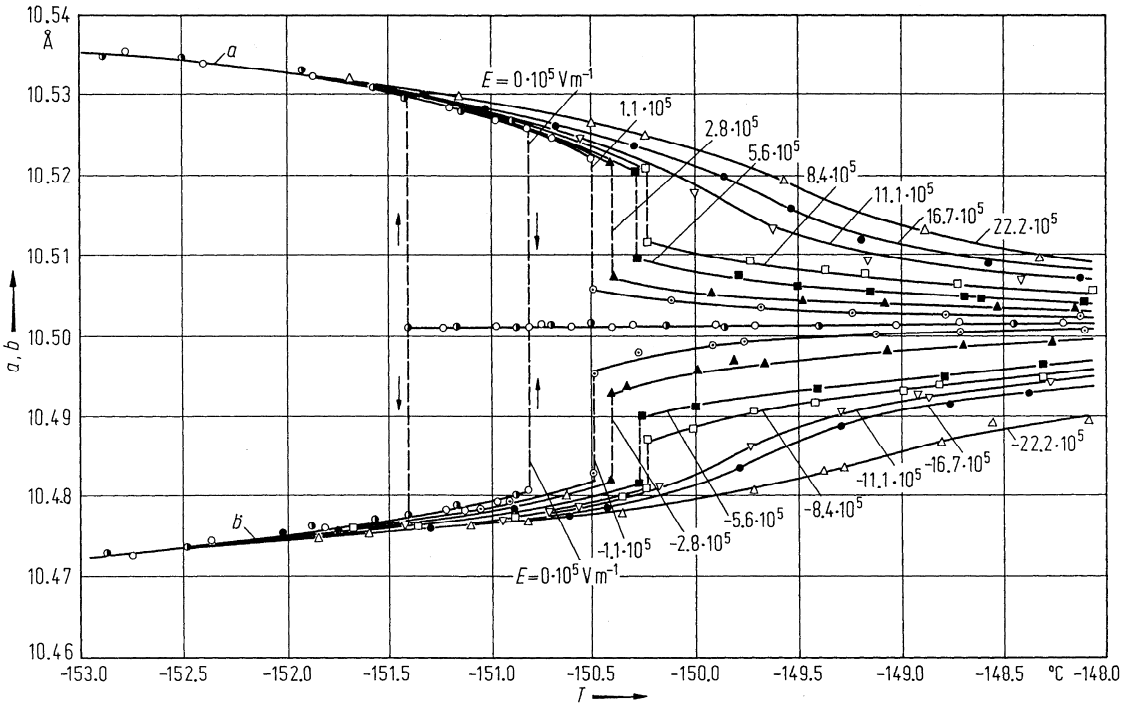

Fig. 33A-1-031. KH_2PO_4 (KDP). *a*, *b* vs. *T* [71Kob]. Parameter: E_{bias}. *a*, *b*: unit cell parameters.

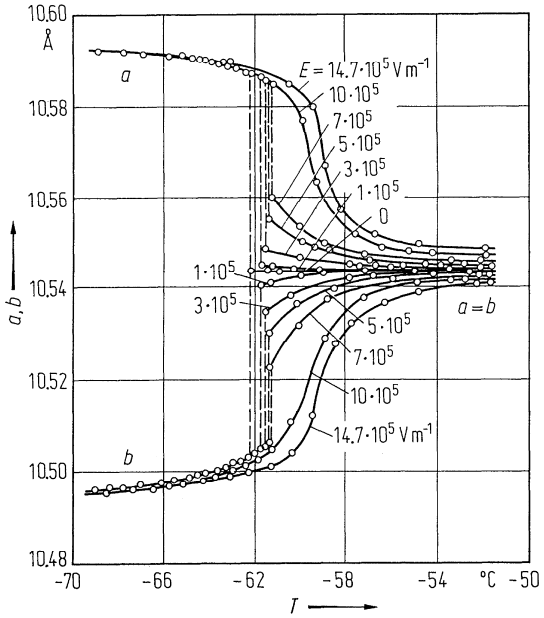

Fig. 33A-1-032. KD_2PO_4 (DKDP). a, b vs. T [74Ues]. Parameter: E_{bias}. a, b: unit cell parameters.

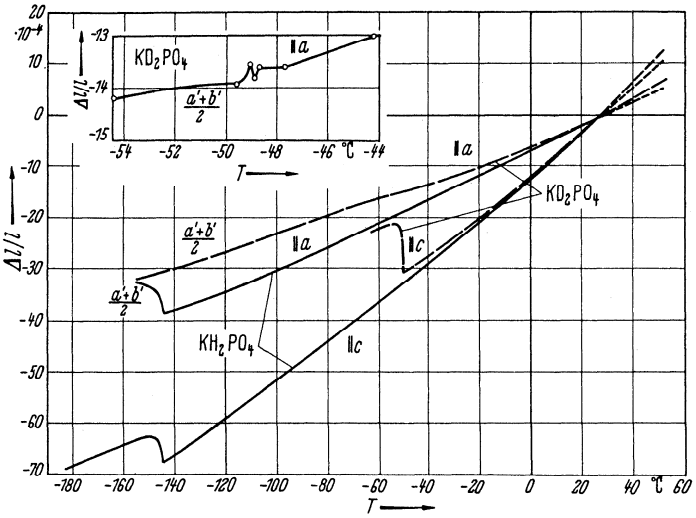

Fig. 33A-1-033. KH_2PO_4 (KDP), KD_2PO_4 (DKDP). $\Delta l/l$ vs. T [67Coo]. Insert shows an expanded plot along a near Θ_f of KD_2PO_4. $(a' + b')/2$ is the mean value along a and b axes of the ferroelectric phase IV.

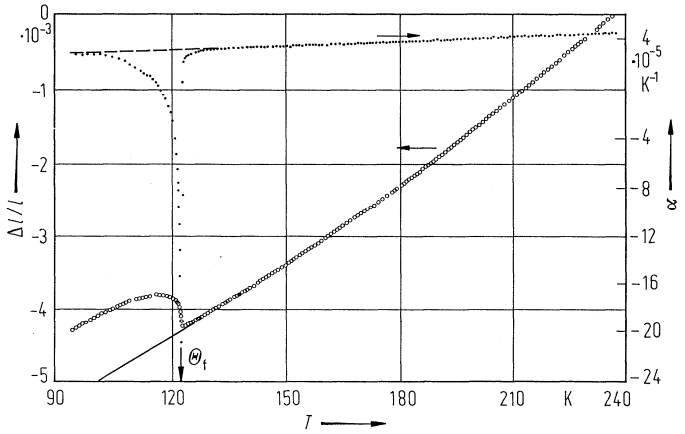

Fig. 33A-1-034. KH_2PO_4 (KDP). $\Delta l/l$, α vs. T along the c axis [80Deg1]. $\Delta l/l$: linear thermal expansion. α: linear thermal expansion coefficient.

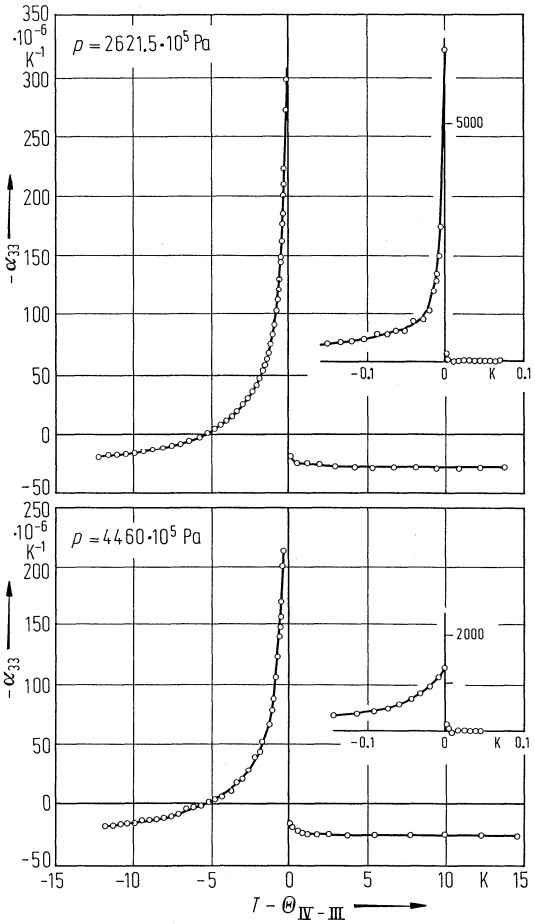

Fig. 33A-1-035. KH_2PO_4 (KDP). $-\alpha_{33}$ vs. $T-\Theta_{IV-III}$ [80Zis]. Parameter: p. $\Theta_{IV-III} = \Theta_f$.

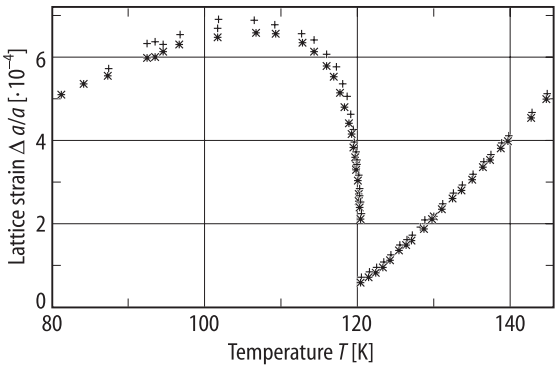

Fig. 33A-1-036. KH_2PO_4 (KDP). $\Delta a/a$ vs. T [87Bas]. $\Delta a/a$: lattice strain along the tetragonal a axis. Cross: coupled neutron-γ ray diffraction method, plus sign: neutron diffraction.

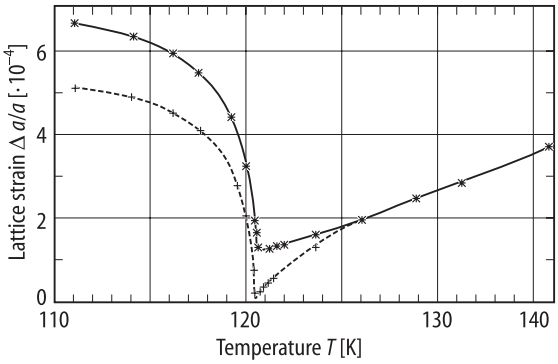

Fig. 33A-1-037. KH_2PO_4 (KDP). $\Delta a/a$ vs. T with E_{bias} applied along the tetragonal c axis [87Bas]. $\Delta a/a$: lattice strain along the tetragonal a axis. Cross: coupled neutron-γ ray diffraction method, plus sign: neutron diffraction. $E_{bias} = 700$ V m^{-1}.

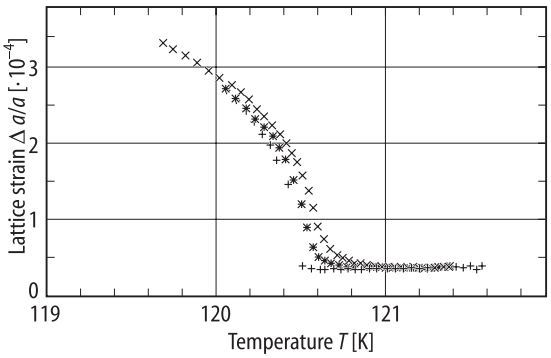

Fig. 33A-1-038. KH_2PO_4 (KDP). $\Delta a/a$ vs. T with E_{bias} applied along the tetragonal c axis [87Bas]. Parameter: E_{bias}. $\Delta a/a$: lattice strain along the tetragonal a axis. Plus sign: $E_{bias} = 320$ V m^{-1}, asterisk: 640 V m^{-1}, cross: 961 V m^{-1}.

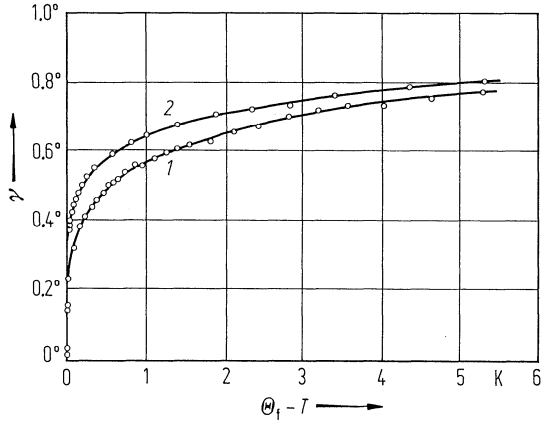

Fig. 33A-1-039. KH_2PO_4 (KDP). γ vs. $\Theta_f - T$ [82Ale2]. Parameter: p. γ: shear angle between X and Y axes. *1*: $2640 \cdot 10^5$ Pa, *2*: $1 \cdot 10^5$ Pa.

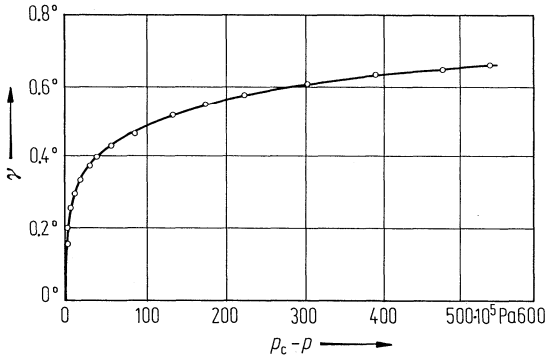

Fig. 33A-1-040. KH_2PO_4 (KDP). γ vs. $p_c - p$ at 109.83 K [82Ale2]. γ: shear angle between X and Y axes. $p_c = 2.64(4) \cdot 10^8$ Pa.

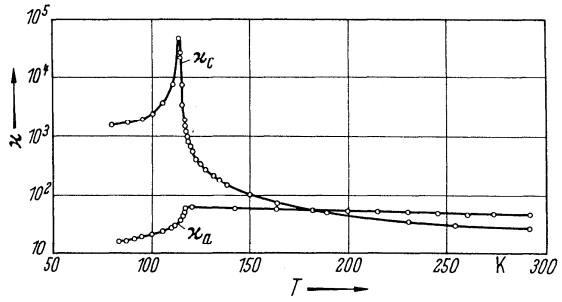

Fig. 33A-1-041. KH_2PO_4 (KDP). κ_a, κ_c vs. T [38Bus]. $f = 800$ Hz.

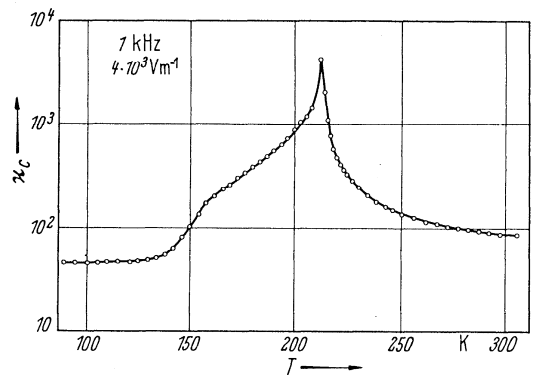

Fig. 33A-1-042. Deuterated KDP. κ_c vs. T [41Ban]. f = 1 kHz.

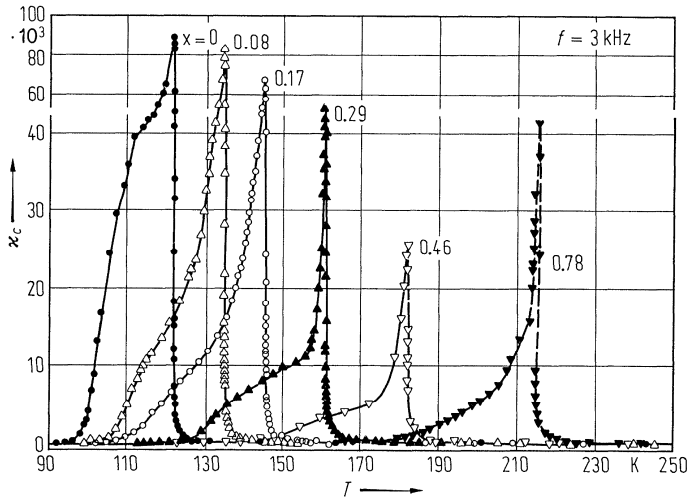

Fig. 33A-1-043. $KH_{2(1-x)}D_{2x}PO_4$. κ_c vs. T [72Str]. Parameter: x. f = 3 kHz.

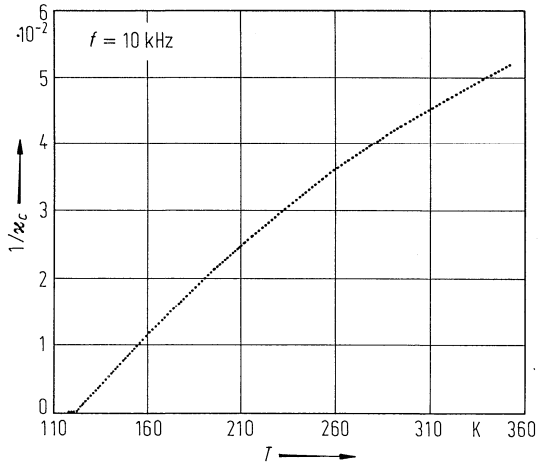

Fig. 33A-1-044. KH_2PO_4 (KDP). $1/\kappa_c$ vs. T [80Deg2]. f = 10 kHz.

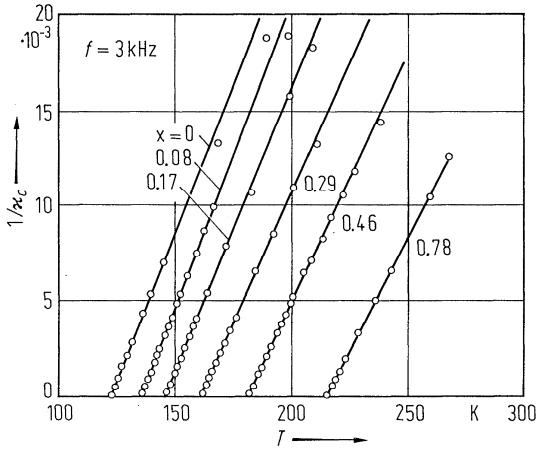

Fig. 33A-1-045. $KH_{2(1-x)}D_{2x}PO_4$. $1/\kappa_c$ vs. T [72Str]. Parameter: x. $f = 3$ kHz.

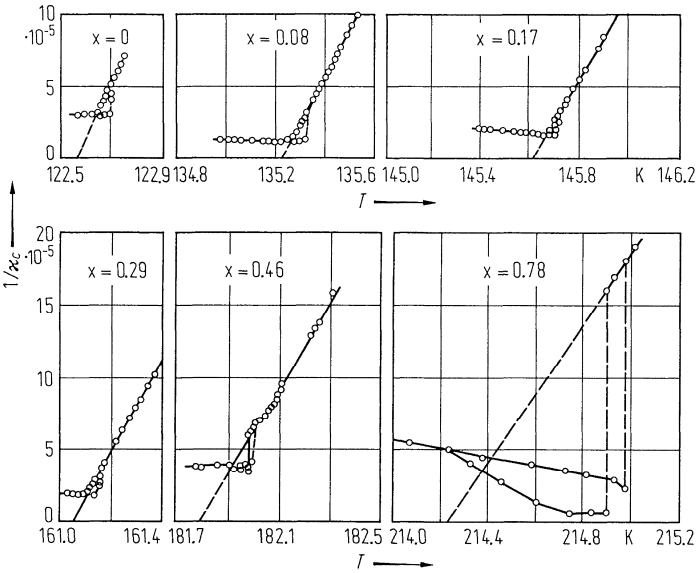

Fig. 33A-1-046. $KH_{2(1-x)}D_{2x}PO_4$. $1/\kappa_c$ vs. T on heating and cooling in the vicinity of Θ_f for various x [72Str]. $f = 3$ kHz.

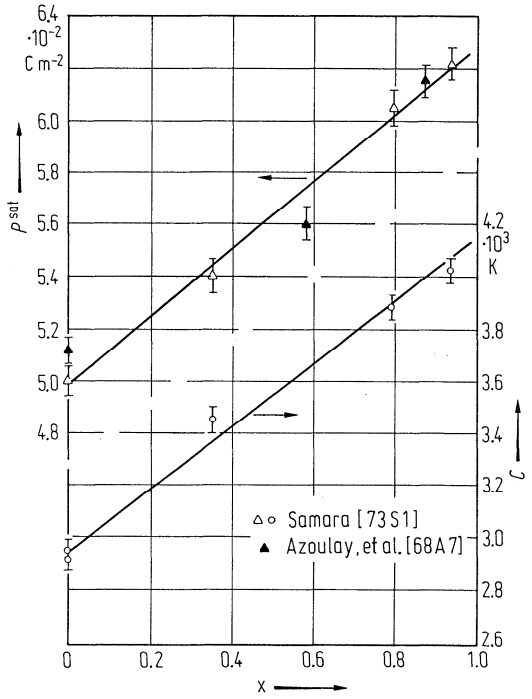

Fig. 33A-1-047. $KH_{2(1-x)}D_{2x}PO_4$. C, P^{sat} vs. x [73Sam, 68Azo]. C: Curie-Weiss constant. P^{sat}: saturation polarization. Open circle, open triangle: [73Sam], full triangle: [68Azo].

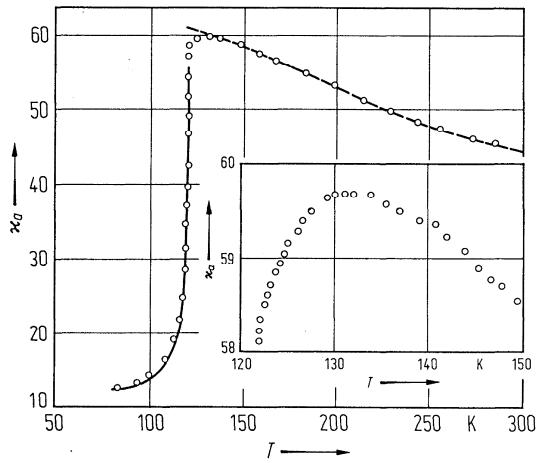

Fig. 33A-1-048. KH_2PO_4 (KDP). κ_a vs. T [75Hav].

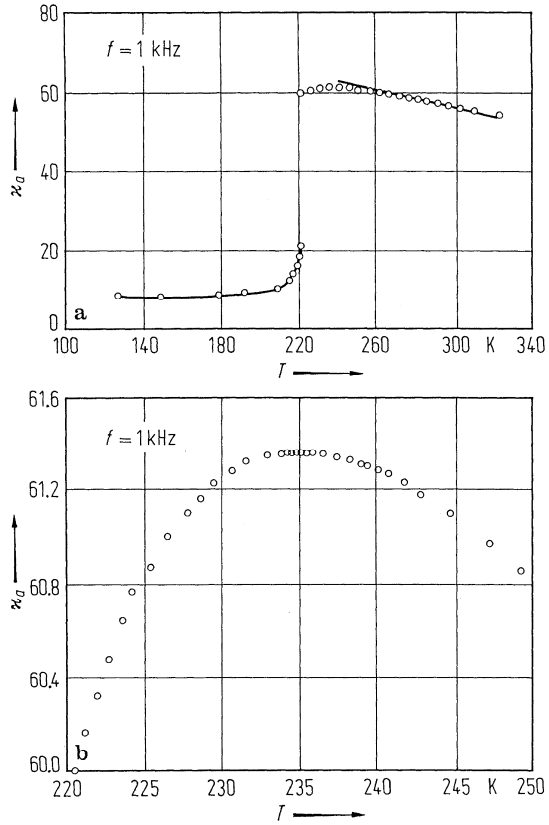

Fig. 33A-1-049. KD_2PO_4 (DKDP). κ_a vs. T [76Hav]. f = 1 kHz. (**a**) 120…320 K. (**b**) 220…250 K.

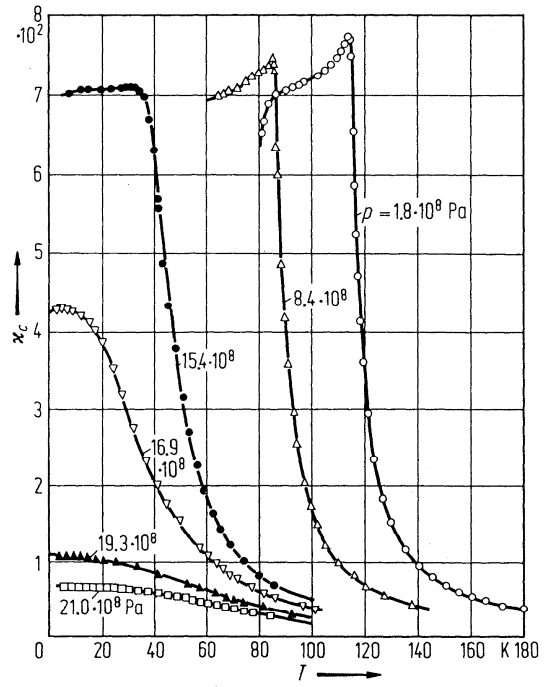

Fig. 33A-1-050. KH_2PO_4 (KDP). κ_c vs. T [71Sam]. Parameter: p.

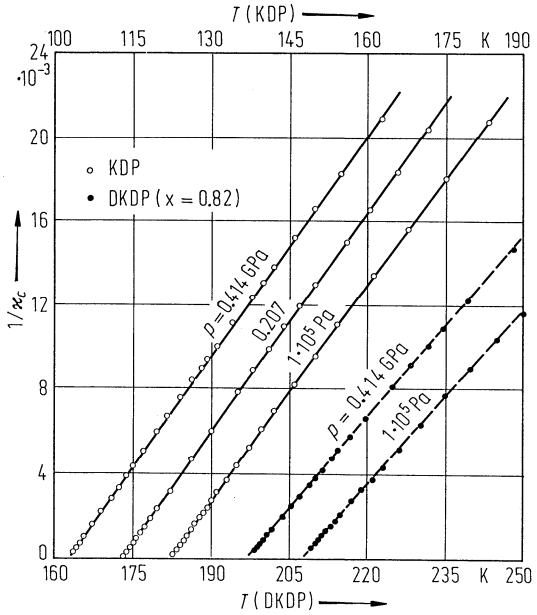

Fig. 33A-1-051. KH_2PO_4 (KDP), $KH_{2(1-x)}D_{2x}PO_4$ (x = 0.82). $1/\kappa_c$ vs. T [79Sam]. Parameter: p.

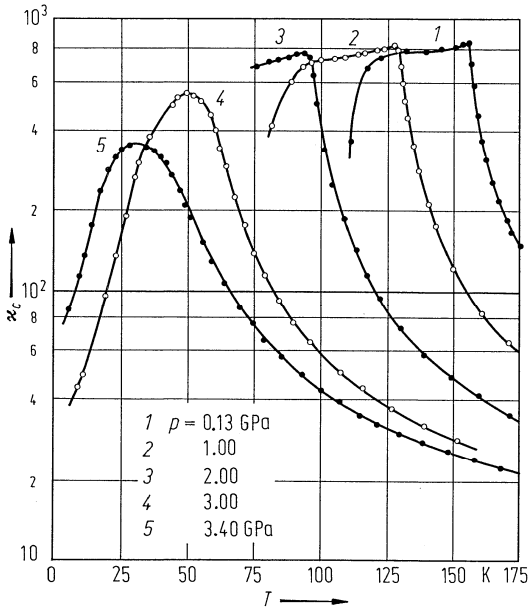

Fig. 33A-1-052. $KH_{2(1-x)}D_{2x}PO_4$ (x = 0.35). κ_c vs. T [79Sam]. Parameter: p.

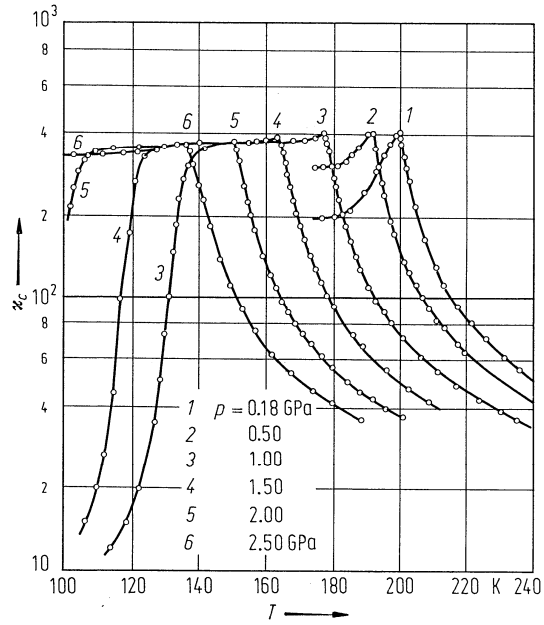

Fig. 33A-1-053. $KH_{2(1-x)}D_{2x}PO_4$ (x = 0.82). κ_c vs. T [79Sam]. Parameter: p.

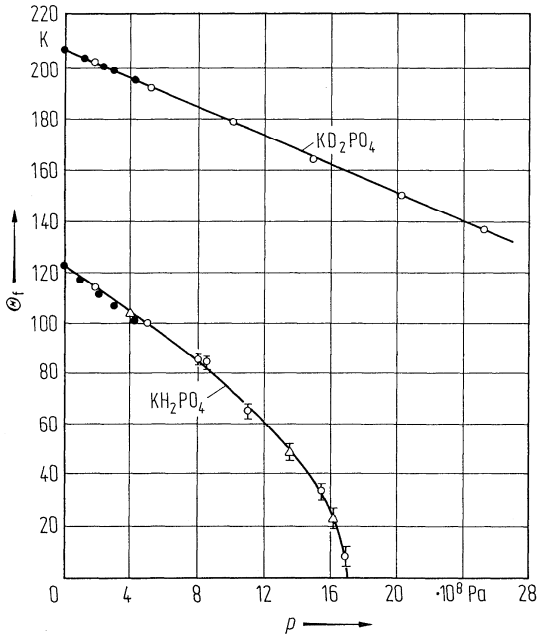

Fig. 33A-1-054. KH_2PO_4 (KDP), KD_2PO_4 (DKDP). Θ_f vs. p [74Sam]. Different symbols correspond to different samples and high pressure cells.

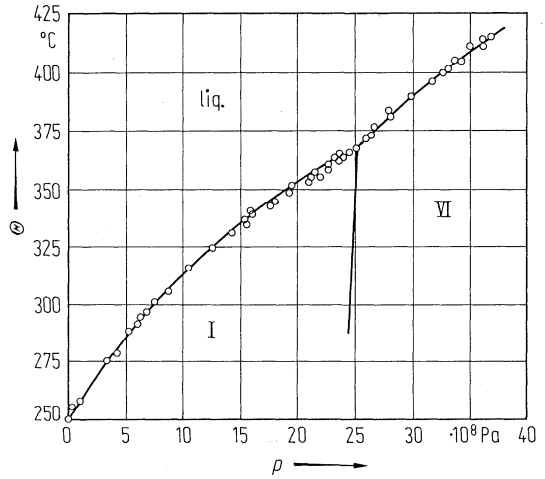

Fig. 33A-1-055. KD_2PO_4 (DKDP). Θ vs. p [78Rap]. See also [70Rap].

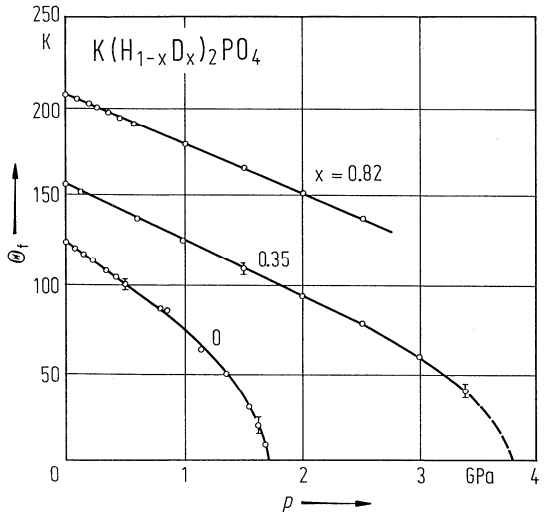

Fig. 33A-1-056. $KH_{2(1-x)}D_{2x}PO_4$ (x = 0, 0.35, 0.82). Θ_f vs. p [79Sam].

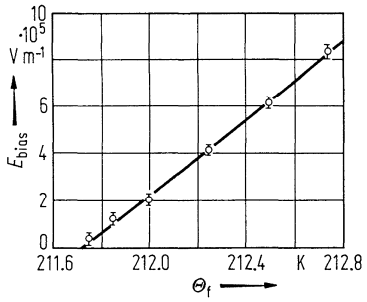

Fig. 33A-1-057. KD_2PO_4 (DKDP). Θ_f vs. E_{bias} [71Gla].

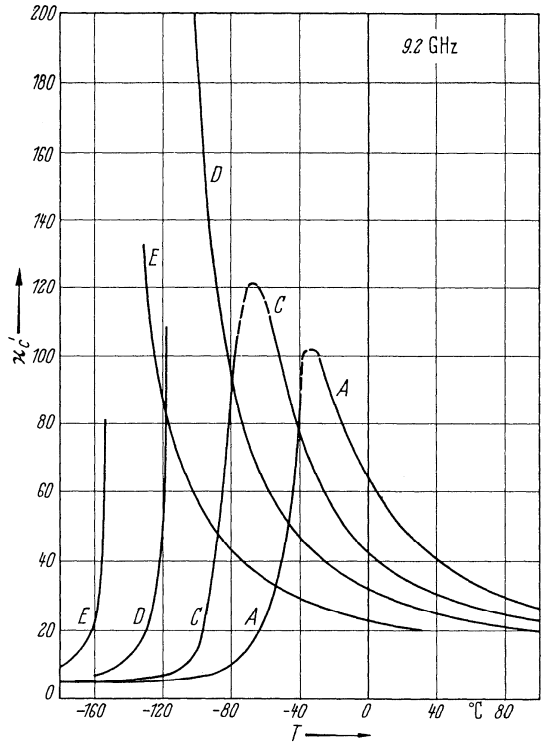

Fig. 33A-1-058. $KH_{2(1-x)}D_{2x}PO_4$. κ_c' vs. T at 9.2 GHz [65Kam]. Curve A: x = 0.96, C: x = 0.66, D: x = 0.35, E: x = 0.

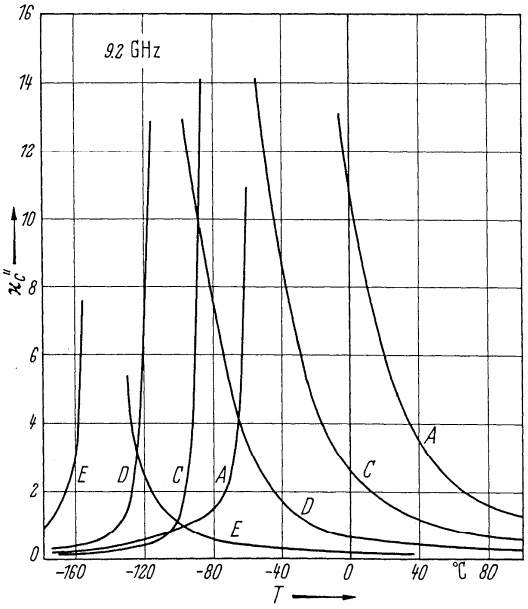

Fig. 33A-1-059. $KH_{2(1-x)}D_{2x}PO_4$. κ_c'' vs. T at 9.2 GHz [65Kam]. Curve A: x = 0.96, C: x = 0.66, D: x = 0.35. E: x = 0.

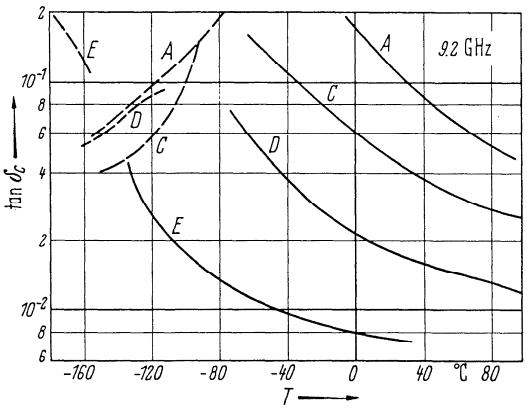

Fig. 33A-1-060. $KH_{2(1-x)}D_{2x}PO_4$. $\tan\delta_c$ vs. T at 9.2 GHz [65Kam]. Curve A: x = 0.96, C: x = 0.66, D: x = 0.35, E: x = 0.

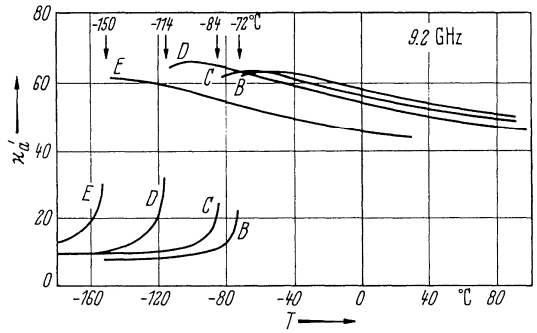

Fig. 33A-1-061. $KH_{2(1-x)}D_{2x}PO_4$. κ'_a vs. T at 9.2 GHz [65Kam]. Curve B: x = 0.68, C: x = 0.66, D: x = 0.35, E: x = 0.

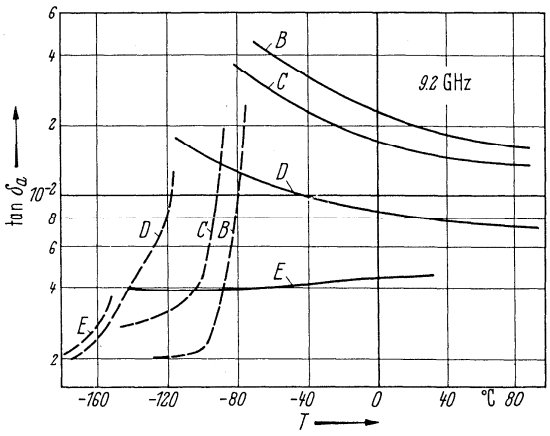

Fig. 33A-1-062. $KH_{2(1-x)}D_{2x}PO_4$. $\tan\delta_a$ vs. T at 9.2 GHz [65Kam]. Curve B: x = 0.68, C: x = 0.66, D: x = 0.35, E: x = 0.

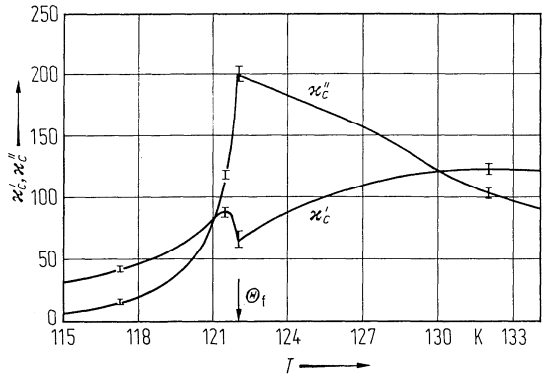

Fig. 33A-1-063. KH_2PO_4 (KDP). κ_c', κ_c'' vs. T at 139 GHz [75Gau].

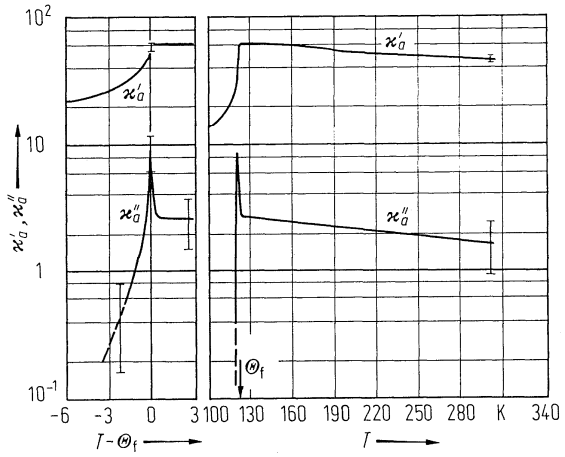

Fig. 33A-1-064. KH_2PO_4 (KDP). κ_a', κ_a'' vs. T at 139 GHz [75Gau].

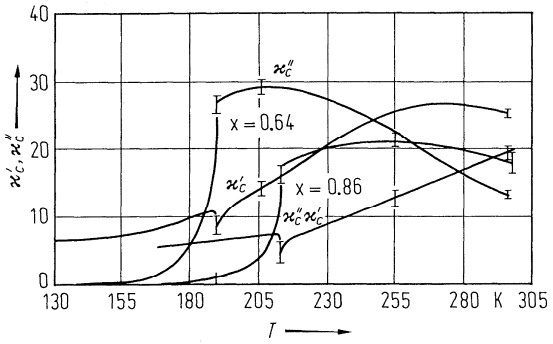

Fig. 33A-1-065. $KH_{2(1-x)}D_{2x}PO_4$. κ_c', κ_c'' vs. T at 139 GHz [76Gau]. Parameter: x.

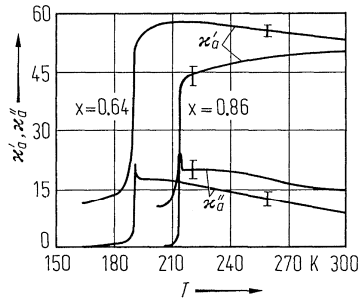

Fig. 33A-1-066. $KH_{2(1-x)}D_{2x}PO_4$. κ'_a, κ''_a vs. T at 139 GHz [76Gau]. Parameter: x.

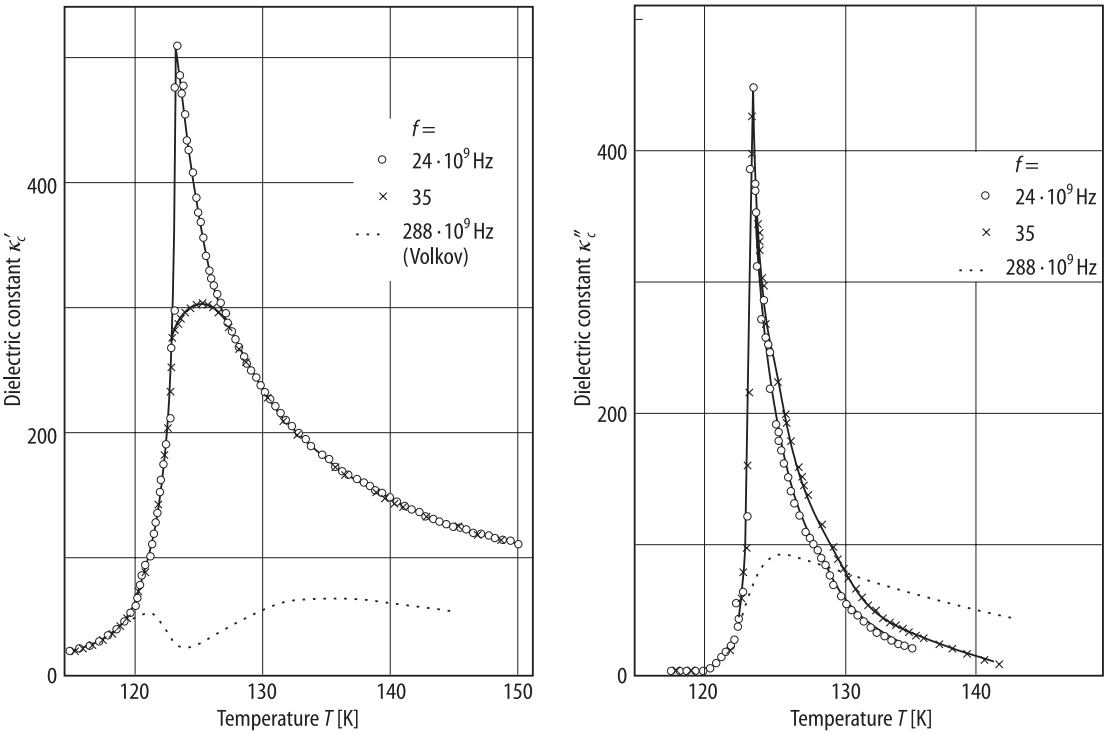

Fig. 33A-1-067. KH_2PO_4 (KDP). κ'_c, κ''_c vs. T [90Hor]. Parameter: f. The data at f = 288 GHz are from [78Vol].

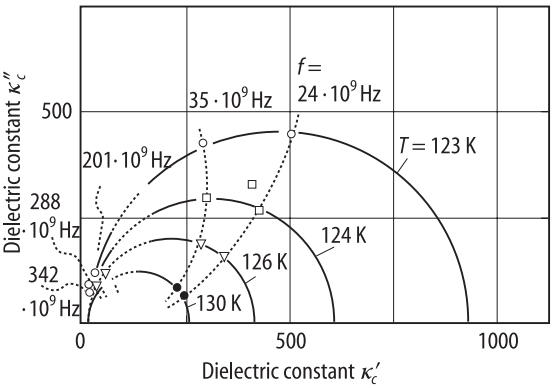

Fig. 33A-1-068. KH_2PO_4 (KDP). κ''_c vs. κ'_c (Cole-Cole diagram) [90Hor]. Parameter: T. The data from f = 201 to 342 GHz are from [78Vol].

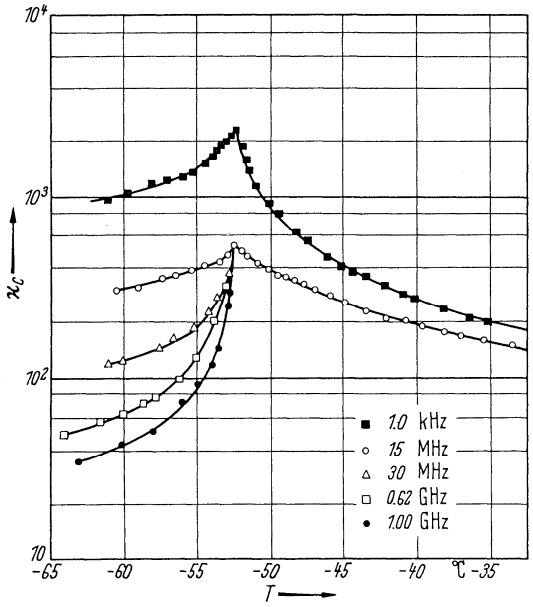

Fig. 33A-1-069. KD_2PO_4 (DKDP). κ_c vs. T [63Hil]. Parameter: f.

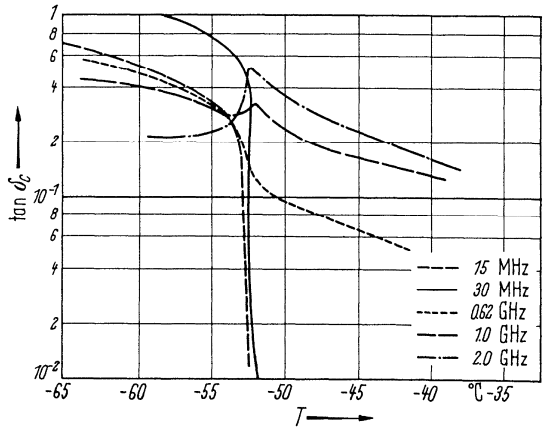

Fig. 33A-1-070. KD_2PO_4 (DKDP). tanδ_c vs. T [63Hil]. Parameter: f.

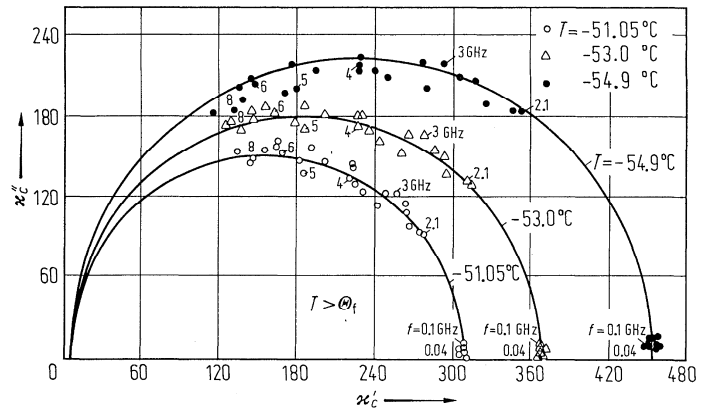

Fig. 33A-1-071. KD_2PO_4 (DKDP). κ_c' vs. κ_c'' (Cole-Cole diagram) in the paraelectric phase [76Lut]. Parameter: T. $\Theta_f = -56.7$ °C.

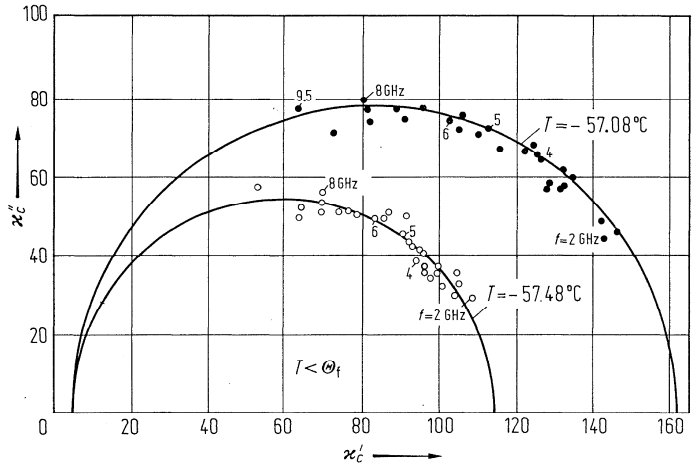

Fig. 33A-1-072. KD_2PO_4 (DKDP). κ_c' vs. κ_c'' (Cole-Cole diagram) in the ferroelectric phase [76Lut]. Parameter: T. $\Theta_f = -56.7$ °C.

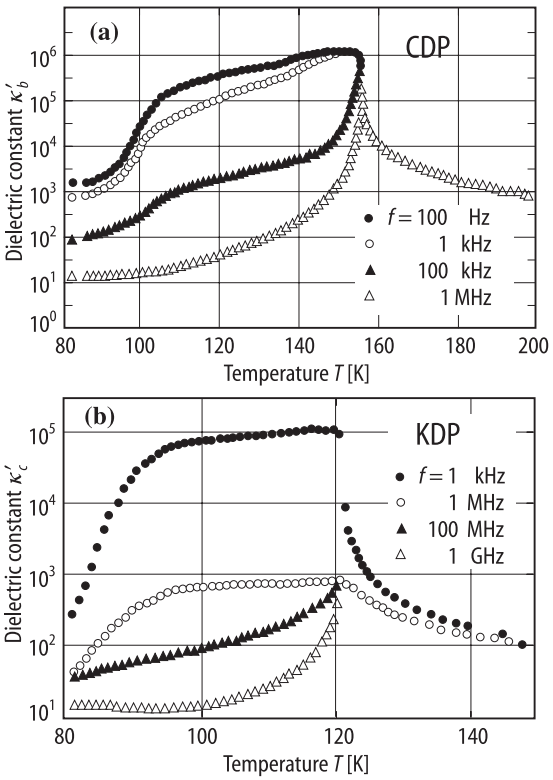

Fig. 33A-1-073. KH_2PO_4 (KDP), CsH_2PO_4 (CDP). κ' vs. T [93Nak]. Parameter: f. (**a**) CDP, κ'_b vs. T. (**b**) KDP, κ'_c vs. T.

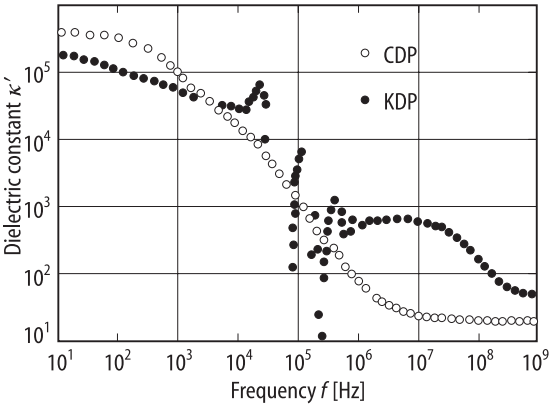

Fig. 33A-1-074. KH_2PO_4 (KDP), CsH_2PO_4 (CDP). κ' vs. f below Θ_t [93Nak]. KDP: κ'_c at 110 K. CDP: κ'_b at 120 K.

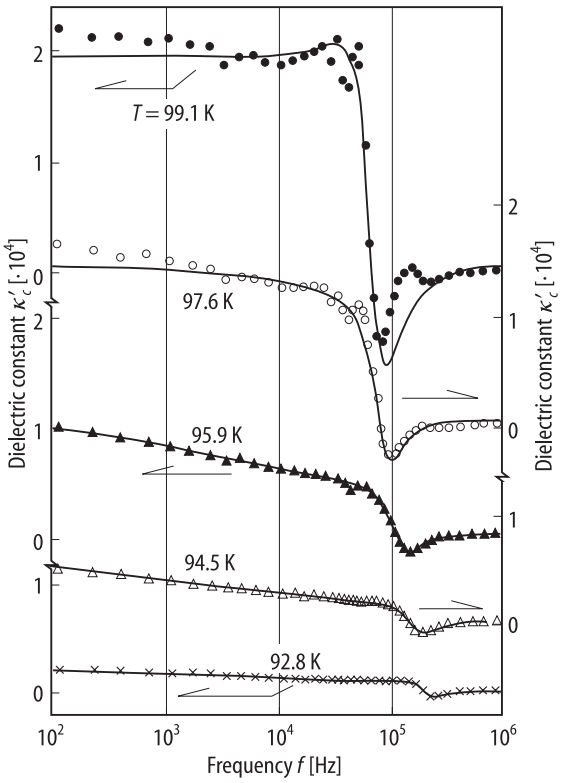

Fig. 33A-1-075. KH_2PO_4 (KDP). κ_c' vs. f around the domain freezing temperature T_f [87Kur]. Parameter: T. $T_f = 95$ K.

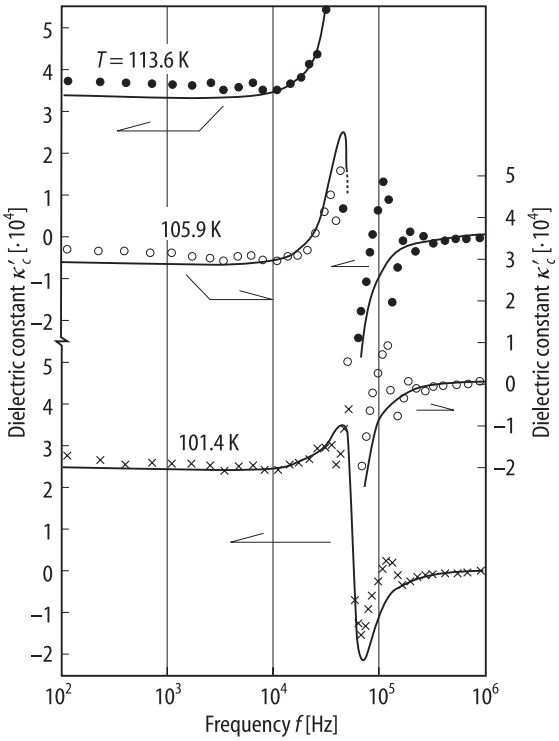

Fig. 33A-1-076. KH_2PO_4 (KDP). κ_c' vs. f in the ferroelectric phase [87Kur]. Parameter: T. 10^2 Hz < f < 1 MHz.

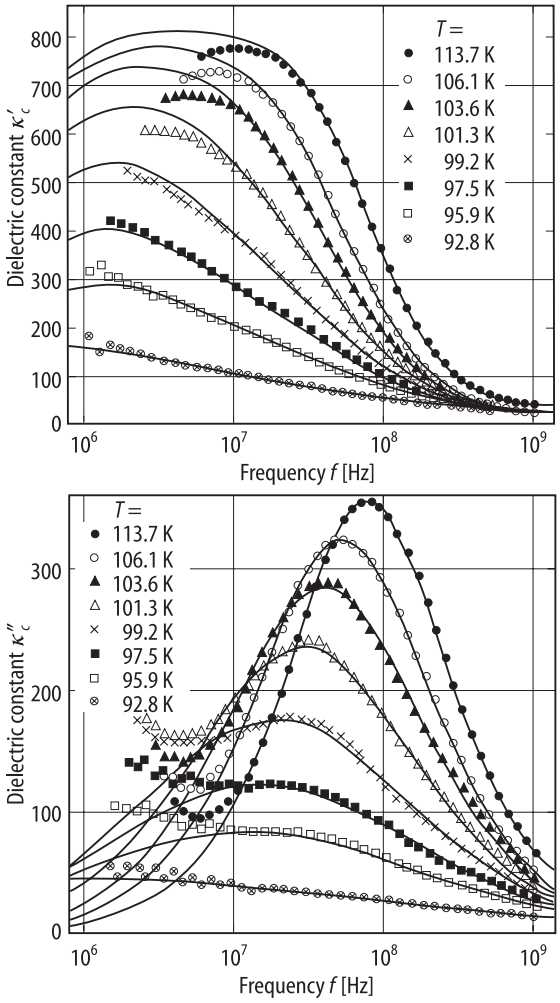

Fig. 33A-1-077. KH_2PO_4 (KDP). κ_c', κ_c'' vs. f in the ferroelectric phase [87Kur]. Parameter: T. 1 MHz < f < 1 GHz.

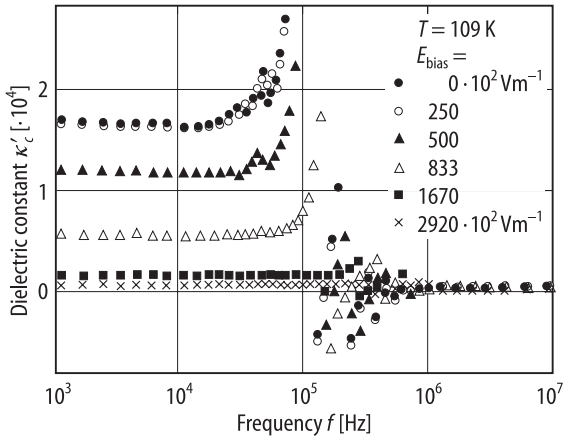

Fig. 33A-1-078. KH_2PO_4 (KDP). κ_c' vs. f in the ferroelectric phase [87Kur]. Parameter: E_{bias}. 1 kHz < f < 10 MHz.

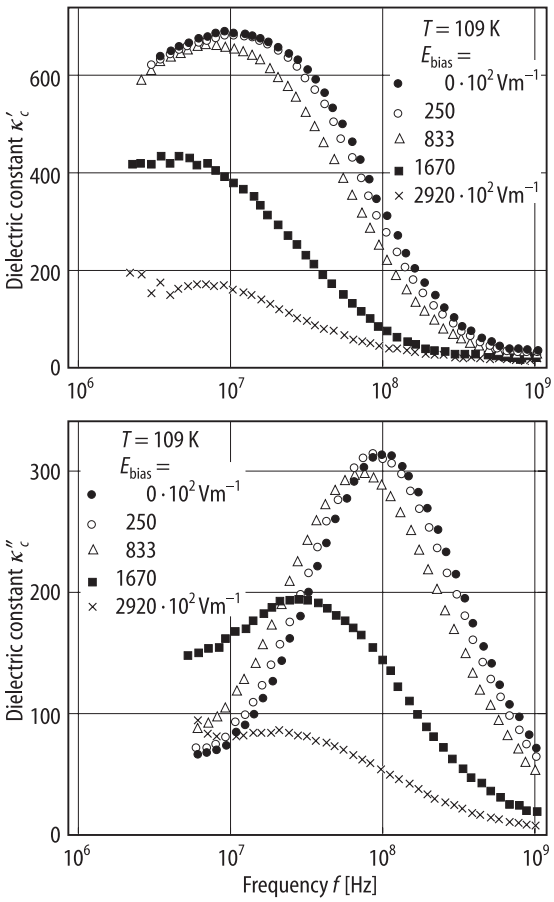

Fig. 33A-1-079. KH_2PO_4 (KDP). κ_c', κ_c'' vs. f in the ferroelectric phase [87Kur]. Parameter: E_{bias}. 1 MHz < f < 1 GHz.

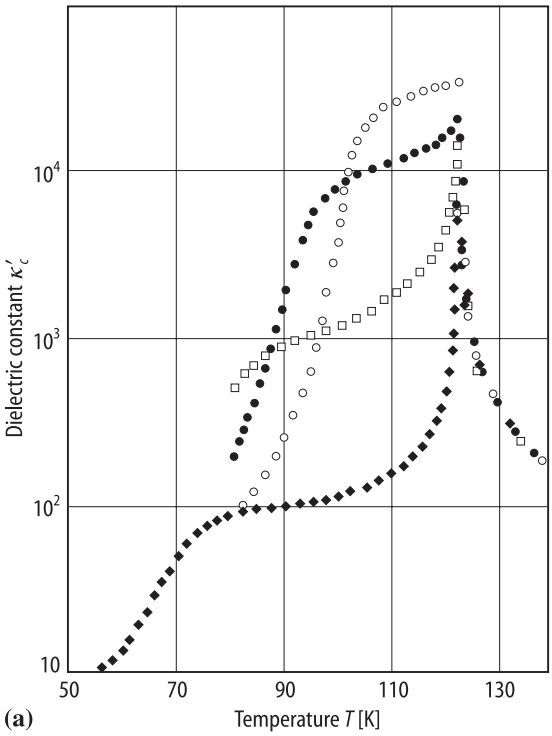

(a)

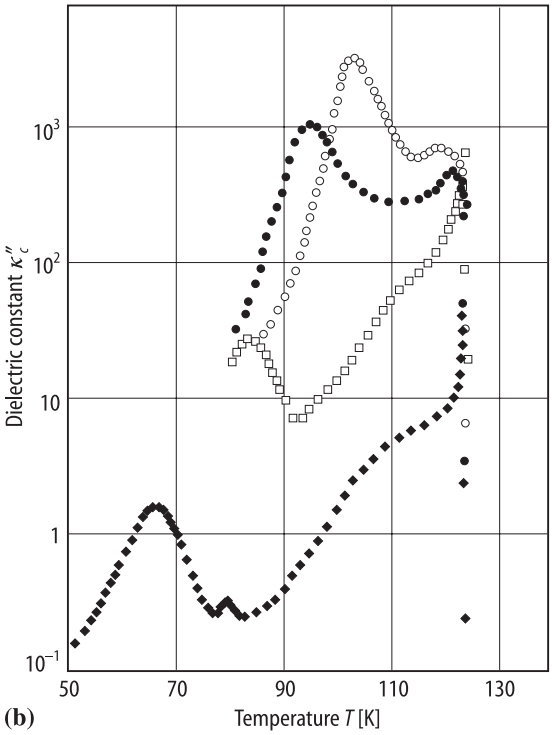

(b)

Fig. 33A-1-080. KH_2PO_4 (KDP). (**a**) κ_c', (**b**) κ_c'' vs. T of lossy crystals [85Kur]. f = 1 kHz. The specimens are specified by tan δ at RT, tan δ_R. Open circle: tan $\delta_R = 7.44 \cdot 10^{-3}$, full circle: $2.27 \cdot 10^{-2}$, open diamond: 6.27, full diamond: 7.48.

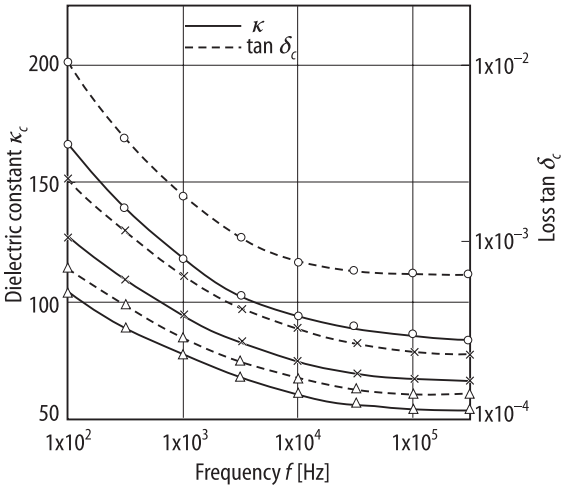

Fig. 33A-1-081. KH_2PO_4 (KDP). κ_c, tan δ_c vs. f for irradiated crystal [89Rou]. T = RT. Full line: κ_c, broken line: tan δ_c. Circle: before irradiation; cross: after X-irradiation for 1 h; triangle: after X-irradiation for 2 h.

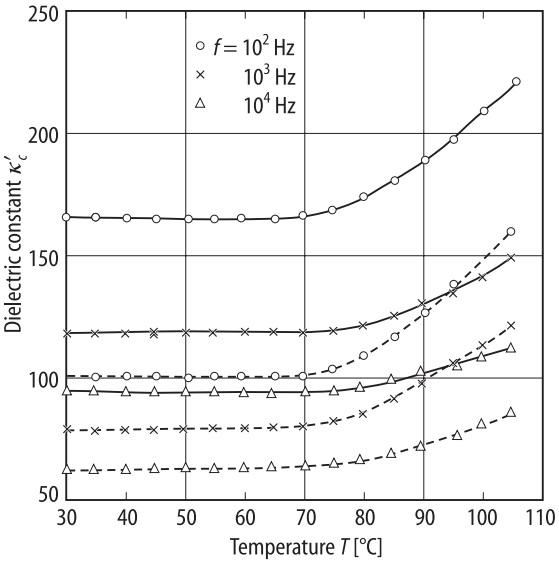

Fig. 33A-1-082. KH_2PO_4 (KDP). κ_c' vs. T for irradiated crystal [89Rou]. Parameter: f. Full line: before irradiation, dashed line: after X-irradiation for 2 h.

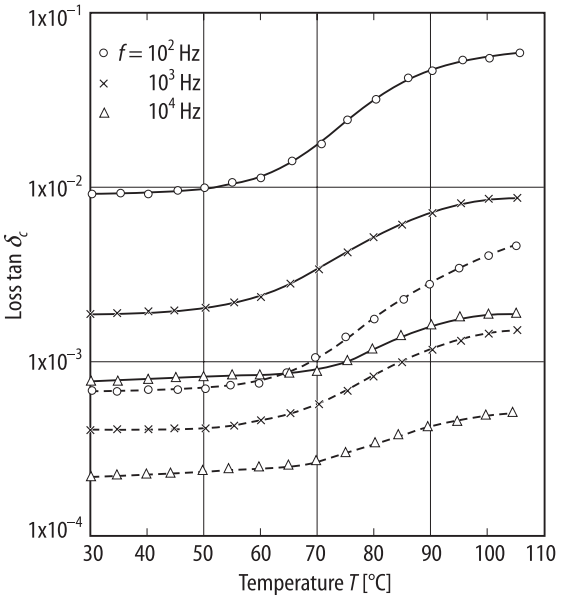

Fig. 33A-1-083. KH_2PO_4 (KDP). tan δ_c vs. T for irradiated crystal [89Rou]. Parameter: f. Full line: before irradiation, dashed line: after X-irradiation for 2 h.

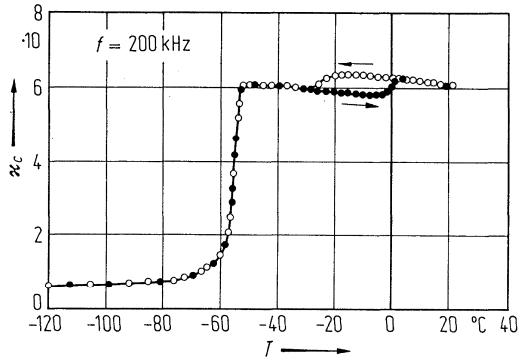

Fig. 33A-1-084. KD_2PO_4 (DKDP) (monoclinic). κ_c vs. T [75Bli]. f = 200 kHz.

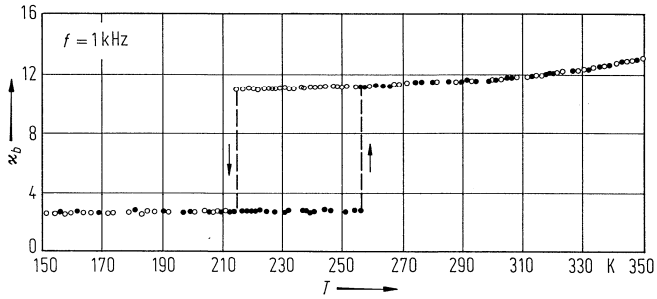

Fig. 33A-1-085. KD_2PO_4 (DKDP) (monoclinic). κ_b vs. T [87Yak]. f = 1 kHz.

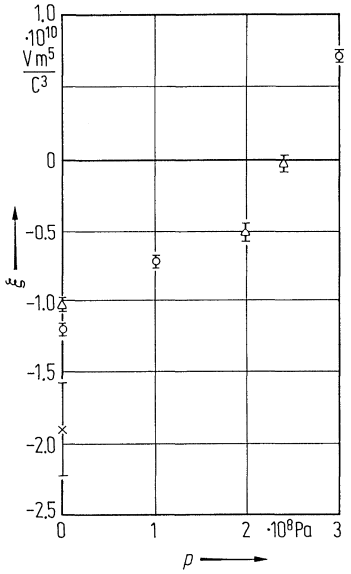

Fig. 33A-1-086. KH_2PO_4 (KDP). ξ vs. p [78Wes]. Different figures correspond to different samples.

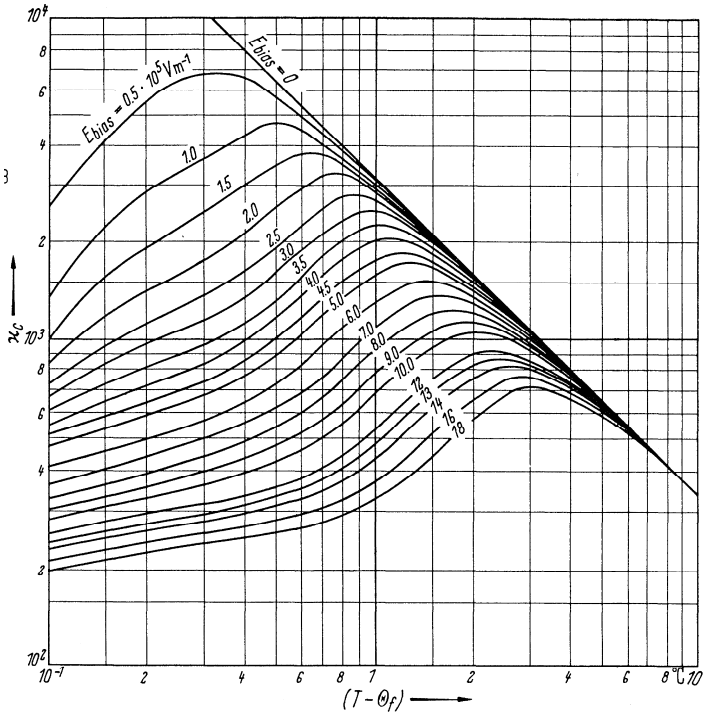

Fig. 33A-1-087. KH_2PO_4 (KDP). κ_c vs. $T - \Theta_f$ [50Bau]. Parameter: E_{bias}. f = 1 kHz.

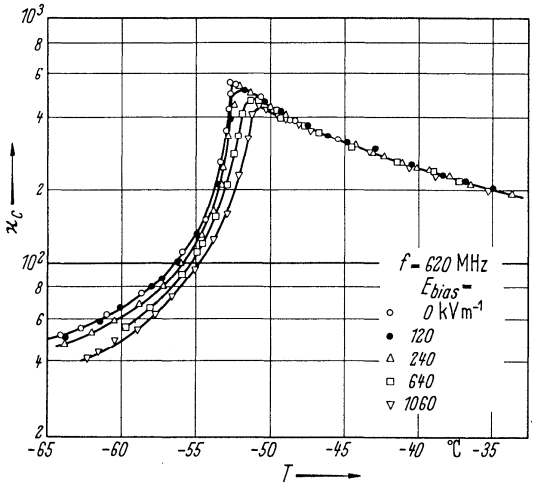

Fig. 33A-1-088. KD_2PO_4 (DKDP). κ_c vs. T at 620 MHz [63Hil]. Parameter: E_{bias}.

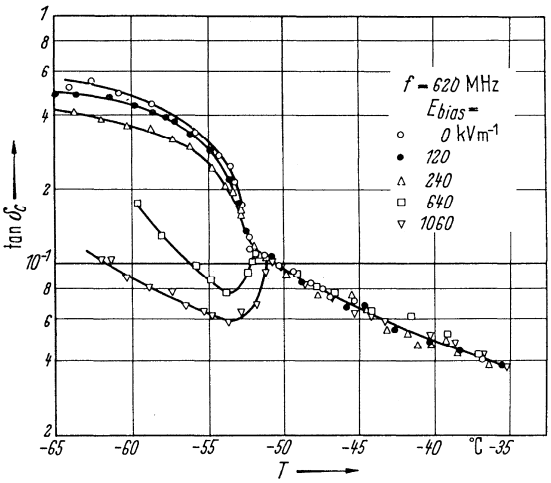

Fig. 33A-1-089. KD_2PO_4 (DKDP). tan δ_c vs. T at 620 MHz [63Hil]. Parameter: E_{bias}.

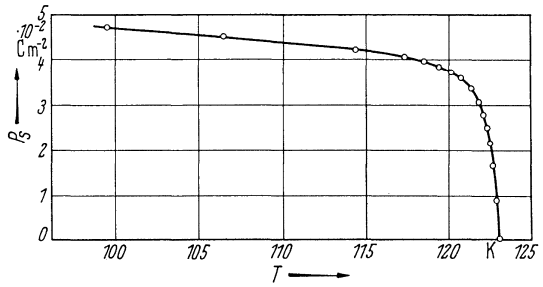

Fig. 33A-1-090. KH_2PO_4 (KDP). P_s vs. T [44von].

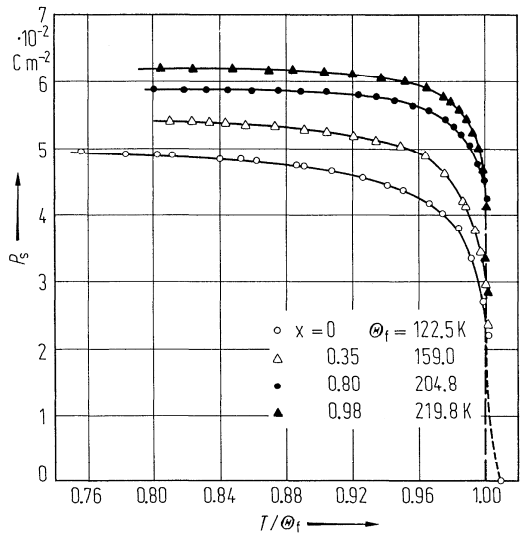

Fig. 33A-1-091. $KH_{2(1-x)}D_{2x}PO_4$. P_s vs. T/Θ_f [73Sam]. Parameter: x.

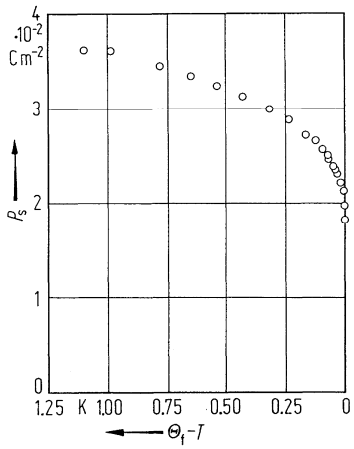

Fig. 33A-1-092. KH_2PO_4 (KDP). P_s vs. ($\Theta_f - T$) in the vicinity of Θ_f [71Ben].

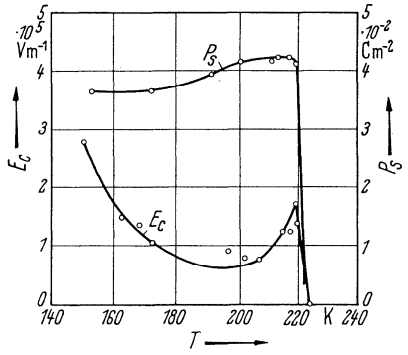

Fig. 33A-1-093. KD_2PO_4 (DKDP). P_s and E_c vs. T [63Sli].

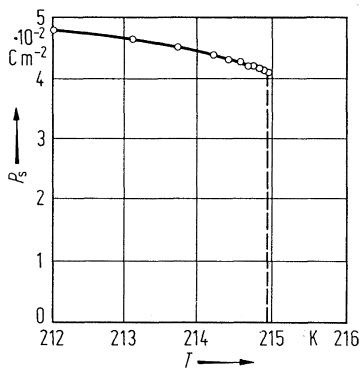

Fig. 33A-1-094. KD_2PO_4 (DKDP). P_s vs. T in the vicinity of Θ_f [71Str].

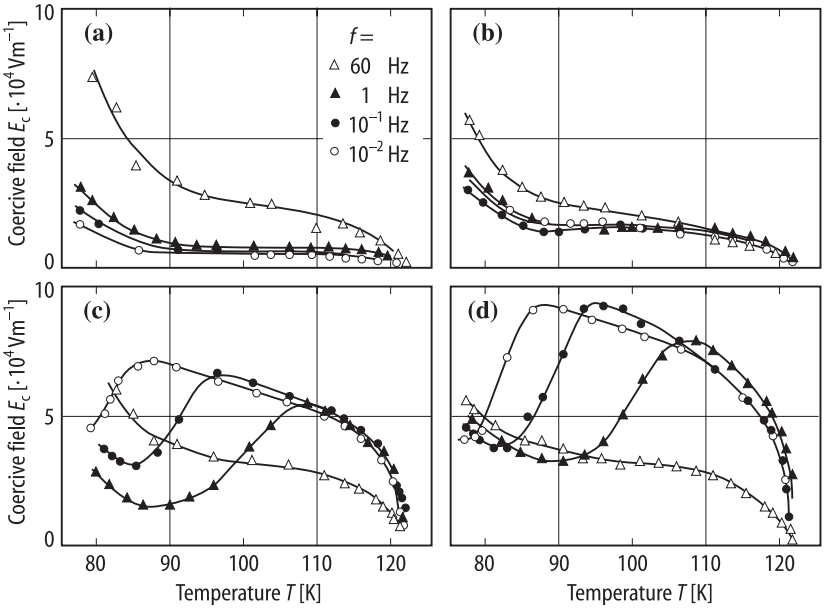

Fig. 33A-1-095. KH_2PO_4 (KDP). E_c vs. T [84Abe]. Parameter: frequency f of P–E hysteresis. Amplitude of the applied field: $2 \cdot 10^5$ V m^{-1}. (**a**) specimen with small signal dielectric loss at 1 kHz at RT, κ_c'' (RT) = $2.3 \cdot 10^{-1}$, (**b**) $2.8 \cdot 10^2$, (**c**) $3.3 \cdot 10^3$, (**d**) $6.7 \cdot 10^3$.

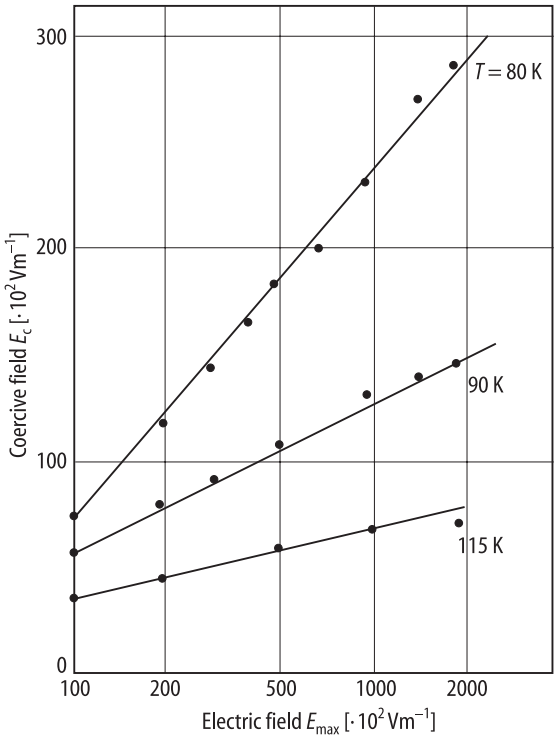

Fig. 33A-1-096. KH_2PO_4 (KDP). E_c vs. E_{max} [95Bor]. Parameter: T. E_{max}: maximum applied field. f = 50 Hz.

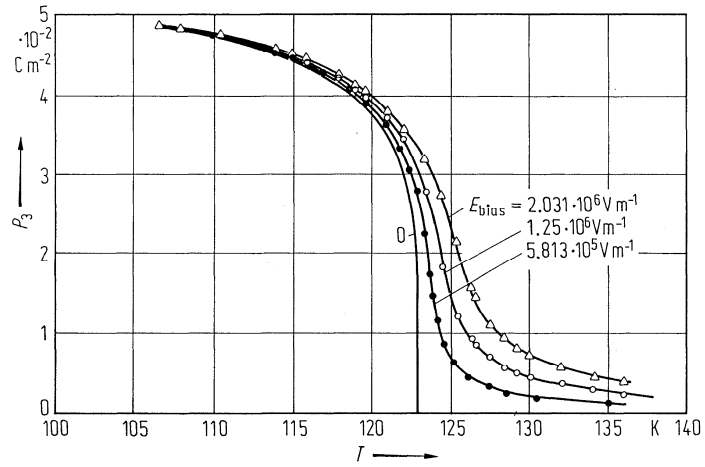

Fig. 33A-1-097. KH_2PO_4 (KDP). P_3 vs. T [77Cha]. Parameter: E_{bias}. P_3: polarization along c axis.

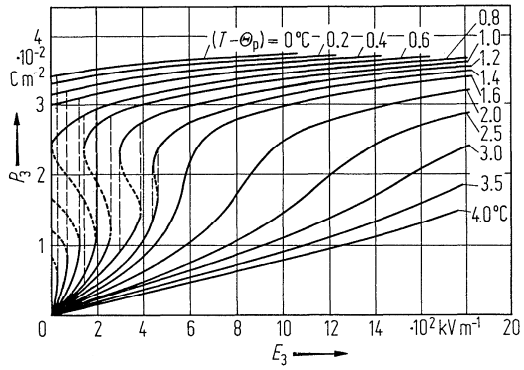

Fig. 33A-1-098. KH_2PO_4 (KDP). P_3 vs. E_3 [71Kob]. Parameter: $T - \Theta_p$. P_3: polarization along *c* axis.

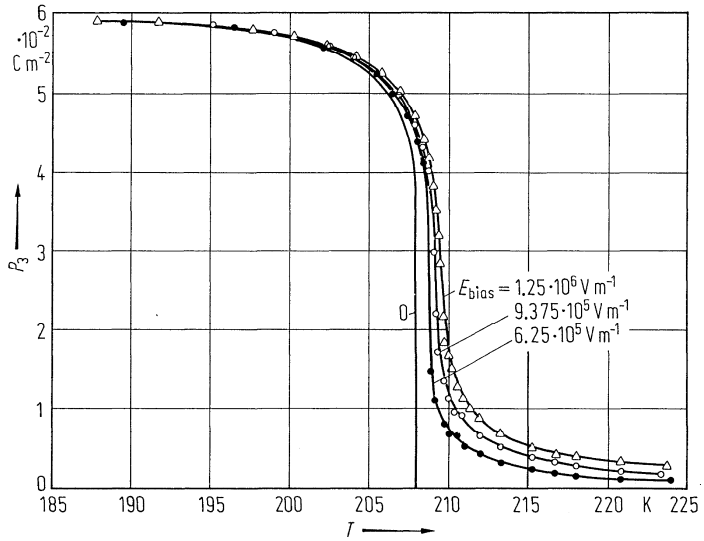

Fig. 33A-1-099. $KH_{2(1-x)}D_{2x}PO_4$ (x = 0.7). P_3 vs. T [77Cha]. Parameter: E_{bias}.

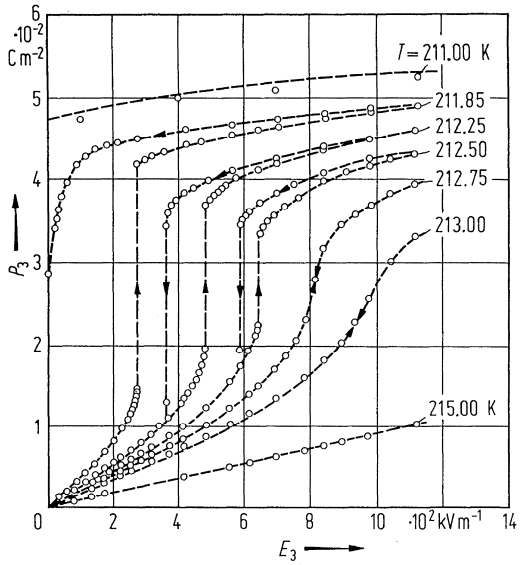

Fig. 33A-1-100. $KH_{2(1-x)}D_{2x}PO_4$ (x = 0.85). P_3 vs. E_3 [72Sid]. Parameter: T.

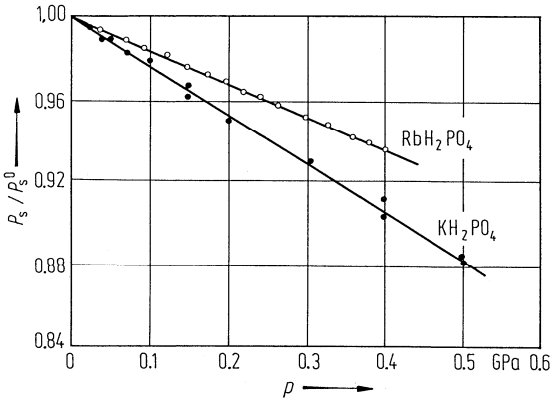

Fig. 33A-1-101. KH_2PO_4 (KDP), RbH_2PO_4(RDP). P_s / P_s^0 vs. p at 75.6 K [79Sam]. P_s^0 : P_s at p = 0.

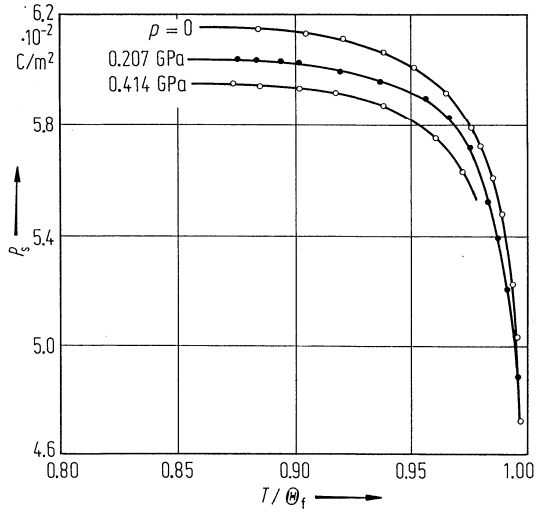

Fig. 33A-1-102. $KH_{2(1-x)}D_{2x}PO_4$ (x = 0.94). P_s vs. T/Θ_f [79Sam]. Parameter: p. Θ_f = 220 K for p = 0.

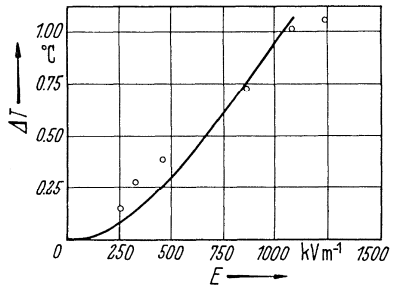

Fig. 33A-1-103. KH_2PO_4 (KDP). ΔT vs. E [50Bau]. ΔT: electrocaloric temperature change.

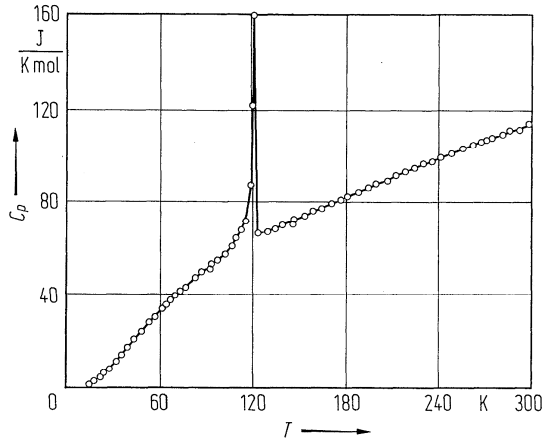

Fig. 33A-1-104. KH_2PO_4 (KDP). C_p vs. T [44Ste]. C_p: molar heat capacity at constant pressure.

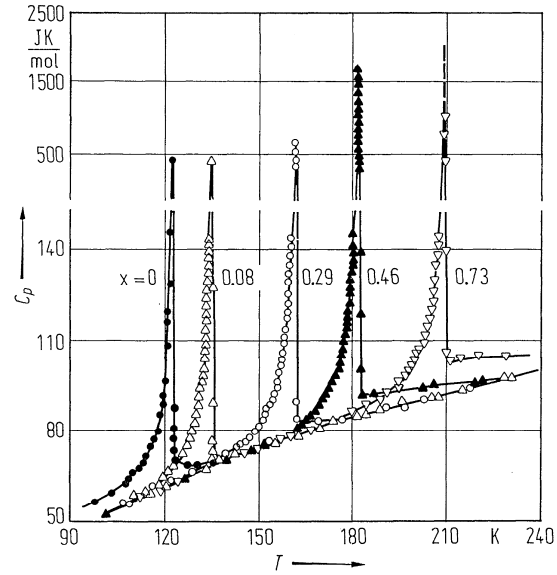

Fig. 33A-1-105. $KH_{2(1-x)}D_{2x}PO_4$. C_p vs. T [72Str]. Parameter: x. C_p: molar heat capacity at constant pressure.

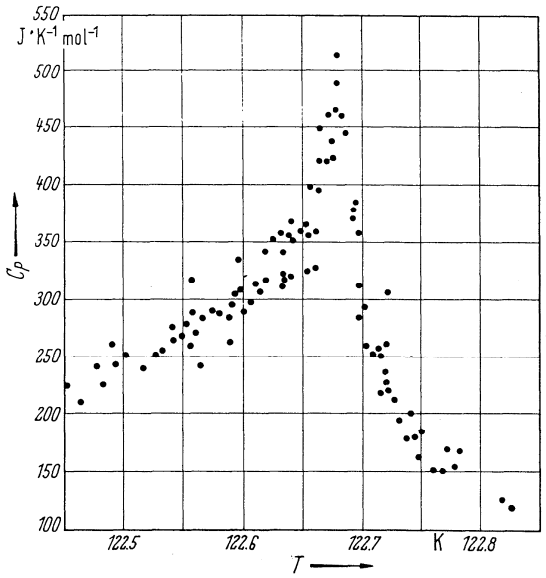

Fig. 33A-1-106. KH_2PO_4 (KDP). C_p vs. T in the vicinity of Θ_t [67Ree]. C_p: molar heat capacity at constant pressure.

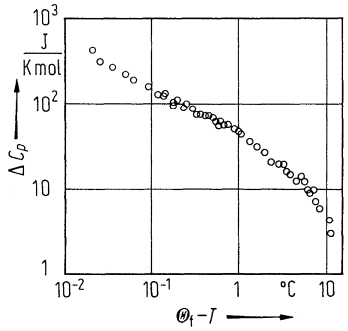

Fig. 33A-1-107. KH_2PO_4 (KDP). ΔC_p vs. $\Theta_t - T$ [68Str]. ΔC_p: anomalous part of C_p. C_p: molar heat capacity at constant pressure.

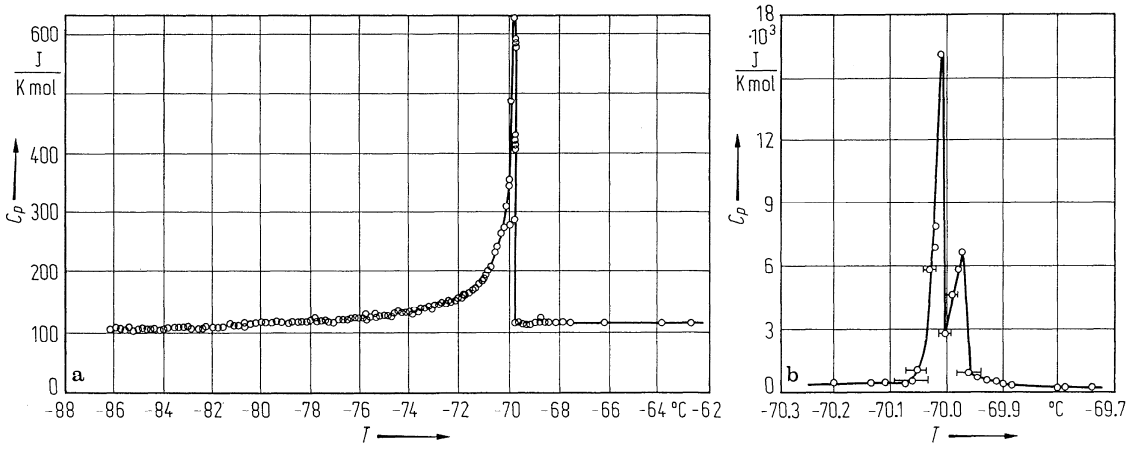

Fig. 33A-1-108. KD_2PO_4 (DKDP). C_p vs. T [67Str]. C_p: molar heat capacity at constant pressure.

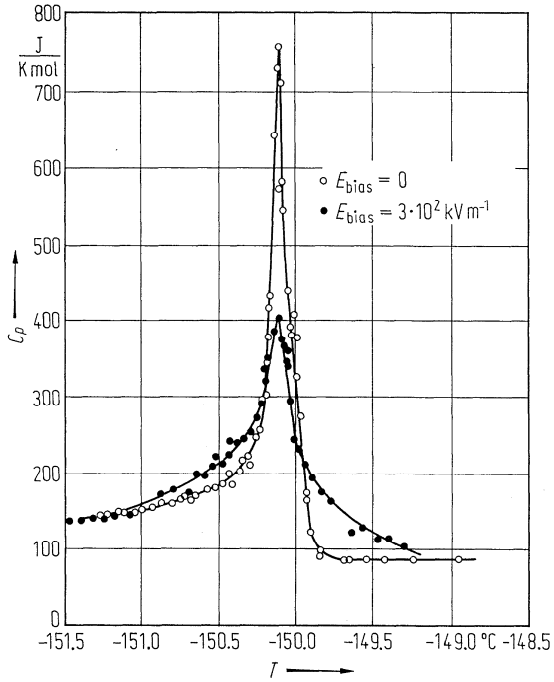

Fig. 33A-1-109. KH_2PO_4 (KDP). C_p vs. T [68Str]. Parameter: E_{bias}. C_p: molar heat capacity at constant pressure.

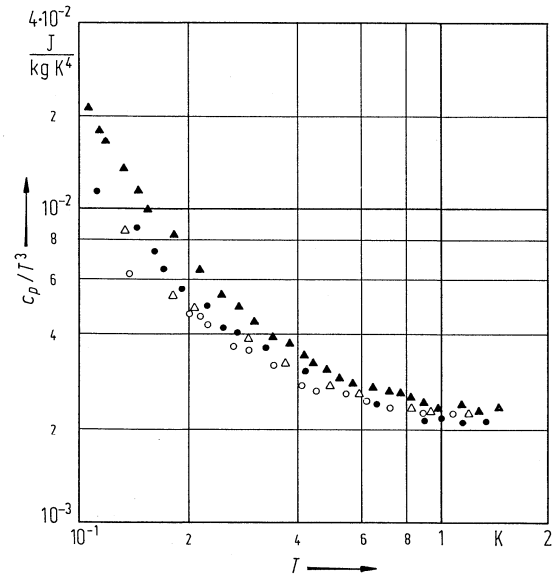

Fig. 33A-1-110. KH_2PO_4 (KDP). c_p/T^3 vs. T [87Zim]. c_p: specific heat capacity at constant pressure. Open circle: with open electrodes; open triangle: with short circuited electrodes; full circle: poled ($E = 2 \cdot 10^5$ V m^{-1}); full triangle: neutron irradiated.

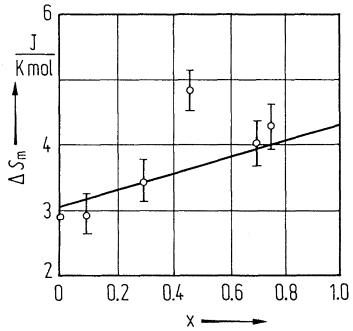

Fig. 33A-1-111. $KH_{2(1-x)}D_{2x}PO_4$. ΔS_m vs. x [72Str]. ΔS_m: transition entropy at Θ_t.

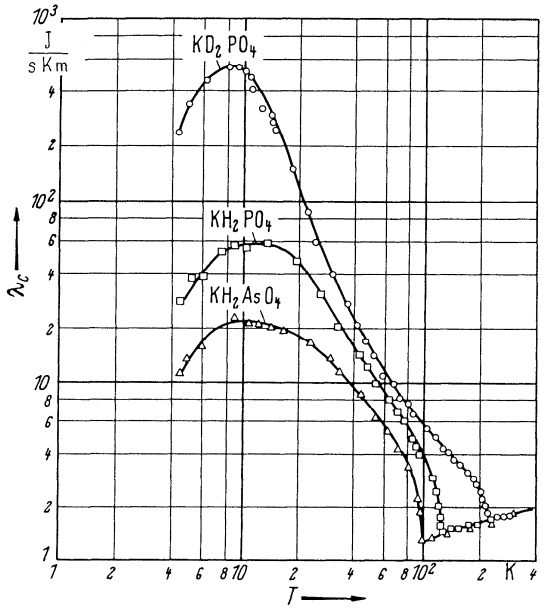

Fig. 33A-1-112. KH_2PO_4 (KDP), KD_2PO_4 (DKDP), KH_2AsO_4 (KDA). λ_c vs. T [67Sue]. λ_c: thermal conductivity along c axis.

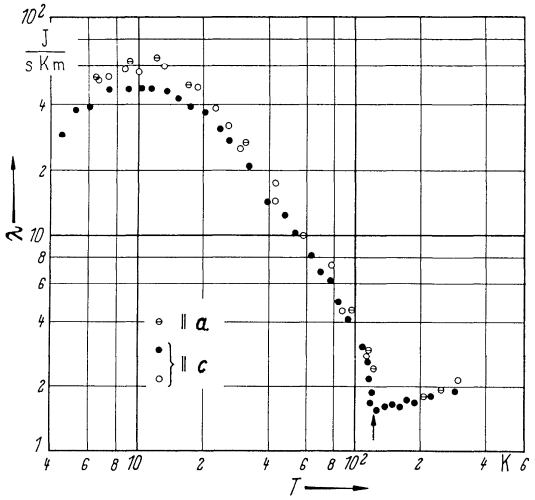

Fig. 33A-1-113. KH_2PO_4 (KDP). λ vs. T [67Sue]. λ: thermal conductivity. Open and full circles correspond to samples of different sizes. Samples are from different crystals.

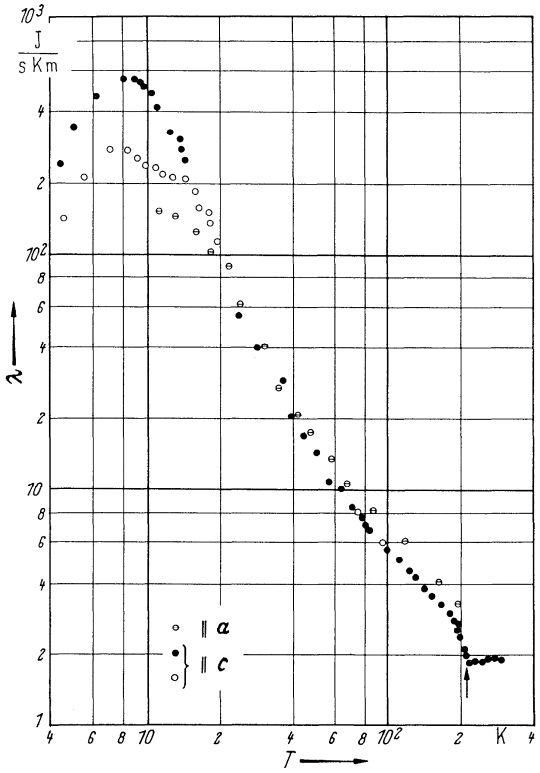

Fig. 33A-1-114. KD_2PO_4 (DKDP). λ vs. T [67Sue]. λ: thermal conductivity. Samples are from the same crystal. See also caption of Fig. 33A-1-113.

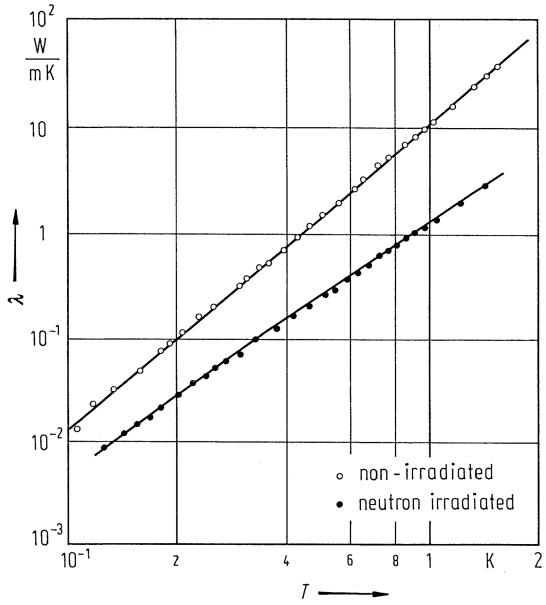

Fig. 33A-1-115. KH_2PO_4 (KDP). λ vs. T [87Zim]. λ: thermal conductivity perpendicular to the c axis.

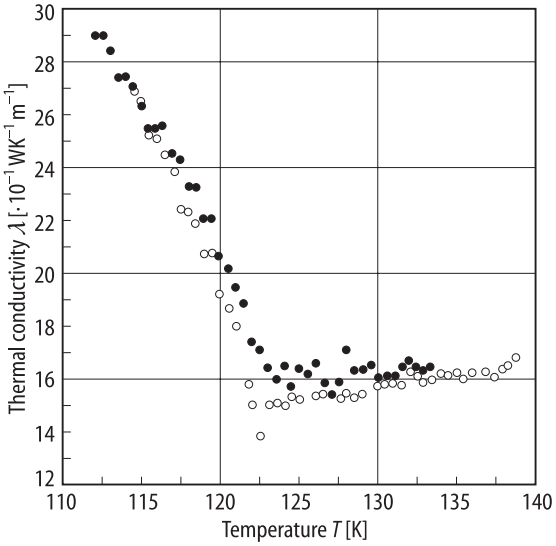

Fig. 33A-1-116. KH_2PO_4 (KDP). λ vs. T [94Lin]. λ: thermal conductivity along the c axis. Open circle: $E_{bias} = 0$; full circle: $E_{bias} = 6 \cdot 10^5$ V m^{-1}.

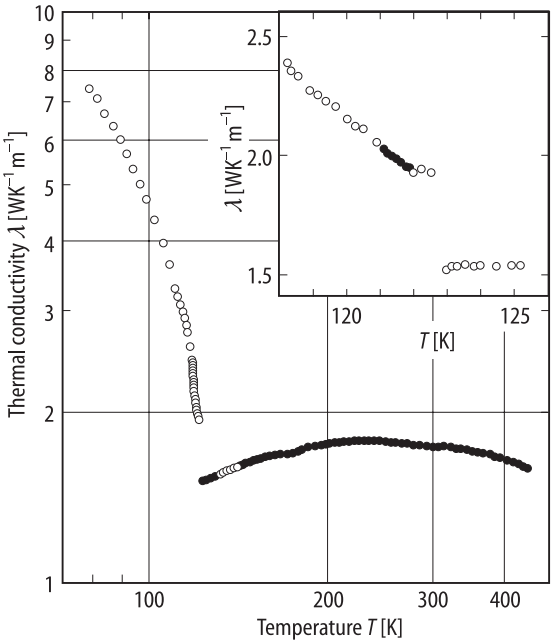

Fig. 33A-1-117. KH_2PO_4 (KDP). λ vs. T [93Lee]. λ: thermal conductivity obtained using the 3ω ac method with a thin line heater along the *a* axis. Insert: the result in the vicinity of Θ_f.

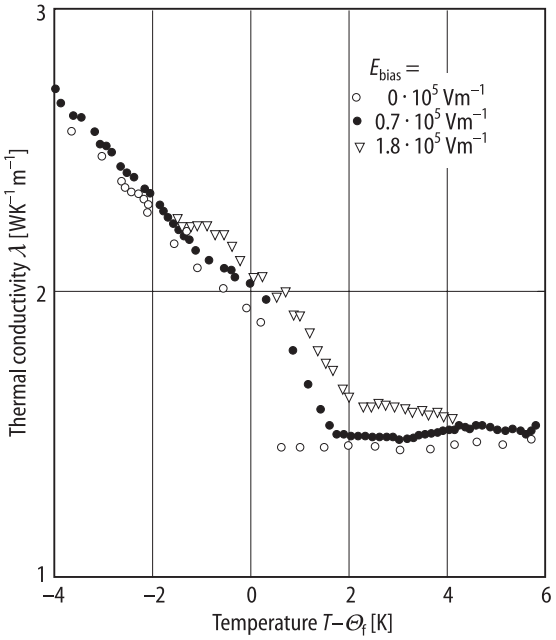

Fig. 33A-1-118. KH_2PO_4 (KDP). λ vs. $T - \Theta_f$ [93Lee]. Parameter: E_{bias}. λ: thermal conductivity obtained using the 3ω ac method with a thin line heater along the *a* axis. E_{bias} was applied along the *c* axis.

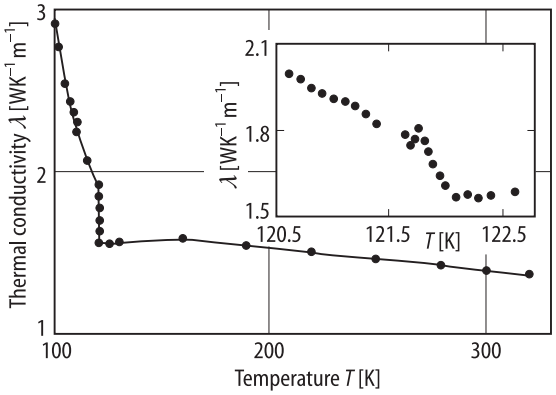

Fig. 33A-1-119. KH_2PO_4 (KDP). λ vs. T [92Str]. λ: thermal conductivity along the c axis. Insert: result in the vicinity of Θ_f.

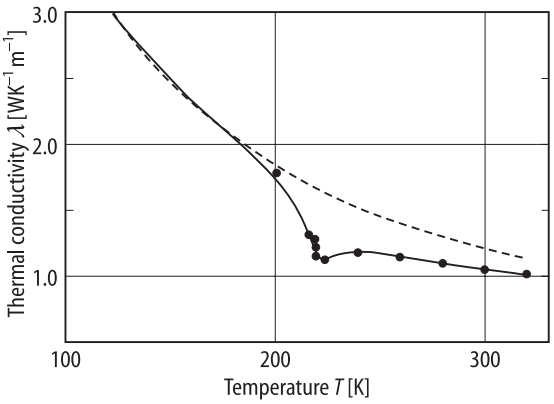

Fig. 33A-1-120. KD_2PO_4 (DKDP). λ vs. T [92Str]. λ: thermal conductivity along the c axis.

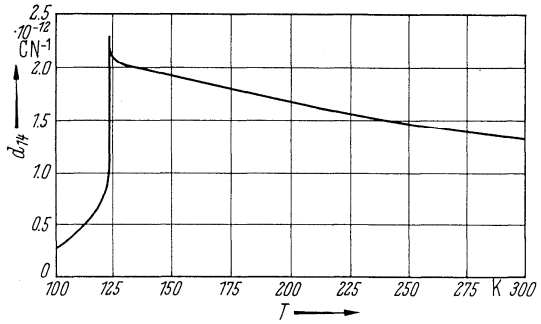

Fig. 33A-1-121. KH_2PO_4 (KDP). d_{14} vs. T [62Jon].

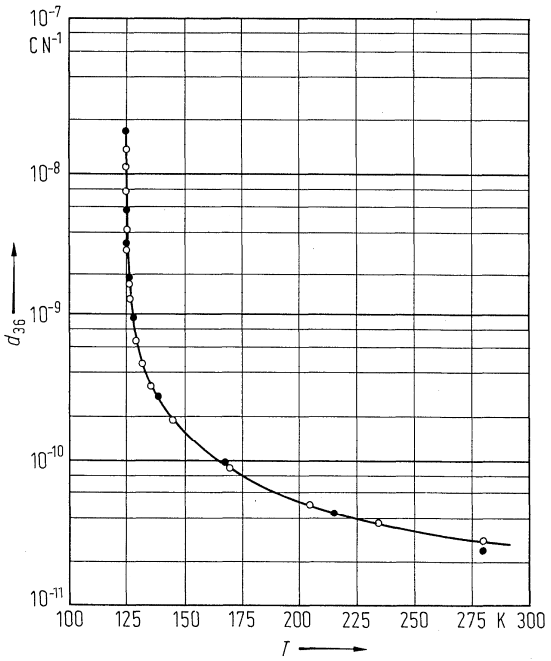

Fig. 33A-1-122. KH_2PO_4 (KDP). d_{36} vs. T. Measurements of the direct effect (full circles) [43Ban] and of the inverse effect (open circles) [44von].

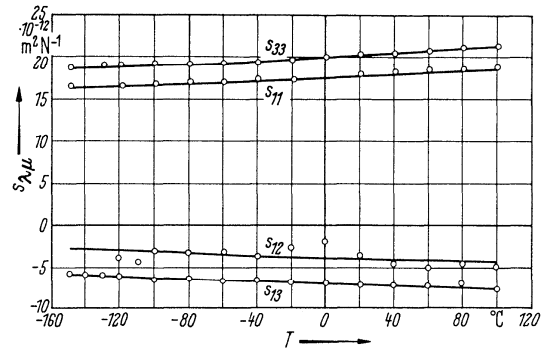

Fig. 33A-1-123. KH_2PO_4 (KDP). $s_{\lambda\mu}$ vs. T [46Mas]. $s_{\lambda\mu}$: elastic compliance.

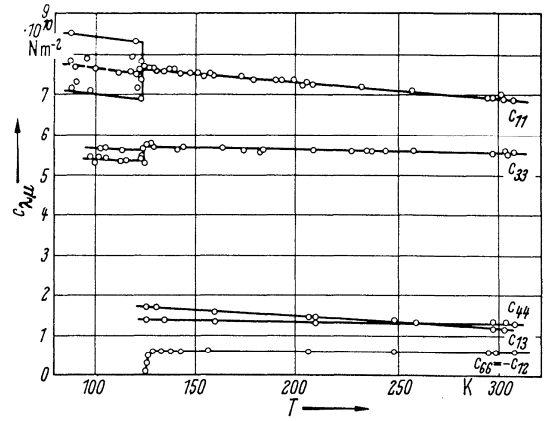

Fig. 33A-1-124. KH_2PO_4 (KDP). $c_{\lambda\mu}$ vs. T [46Zwi]. $c_{\lambda\mu}$: elastic stiffness.

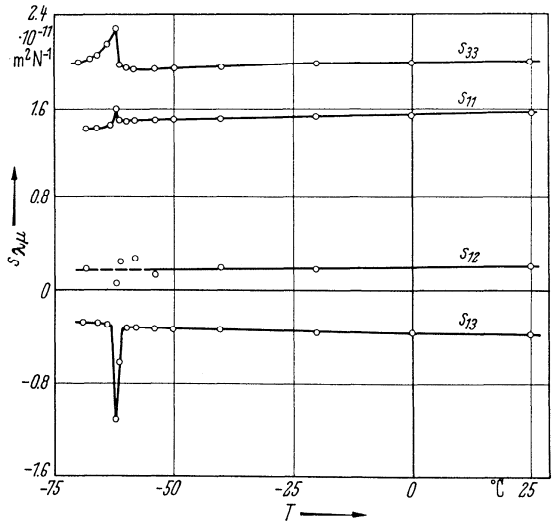

Fig. 33A-1-125. KD_2PO_4 (DKDP). $s_{\lambda\mu}$ vs. T [66Shu]. $s_{\lambda\mu}$: elastic compliance.

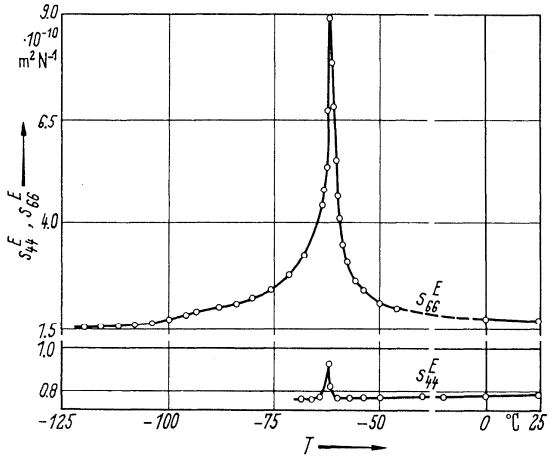

Fig. 33A-1-126. KD_2PO_4 (DKDP). s_{44}^{E}, s_{66}^{E} vs. T [66Shu].

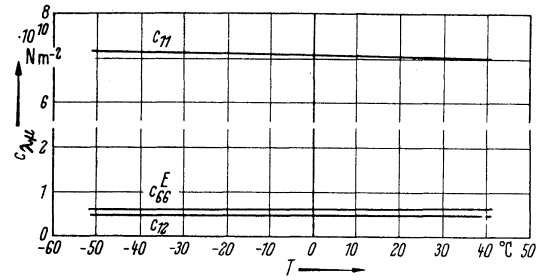

Fig. 33A-1-127. KD_2PO_4 (DKDP). $c_{\lambda\mu}$ vs. T [50Jon]. $c_{\lambda\mu}$: elastic stiffness.

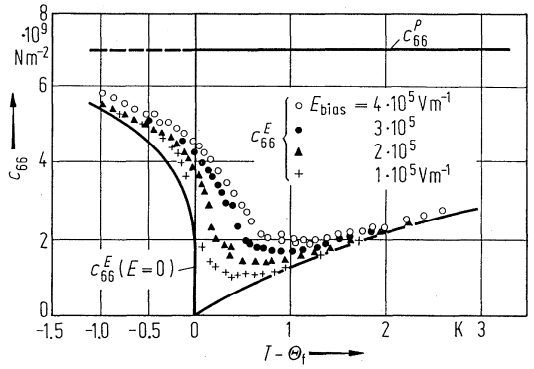

Fig. 33A-1-128. KH_2PO_4 (KDP). c_{66}^{E}, c_{66}^{P} vs. $T - \Theta_f$ [70Lit1]. Parameter: E_{bias}.

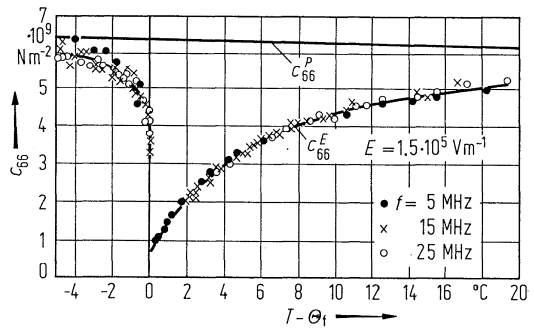

Fig. 33A-1-129. KD_2PO_4 (DKDP). c_{66}^{E}, c_{66}^{P} vs. $T - \Theta_f$ [70Lit2]. Parameter: f.

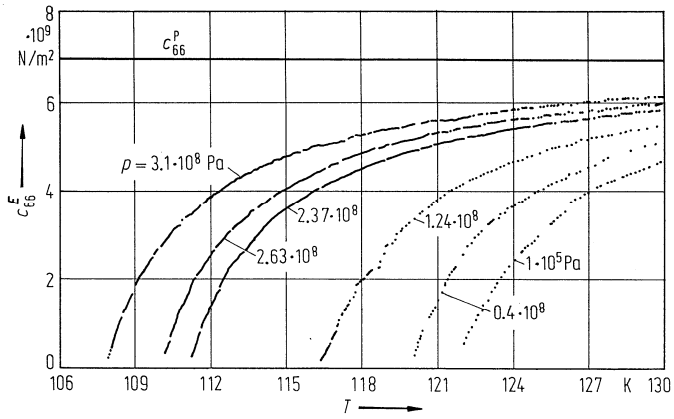

Fig. 33A-1-130. KH_2PO_4 (KDP). c_{66}^{E} vs. T [84Hik]. Parameter: p.

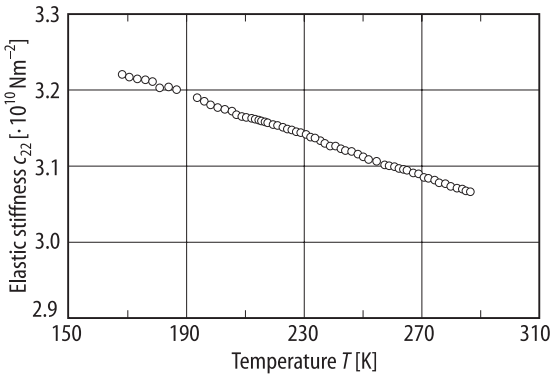

Fig. 33A-1-131. KD_2PO_4 (monoclinic). c_{22} vs. T [88Yak]. f = 10 MHz. Deuterium concentration is about 98 %.

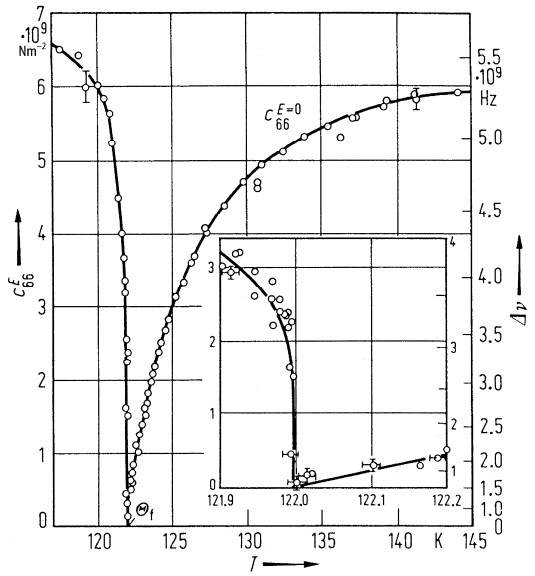

Fig. 33A-1-132. KH_2PO_4 (KDP). c_{66}^{E}, $\Delta\nu$ vs. T [68Bro]. $\Delta\nu$: Brillouin shift.

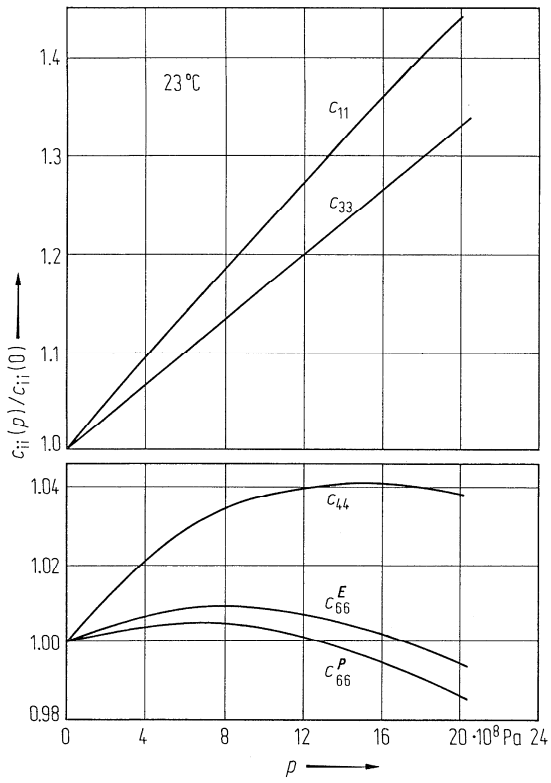

Fig. 33A-1-133. KH_2PO_4 (KDP). $c_{ii}(p)/c_{ii}(0)$ vs. p [76Fri]. $c_{ii}(p)$: elastic stiffness under hydrostatic pressure p. $T = 23$ °C.

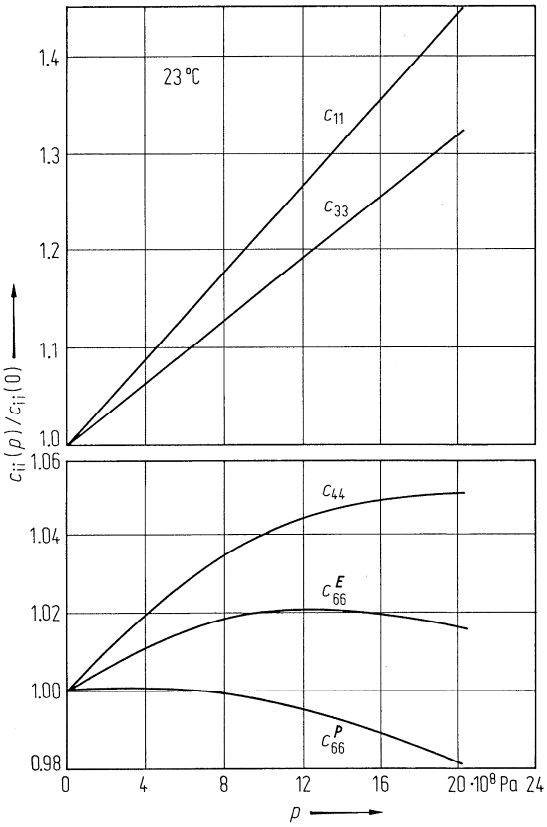

Fig. 33A-1-134. KD_2PO_4 (DKDP). $c_{ii}(p)/c_{ii}(0)$ vs. p [76Fri]. $c_{ii}(p)$: elastic stiffness under hydrostatic pressure p. $T = 23$ °C.

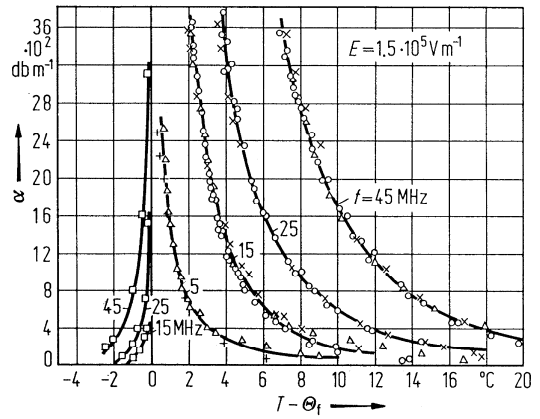

Fig. 33A-1-135. KD_2PO_4 (DKDP). α vs. $T - \Theta_f$ [70Lit2]. Parameter: f. α: attenuation coefficient of transverse ultrasonic wave propagating along the a axis with its polarization along the b axis. $E_{bias} = 1.5 \cdot 10^5$ V m^{-1} was applied along the c axis.

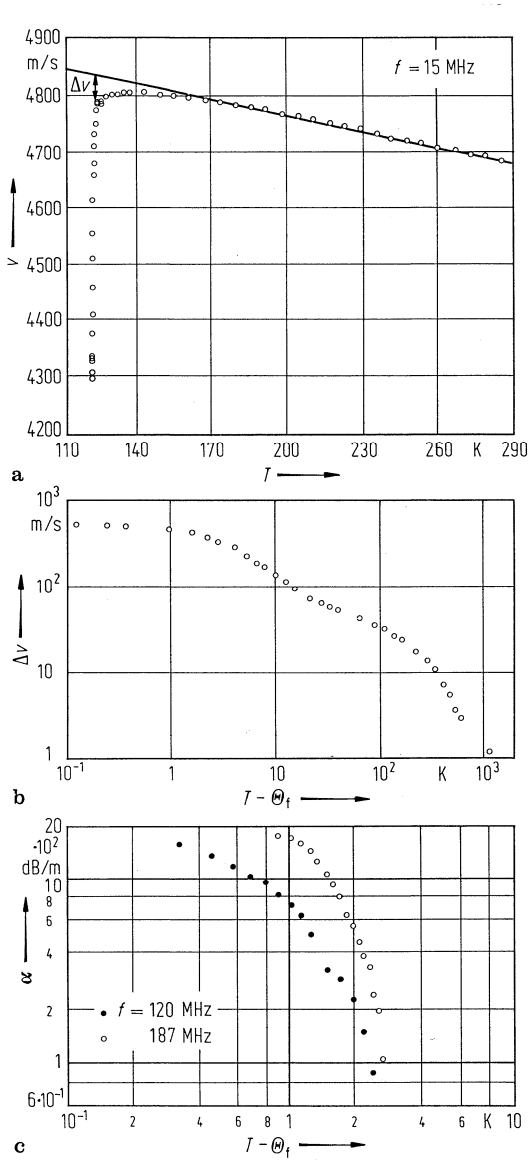

Fig. 33A-1-136. KH_2PO_4 (KDP). (**a**) Velocity v vs. T, (**b**) Δv vs. $T - \Theta_f$, and (**c**) attenuation α vs. $T - \Theta_f$ of longitudinal sound wave along the c axis [84Lae].

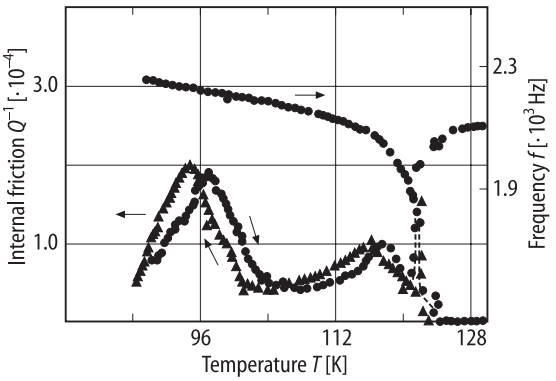

Fig. 33A-1-137. KH_2PO_4 (KDP). Q^{-1}, f vs. T [92Hua]. Q^{-1}: internal friction. f: resonant frequency.

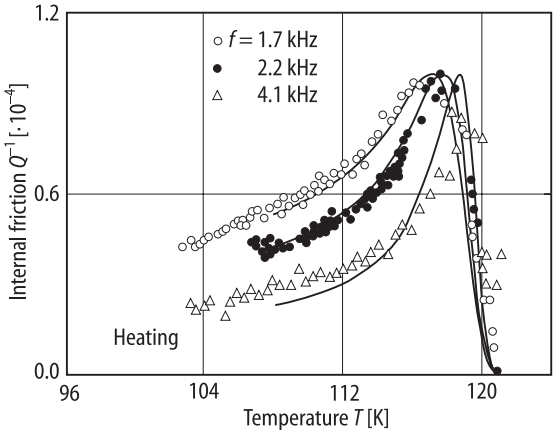

Fig. 33A-1-138. KH_2PO_4 (KDP). Q^{-1} vs. T [92Hua]. Parameter: f. Q^{-1}: internal friction. f: resonant frequency. Heating run. Full line: theoretical curve of monodispersive formula with relaxation time $\tau = A_0 \exp[-B/(\Theta_f - T)]$, where A_0 and B are constants independent of temperature.

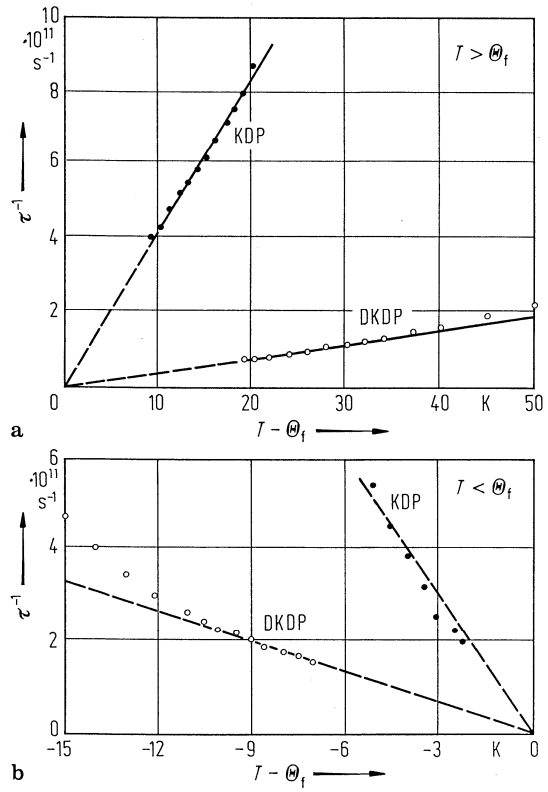

Fig. 33A-1-139. KH_2PO_4 (KDP), KD_2PO_4 (DKDP). τ^{-1} vs. $T - \Theta_f$ [80Vaj]. (**a**) $T > \Theta_f$, (**b**) $T < \Theta_f$. τ: polarization relaxation time by ultrasonic measurements at $f = 60\ldots500$ MHz.

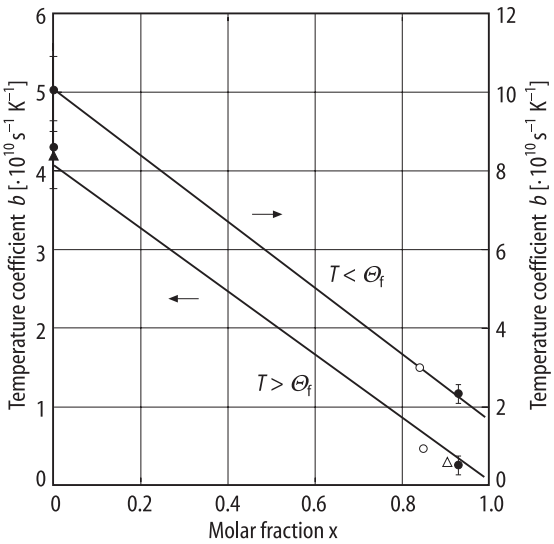

Fig. 33A-1-140. $KH_{2(1-x)}D_{2x}PO_4$. b vs. x [80Vaj]. b: coefficient given in the expression $\tau^{-1} = b\,|T - \Theta_f|$. τ: polarization relaxation time determined by ultrasonic measurements at $f = 60\ldots500$ MHz. Different symbols are from different authors. Full circle: [80Vaj]; open triangle: [63Hil]; open circle: [70Lit2]; full triangle: [69Gar].

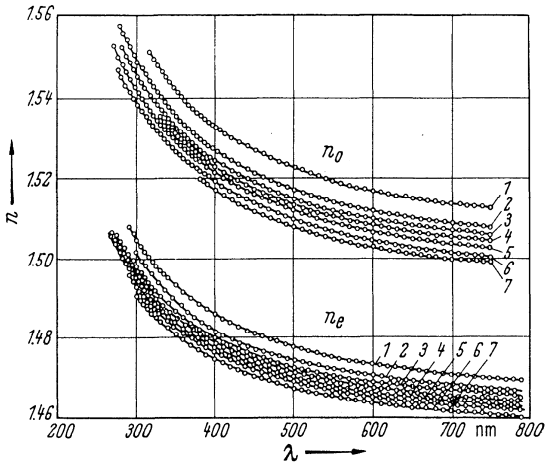

Fig. 33A-1-141. KH_2PO_4 (KDP). n_o, n_e vs. λ [66Vis]. Parameter: *T*. Curve *1*: *T* = –196 °C, *2*: –50 °C, *3*: +20 °C, *4*: +64 °C, *5*: +100 °C, *6*: +150 °C, *7*: +200 °C.

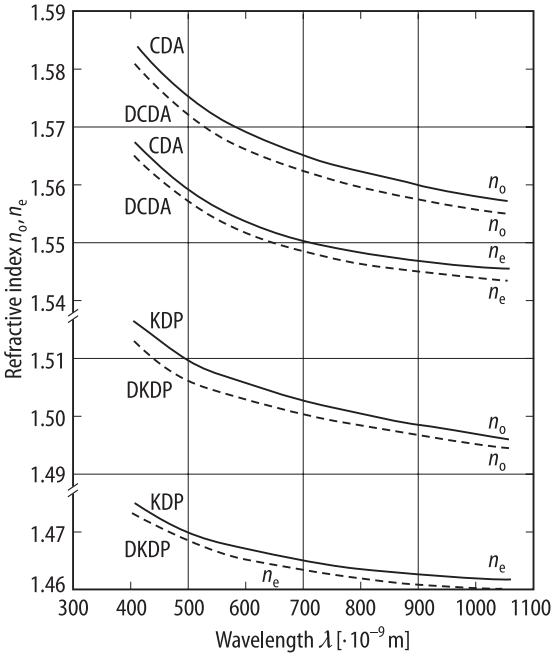

Fig. 33A-1-142. KH_2PO_4 (KDP), KD_2PO_4 (DKDP), CsH_2AsO_4 (CDA), CsD_2AsO_4 (DCDA). n_o, n_e vs. λ [87Kir]. *T* = 33 °C.

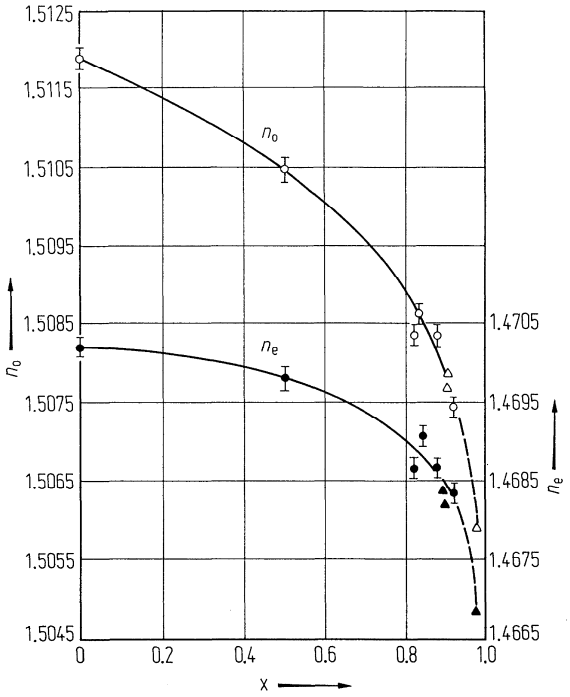

Fig. 33A-1-143. $KH_{2(1-x)}D_{2x}PO_4$. n_o, n_e vs. x [75Vlo]. $\lambda = 546.1$ nm. Open and full triangles are from literature.

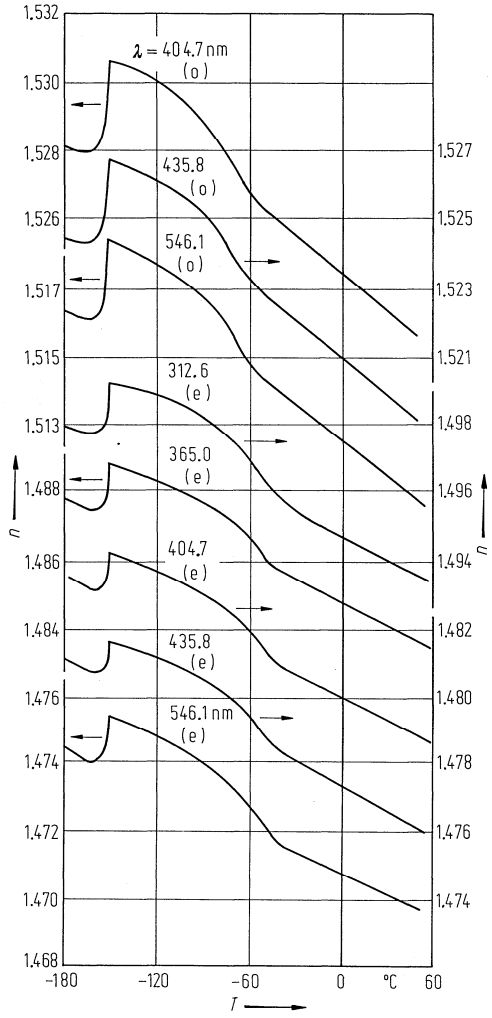

Fig. 33A-1-144. KH_2PO_4 (KDP). n vs. T [81Ona]. Parameter: λ. o: ordinary light. e: extraordinary light. Heating run.

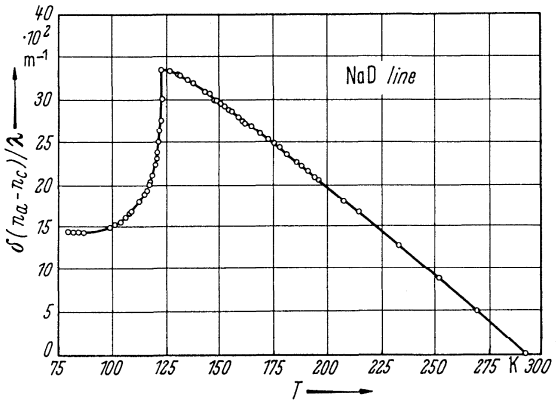

Fig. 33A-1-145. KH_2PO_4 (KDP). $\delta(n_a - n_c)/\lambda$ vs. T [44Zwi].

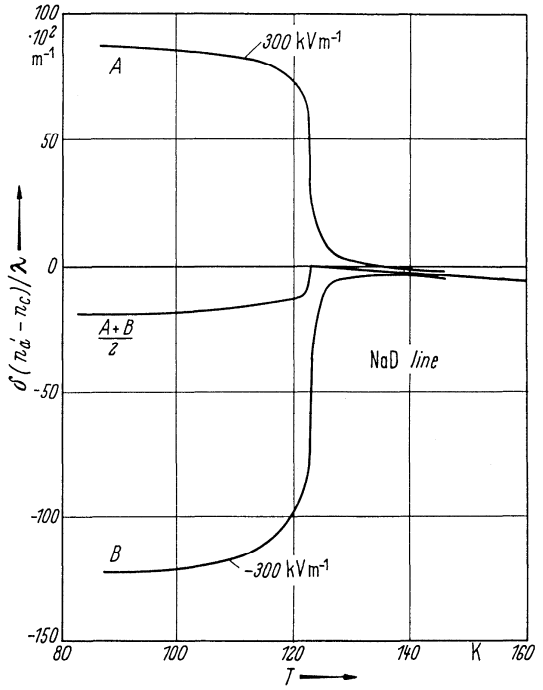

Fig. 33A-1-146. KH_2PO_4 (KDP). $\delta(n'_a - n_c)/\lambda$ vs. T at biasing field E_3 = 300 kV m^{-1} [44Zwi]. n'_a, n_c : refractive indices along [110], [001]. E_3: electric field || ***c***.

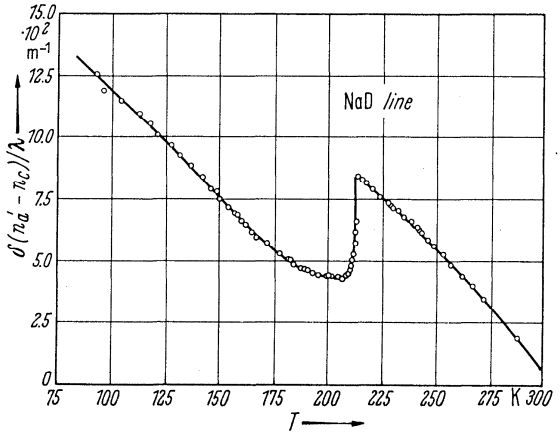

Fig. 33A-1-147. KD_2PO_4 (DKDP). $\delta(n'_a - n_c)/\lambda$ vs. T [44Zwi]. n'_a, n_c : refractive indices along [110], [001].

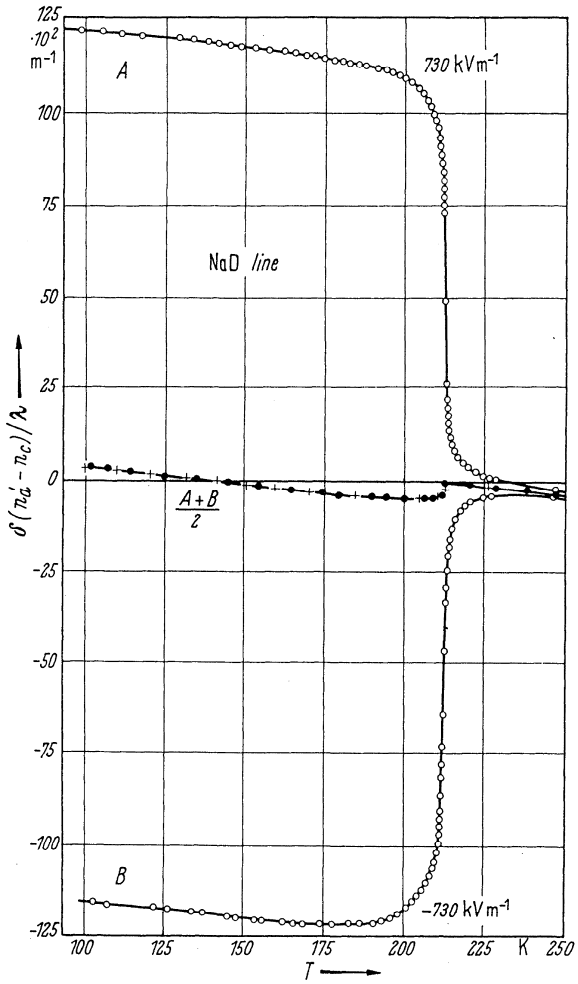

Fig. 33A-1-148. KD_2PO_4 (DKDP). $\delta(n'_a - n_c)/\lambda$ vs. T at biasing field E_3 = 730 kV m^{-1} [44Zwi]. n'_a, n_c : refractive indices along [110], [001]. E_3: electric field || ***c***.

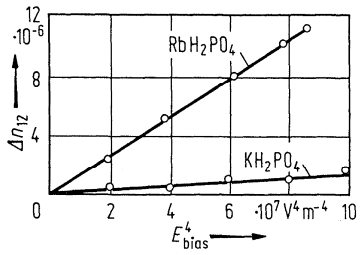

Fig. 33A-1-149. KH_2PO_4 (KDP), RbH_2PO_4 (RDP). Induced birefringence Δn_{12} vs. E^4_{bias} [69Per]. $\Delta n_{12} = |n_1 - n_2|$. λ = 540 nm, T = 25 °C.

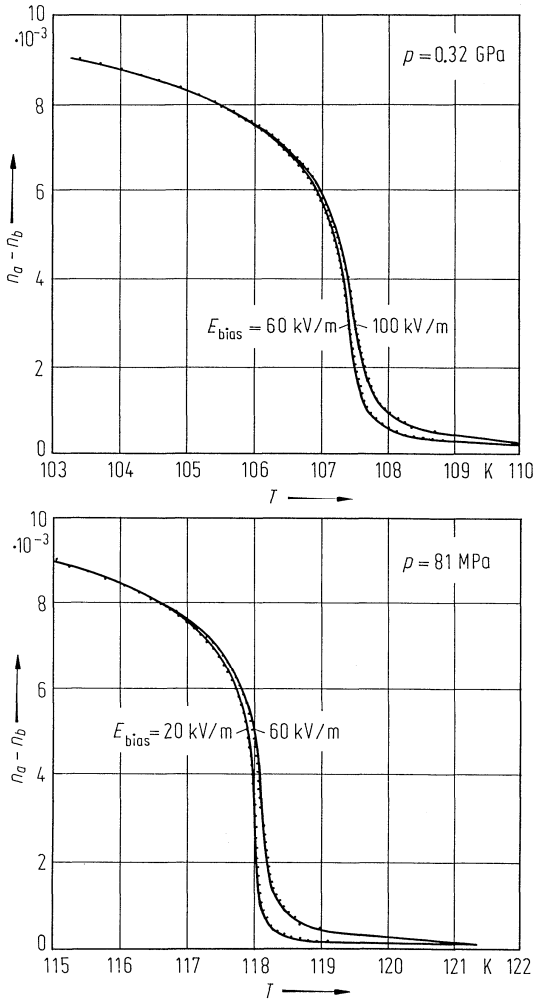

Fig. 33A-1-150. KH_2PO_4 (KDP). $n_a - n_b$ vs. T [85Tro]. Parameter: p, E_{bias}.

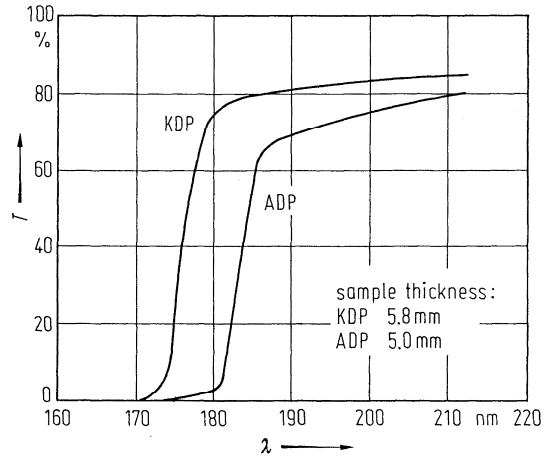

Fig. 33A-1-151. KH_2PO_4 (KDP), $NH_4H_2PO_4$ (ADP). T vs. λ [77Smi]. T: transmission in vacuum ultraviolet region. The data include losses from surface reflection.

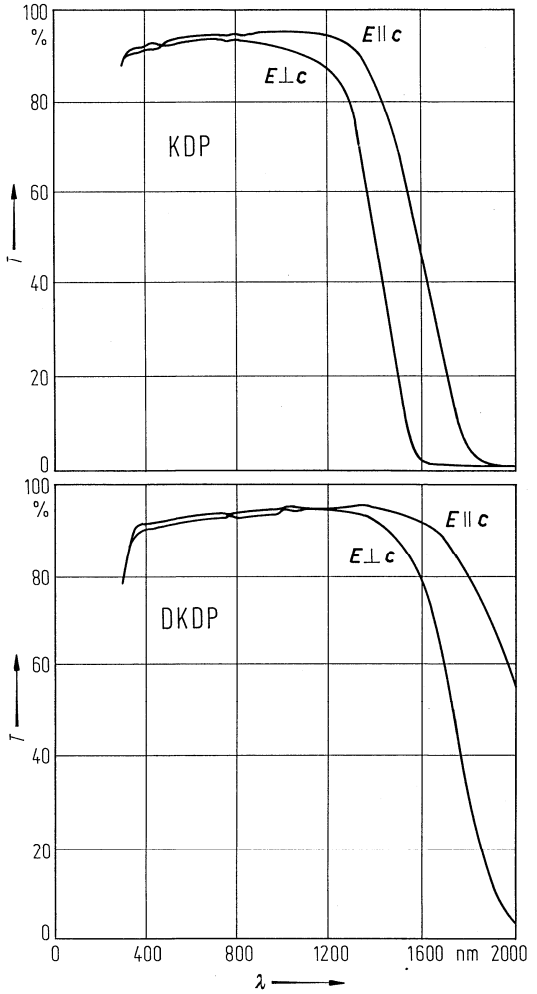

Fig. 33A-1-152. KH_2PO_4 (KDP), KD_2PO_4 (DKDP). T vs. λ [87Eim]. T: transmission. Sample thickness: 11 mm.

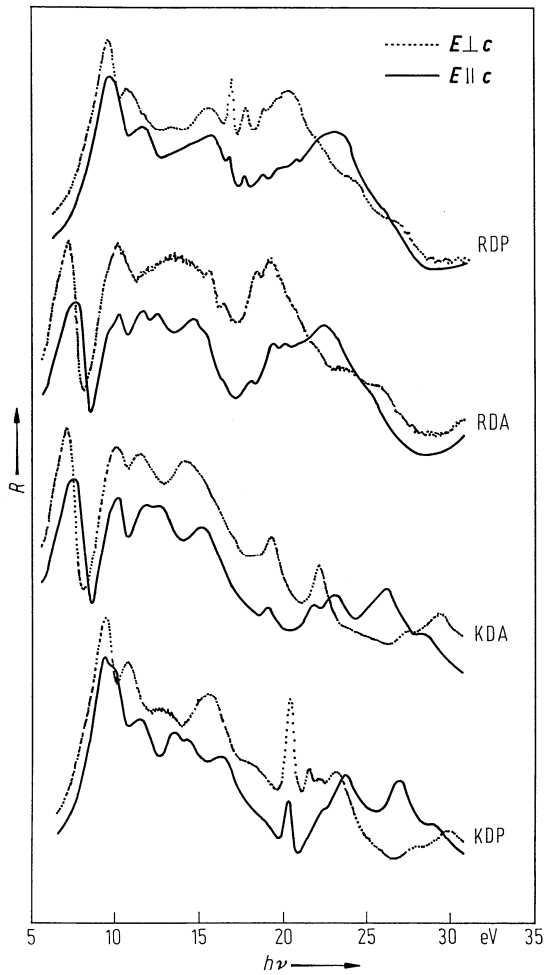

Fig. 33A-1-153. KH_2PO_4 (KDP), RbH_2PO_4 (RDP), KH_2AsO_4 (KDA), RbH_2AsO_4 (RDA). R vs. $h\nu$ [85Mat]. R: reflectivity. $h\nu$: photon energy.

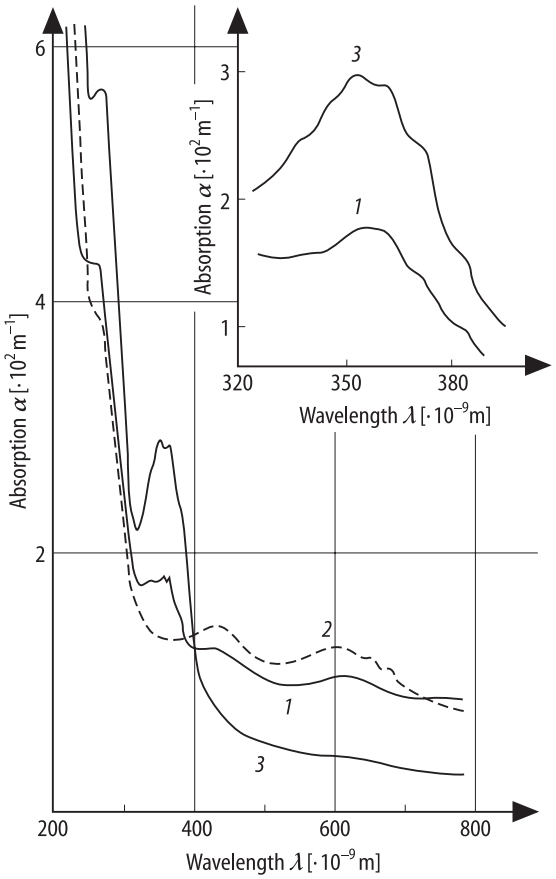

Fig. 33A-1-154. KH_2PO_4 (KDP). α vs. λ [88Aly]. α: optical absorption coefficient. λ: wavelength. *1*, *3*: sample doped with $K_2Cr_2O_7$; *2*: sample doped with $Cr_2(SO_4)_3 \cdot 6H_2O$. *1*: before X-ray irradiation; *3*: after 7 h of X-ray irradiation.

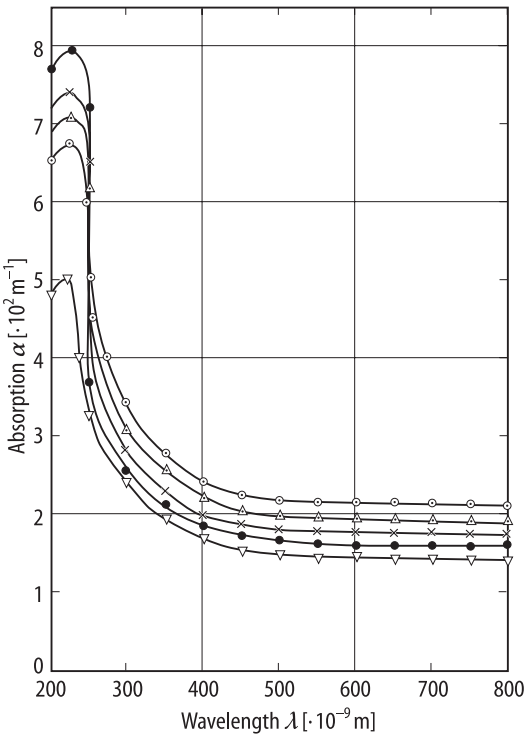

Fig. 33A-1-155. KH_2PO_4 (KDP). α vs. λ [89Rou]. α: optical absorption coefficient. T = RT. Open circle: before irradiation; open upside triangle: X-irradiation for 0.5 h; cross: X-irradiation for 1.0 h; full circle: X-irradiation for 1.5 h; open downside triangle: X-irradiaion for 2.0 h.

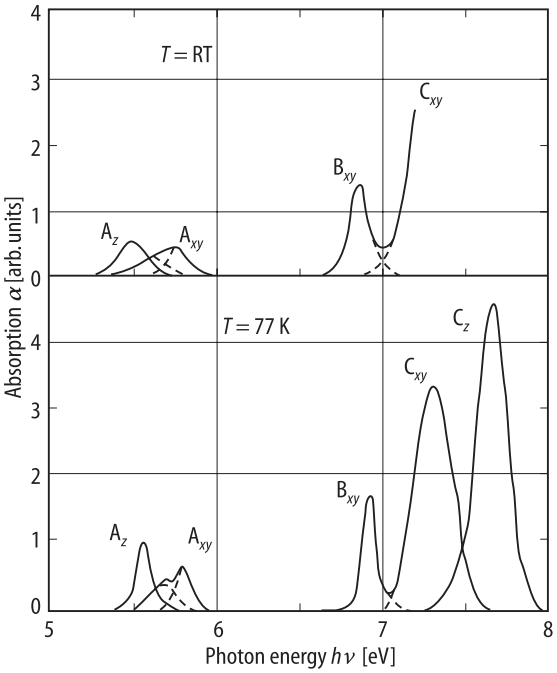

Fig. 33A-1-156. KH_2PO_4:Tl. α vs. $h\nu$ [94Fuj]. α: absorption of polarized light. $h\nu$: photon energy. A, B, C stand for corresponding absorption bands A, B, C of Tl^+ centers in alkali halides, respectively. Polarization of light is parallel (z) or perpendicular (xy) to z axis.

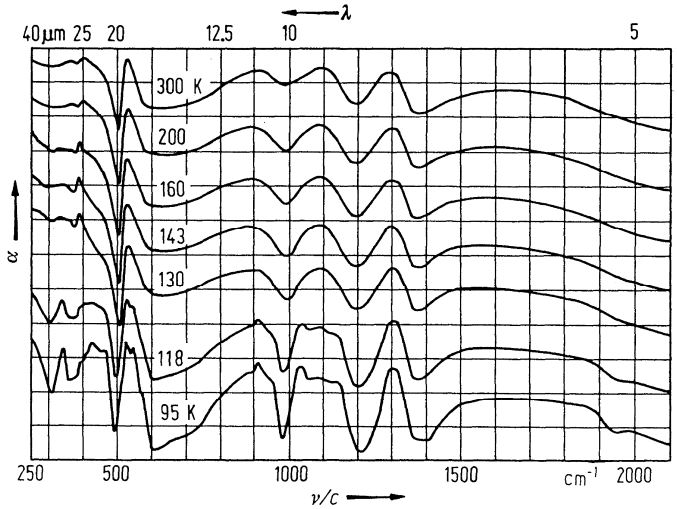

Fig. 33A-1-157. KH_2PO_4 (KDP). α vs. ν/c [70Wie]. α: infrared absorption. Parameter: T.

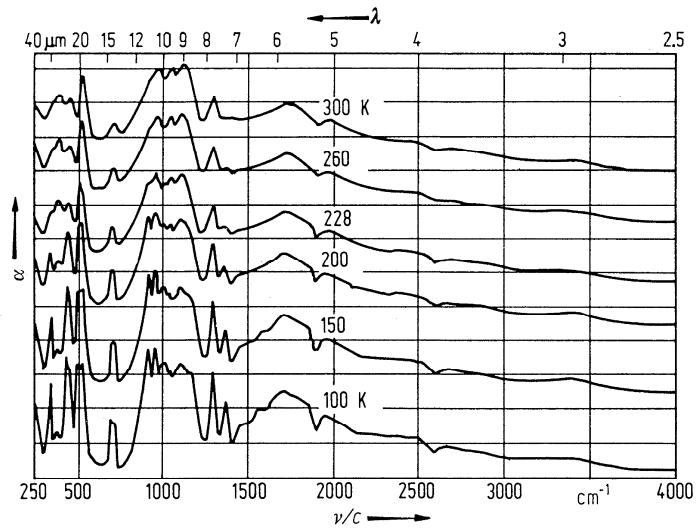

Fig. 33A-1-158. $K(H_{0.1}D_{0.9})_2PO_4$. α vs. ν/c [70Wie]. α: infrared absorption. Parameter: T.

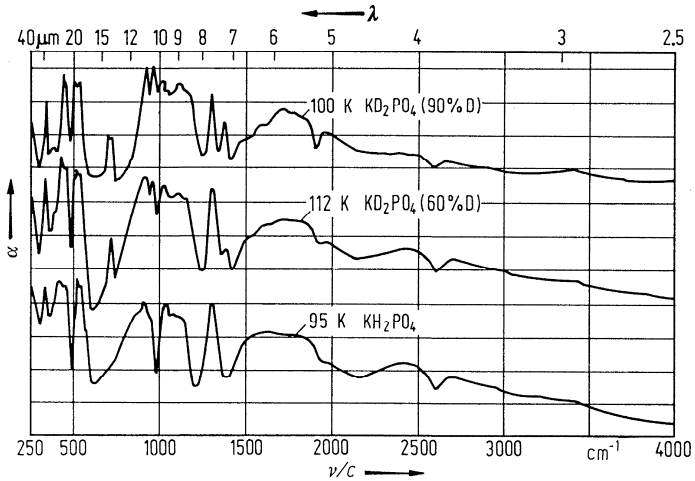

Fig. 33A-1-159. $KH_{2(1-x)}D_{2x}PO_4$. α vs. ν/c in the ferroelectric states [70Wie]. Parameter: x. α: infrared absorption.

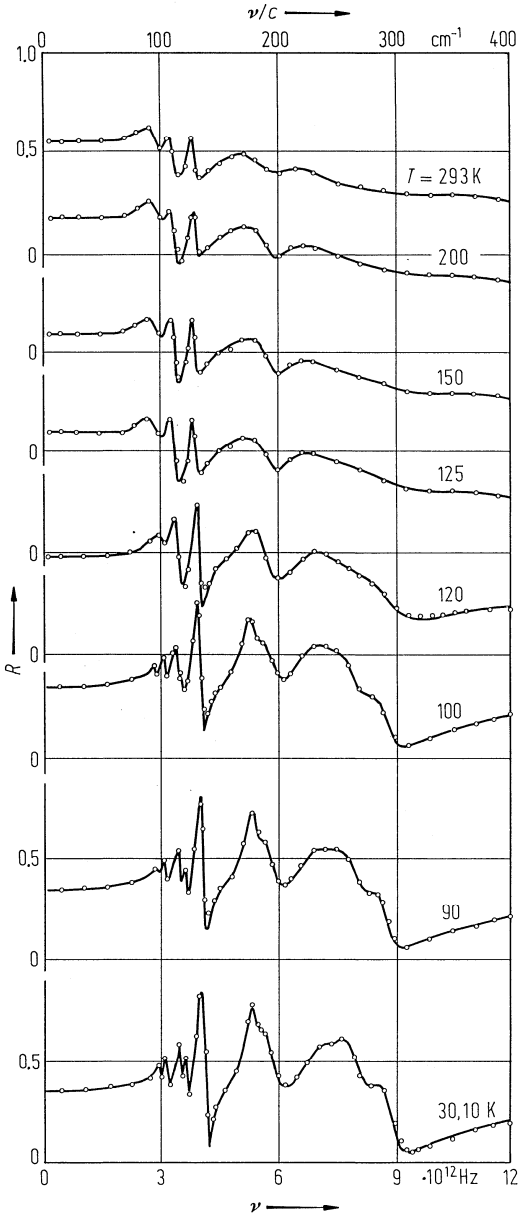

Fig. 33A-1-160. KH_2PO_4 (KDP). R vs. ν [86Wyn]. Parameter: T. R: far-infared reflectivity.

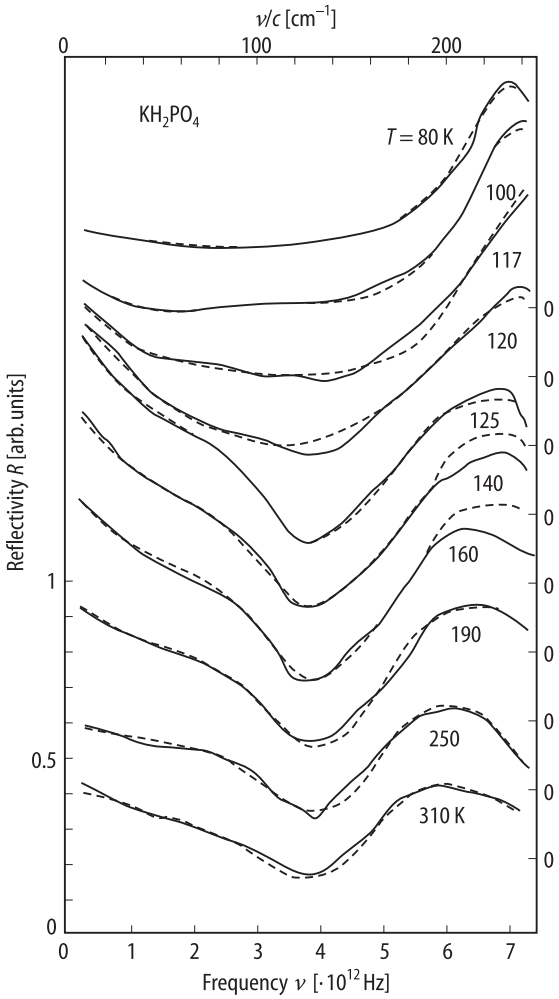

Fig. 33A-1-161. KH_2PO_4 (KDP). R vs. ν [94Shi1]. R: reflectivity of far-infrared ray with electric field parallel to the c axis. Parameter: T. Full line: measured spectra; dashed line: spectra calculated by factorized form.

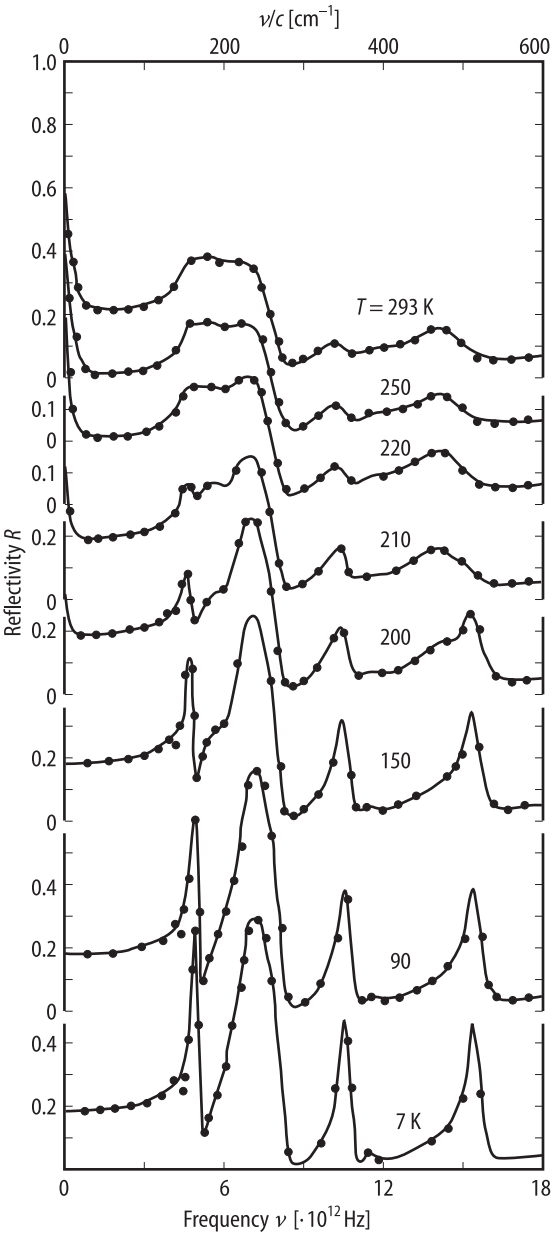

Fig. 33A-1-162. KD_2PO_4 (DKDP). R vs. ν [88Bre]. Parameter: T. R: reflectivity measured along the c axis. The data below 15 cm^{-1} are from [79Vol]. Full line: the best fit of the dielectric function of factorized form.

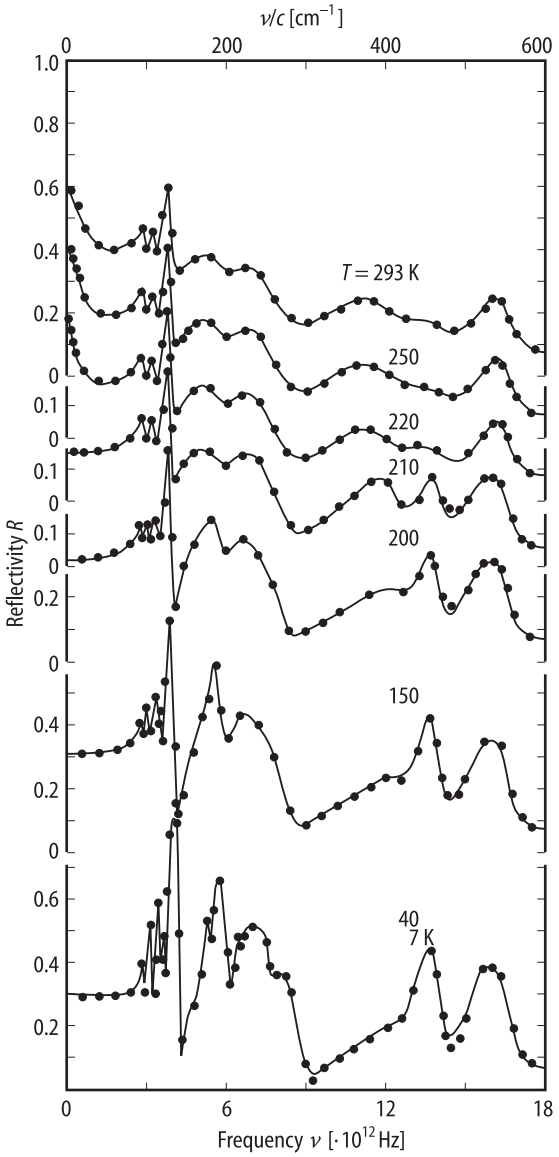

Fig. 33A-1-163. KD_2PO_4 (DKDP). R vs. ν [88Bre]. Parameter: T. R: reflectivity measured in direction perpendicular to the c axis. The data below 15 cm^{-1} are from [79Vol]. Full line: the best fit of the dielectric function of factorized form.

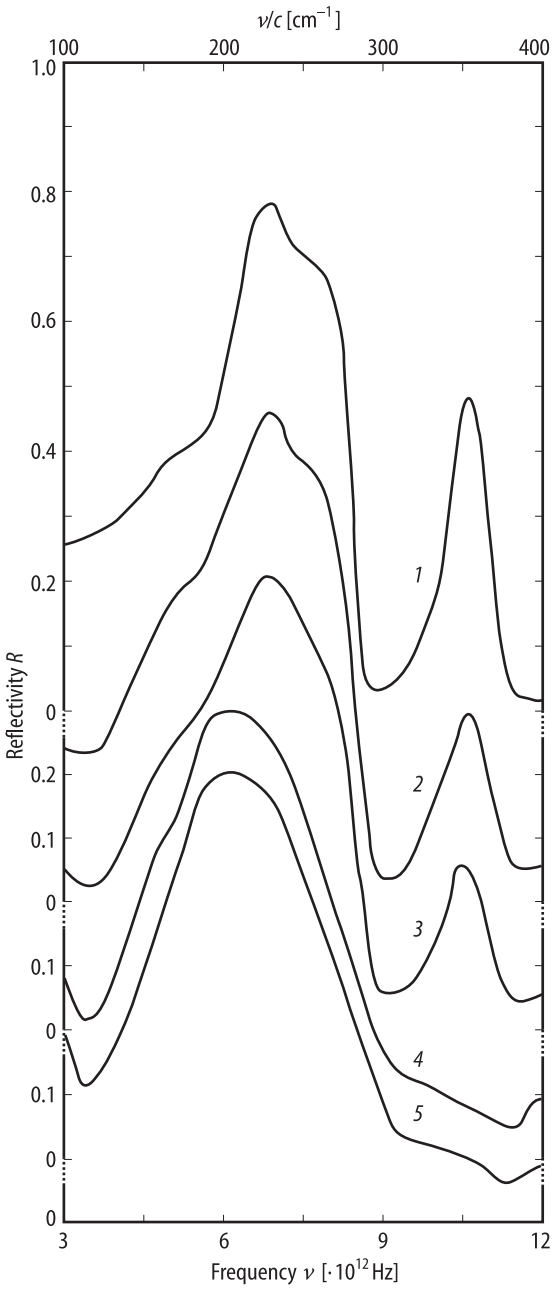

Fig. 33A-1-164. KH_2PO_4 (KDP). R vs. ν [92Bre]. Parameter: T. R: reflectivity measured along the c axis. *1*: 100 K, *2*: 115 K, *3*: 120 K, *4*: 125 K, *5*: 130 K.

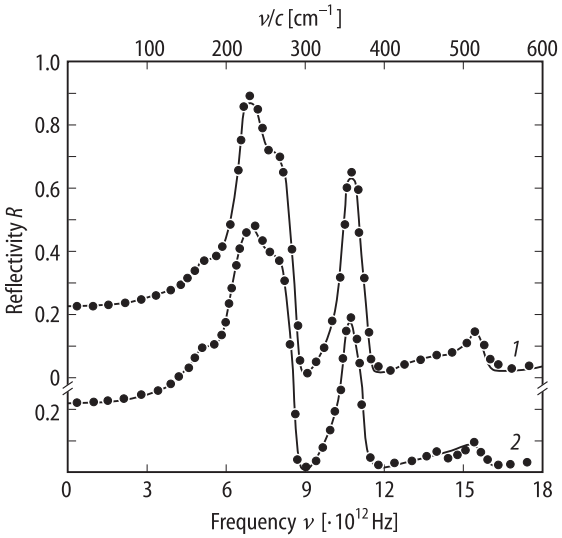

Fig. 33A-1-165. KH_2PO_4 (KDP). R vs. ν [92Bre]. Parameter: T. R: reflectivity measured along the c axis. *1*: 7 K, *2*: 100 K. Full line: the best fit of the dielectric function of factorized form.

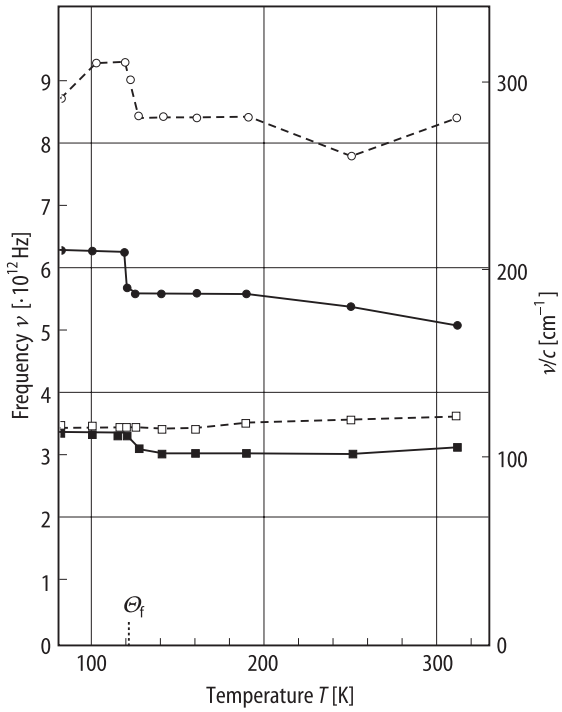

Fig. 33A-1-166. KH_2PO_4 (KDP). ν vs. T [94Shi1]. ν: optical mode frequency. Full circle, full square: TO modes; open circle, open square: LO modes.

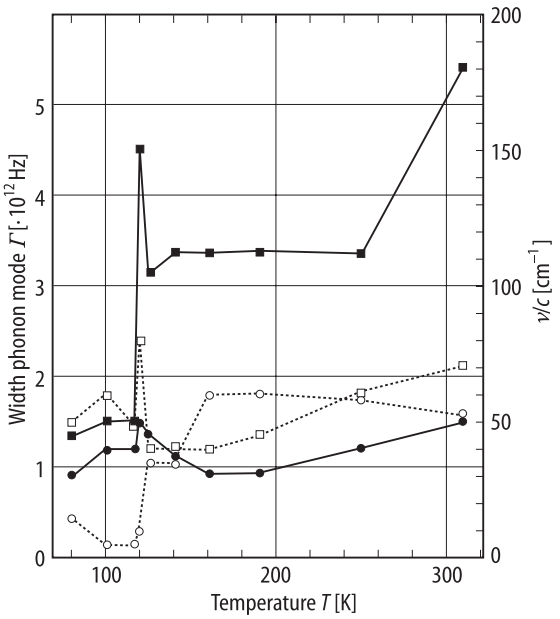

Fig. 33A-1-167. KH_2PO_4 (KDP). Γ vs. T [94Shi1]. Γ: width of the phonon mode. Full circle, full square: TO modes; open circle, open square: LO modes.

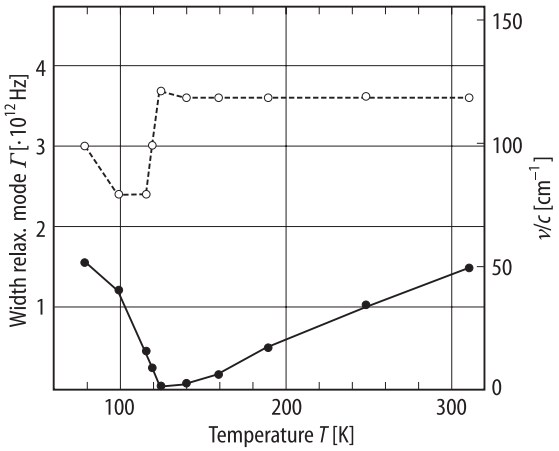

Fig. 33A-1-168. KH_2PO_4 (KDP). Γ vs. T [94Shi1]. Γ: width of the relaxational mode. Full circle: TO mode; open circle: LO mode.

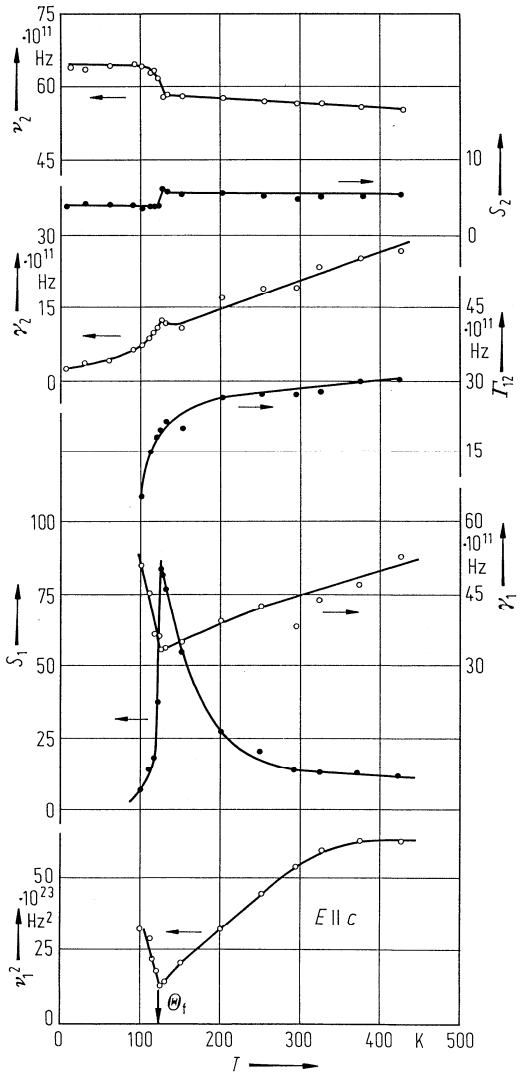

Fig. 33A-1-169. KH_2PO_4 (KDP). ν, γ, S and Γ_{12} vs. T [84ElS]. ν: frequency. γ: damping constant. S: mode strength. Γ_{12}: coupling coefficient obtained from infrared reflectivity.

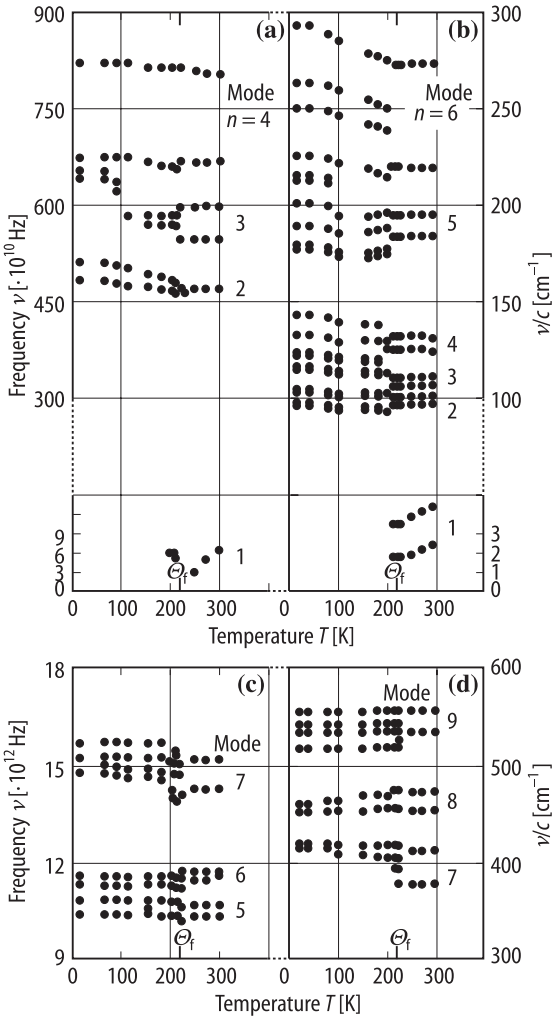

Fig. 33A-1-170. KD_2PO_4 (DKDP). ν vs. T [88Bre]. ν: frequency of infrared active mode. (**a**), (**b**) external mode, (**c**), (**d**) internal mode. (**a**), (**c**) $\boldsymbol{E} \parallel \boldsymbol{c}$. (**b**), (**d**) $\boldsymbol{E} \perp \boldsymbol{c}$. See Table 33A-1-045 for (**a**), (**c**) and Table 33A-1-046 for (**b**), (**d**) mode assignments.

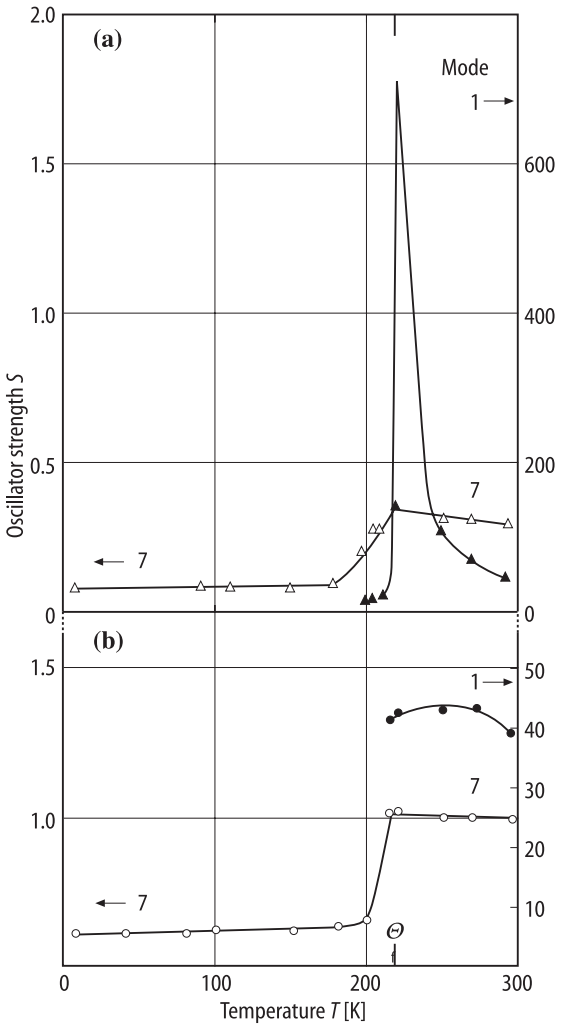

Fig. 33A-1-171. KD_2PO_4 (DKDP). *S* vs. *T* of TO mode [88Bre]. *S*: oscillator strength. (**a**) $\boldsymbol{E} \parallel \boldsymbol{c}$. (**b**) $\boldsymbol{E} \perp \boldsymbol{c}$. *1*: lowest frequency mode; *7*: 7th mode. See Fig. 33A-1-170 for the mode number.

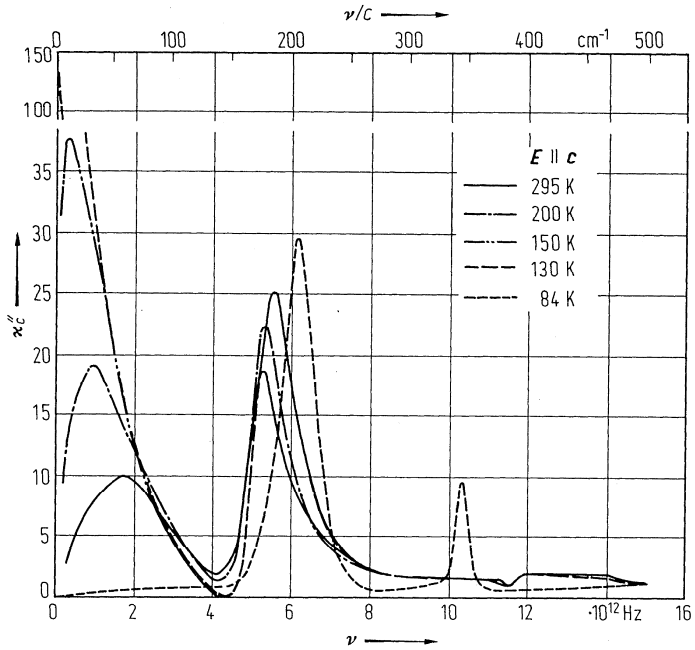

Fig. 33A-1-172. KH_2PO_4 (KDP). κ_c'' vs. ν [73Kaw]. Parameter: *T*. The curves were obtained from reflectivity data using Kramers-Kronig relation.

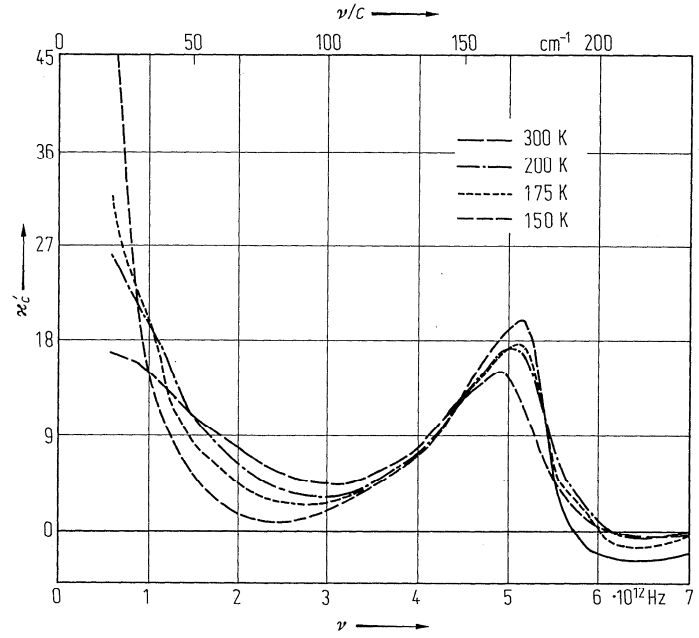

Fig. 33A-1-173. KH_2PO_4 (KDP). κ_c' vs. ν [77Led]. Parameter: *T*.

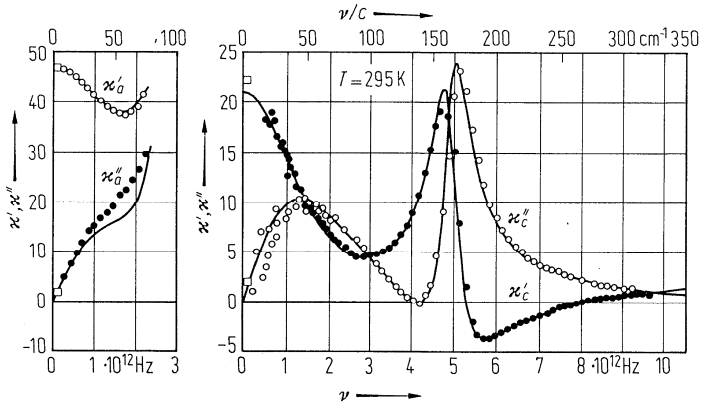

Fig. 33A-1-174. KH_2PO_4 (KDP). κ', κ'' vs. ν [75Gau]. T = 295 K. Squares: millimeter wave points. Solid line: oscillator fit.

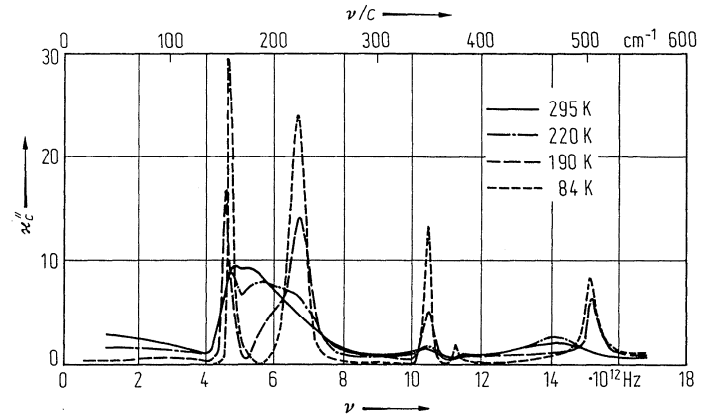

Fig. 33A-1-175. KD_2PO_4 (DKDP). κ_c'' vs. ν [74Kaw]. Parameter: T. Curves were obtained from reflectivity data using Kramers-Kronig relation.

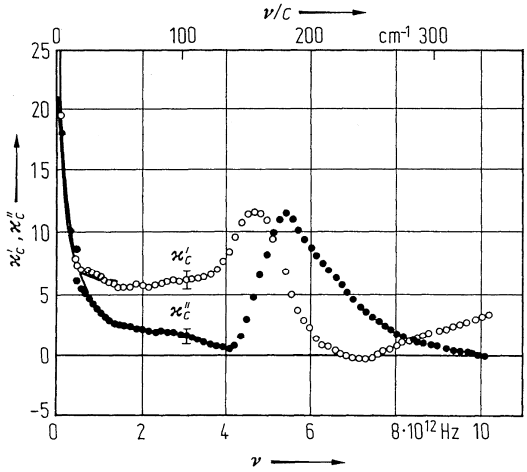

Fig. 33A-1-176. $KH_{2(1-x)}D_{2x}PO_4$ (x = 0.86). κ_c', κ_c'' vs. ν at 295 K [77Hap].

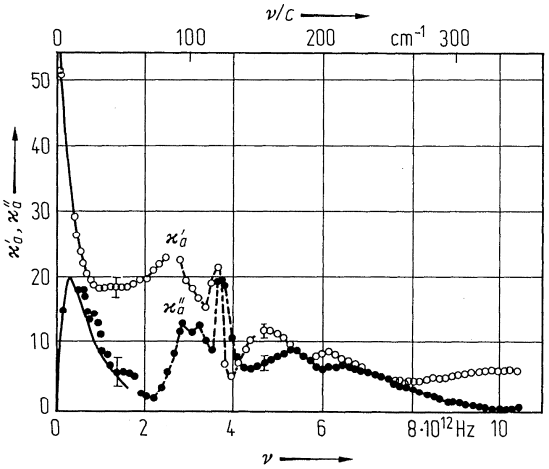

Fig. 33A-1-177. $KH_{2(1-x)}D_{2x}PO_4$ (x = 0.86). κ'_a, κ''_a vs. ν at 295 K [77Hap].

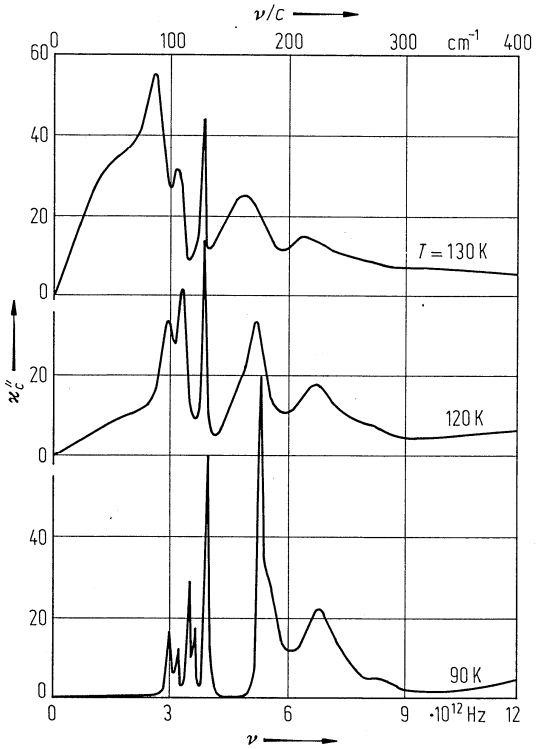

Fig. 33A-1-178. KH_2PO_4 (KDP). κ''_c vs. ν [86Wyn]. Parameter: T. κ''_c : imaginary part of complex dielectric constant along the c axis determined from the reflectivity data of Fig. 33A-1-160.

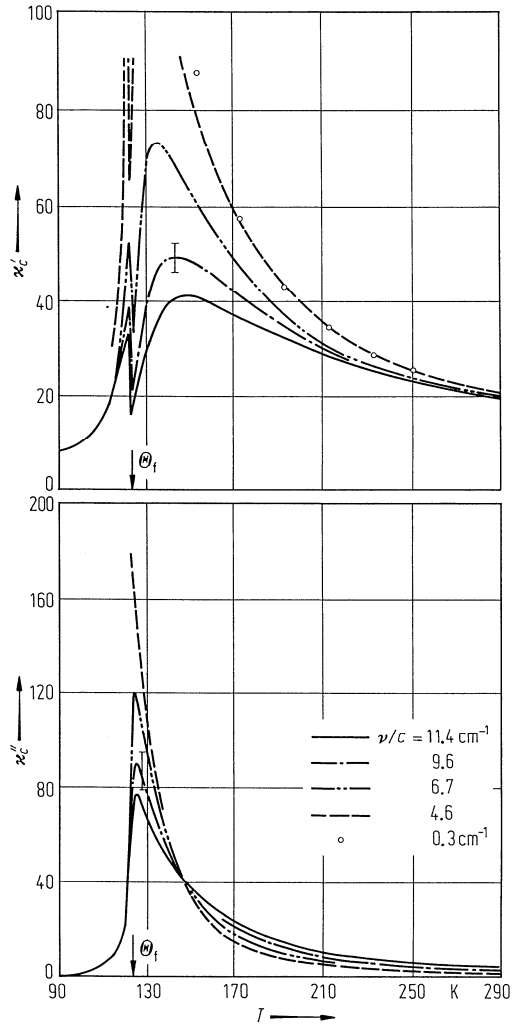

Fig. 33A-1-179. KH_2PO_4 (KDP). κ_c', κ_c'' vs. T [78Koz2]. Parameter: ν/c. Circles: data from [65Kam]. Dashed line: data from [75Gau].

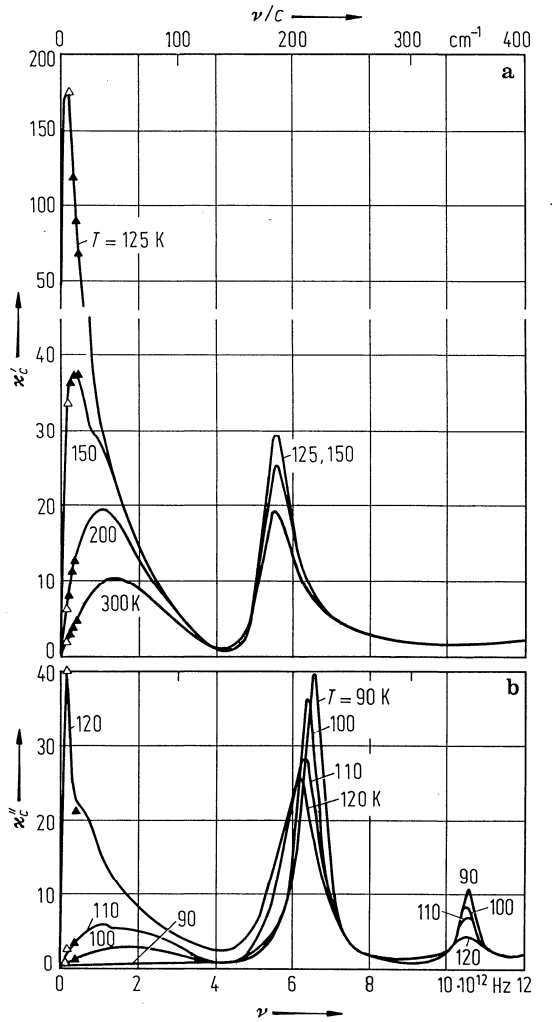

Fig. 33A-1-180. KH_2PO_4 (KDP). κ_c', κ_c'' vs. ν [85Bre]. Parameter: T. (**a**) $T > \Theta_f$, (**b**) $T < \Theta_f$. Full triangle: [78Vol]; open triangle: [75Gau].

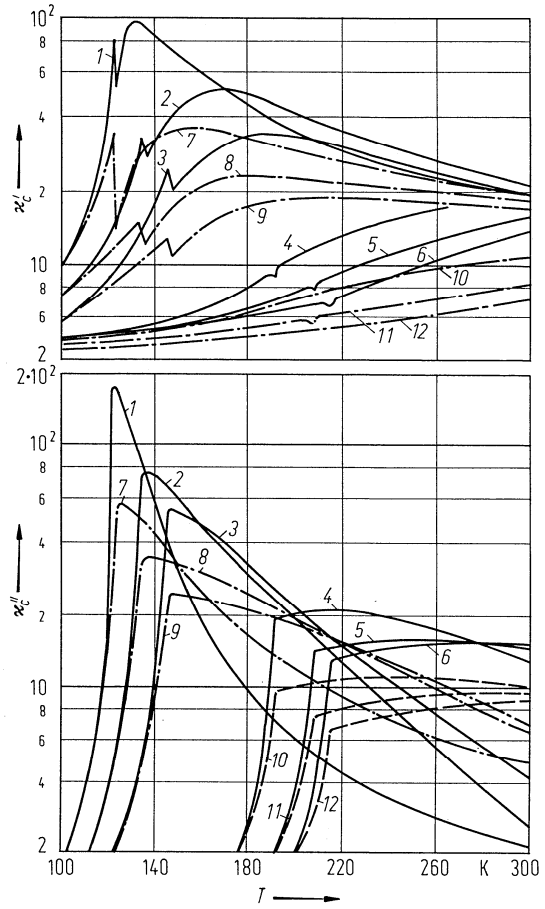

Fig. 33A-1-181. $KH_{2(1-x)}D_{2x}PO_4$. κ_c', κ_c'' vs. T [79Vol]. Parameter: x. *1*, *7*: x = 0; *2*, *8*: x = 0.15; *3*, *9*: x = 0.23; *4*, *10*: x = 0.67; *5*, *11*: x = 0.84; *6*, *12*: x = 0.93. Solid lines: 153 GHz; dashed lines: 372 GHz.

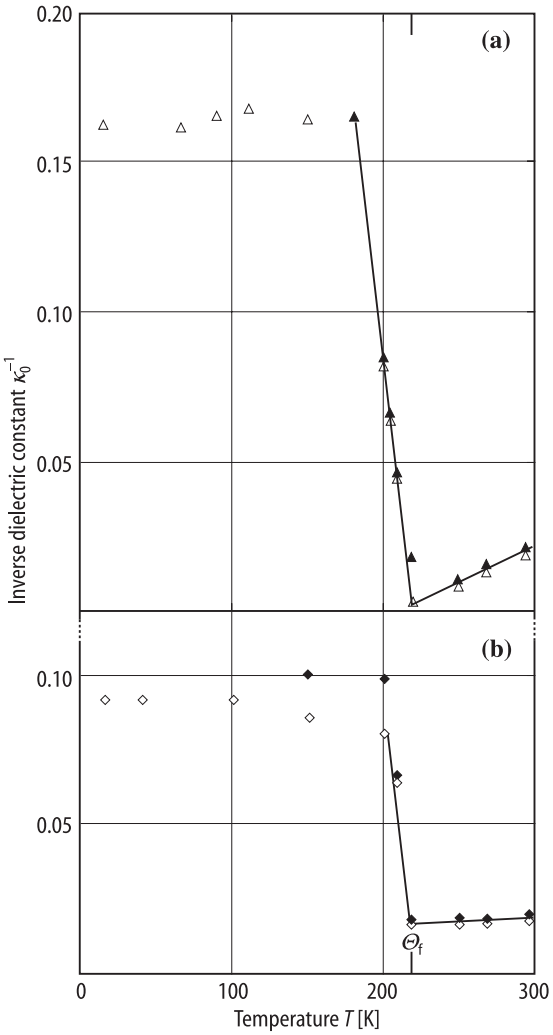

Fig. 33A-1-182. KD_2PO_4 (DKDP). $1/\kappa_0$ vs. T [88Bre]. κ_0: dielectric constant deduced from the TO mode oscillator strength (open symbols). (**a**) $\boldsymbol{E} \parallel \boldsymbol{c}$. (**b**) $\boldsymbol{E} \perp \boldsymbol{c}$. Dielectric constants determined from dielectric measurements are shown as full symbols.

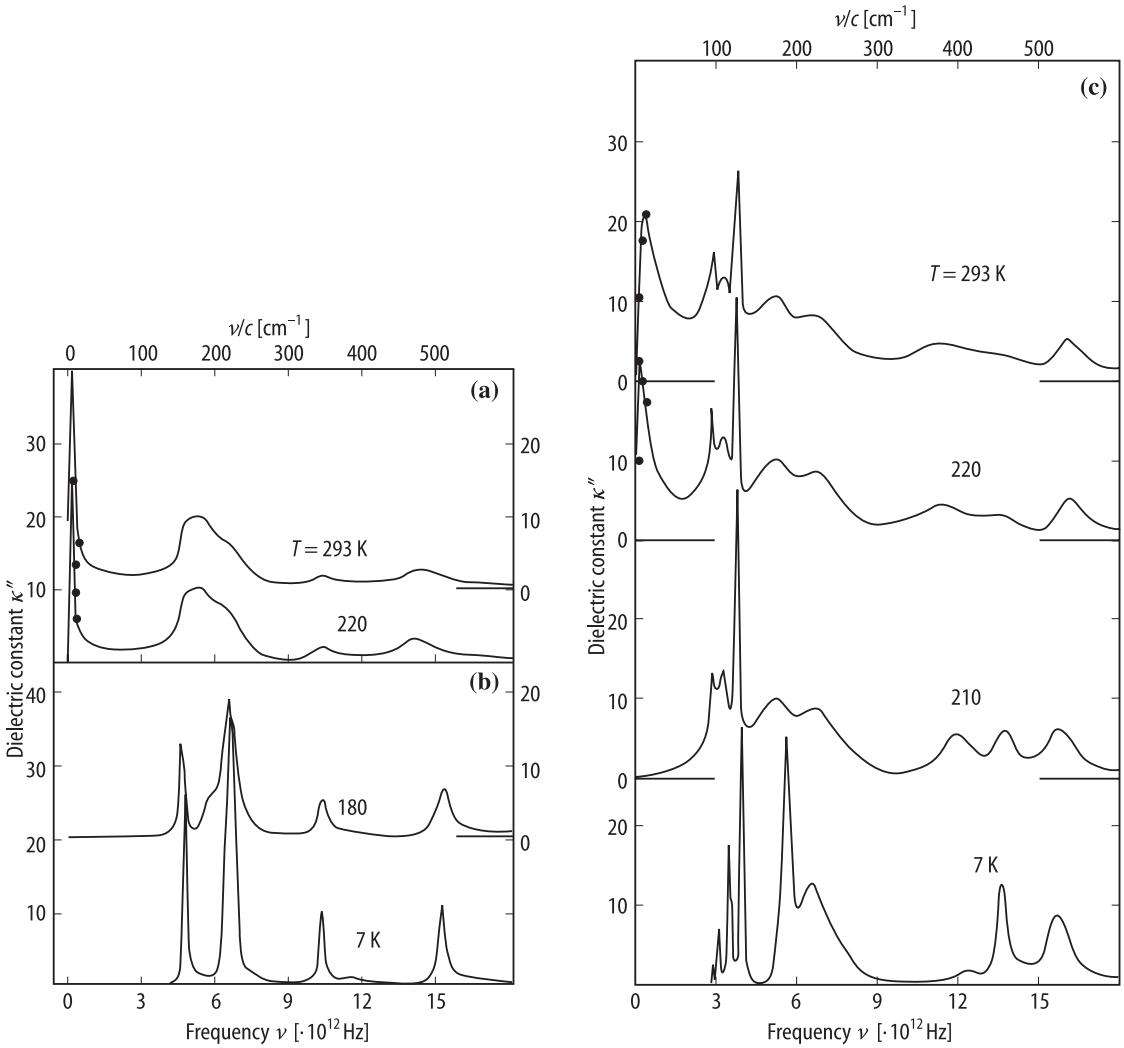

Fig. 33A-1-183. KD_2PO_4 (DKDP). κ'' vs. ν [88Bre]. Parameter: T. κ'': dielectric loss deduced from far-infrared reflectivity. (**a**), (**b**) $\boldsymbol{E} \parallel \boldsymbol{c}$; (**c**) $\boldsymbol{E} \perp \boldsymbol{c}$.

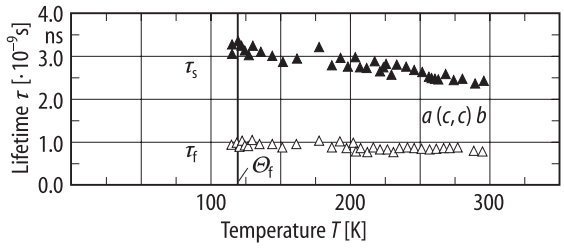

Fig. 33A-1-184. KH_2PO_4 (KDP). τ_s, τ_f vs. T [94Shi2]. τ_s, τ_f: slow and fast components of fluorescence life time, respectively.

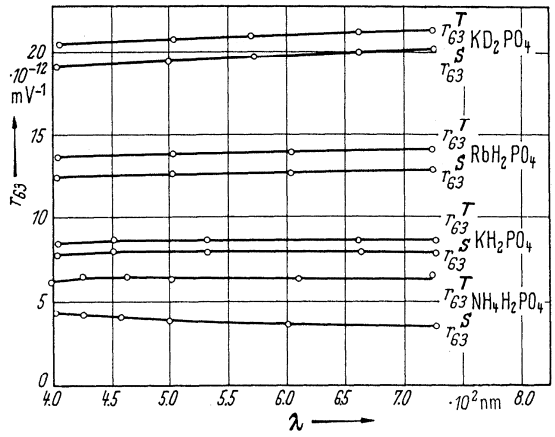

Fig. 33A-1-185. KH_2PO_4 (KDP), KD_2PO_4 (DKDP), RbH_2PO_4 (RDP), $NH_4H_2PO_4$ (ADP). r_{63} vs. λ [66Vas].

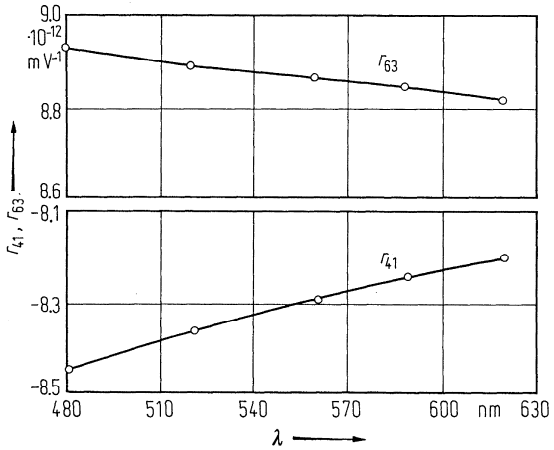

Fig. 33A-1-186. KH_2PO_4 (KDP). r_{41}, r_{63} vs. λ [78Vee].

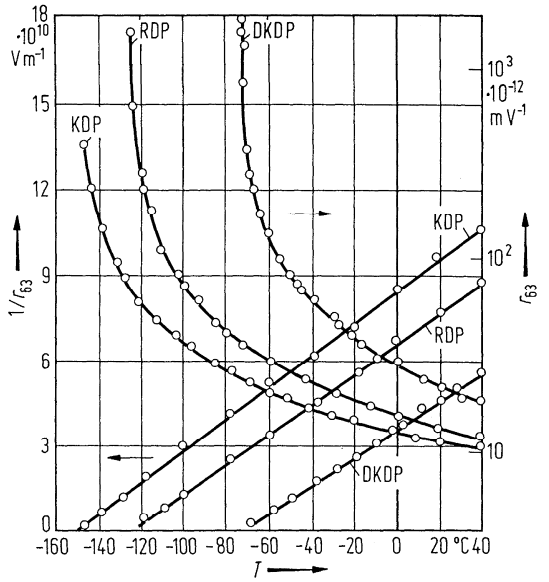

Fig. 33A-1-187. KH_2PO_4 (KDP), KD_2PO_4 (DKDP), RbH_2PO_4 (RDP). r_{63}, $1/r_{63}$ vs. T [71Vas]. r_{63}: electrooptic constant for E.

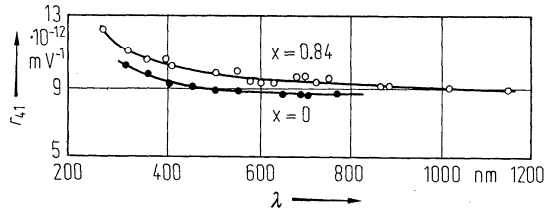

Fig. 33A-1-188. $KH_{2(1-x)}D_{2x}PO_4$. r_{41} vs. λ [75Vlo]. Parameter: x.

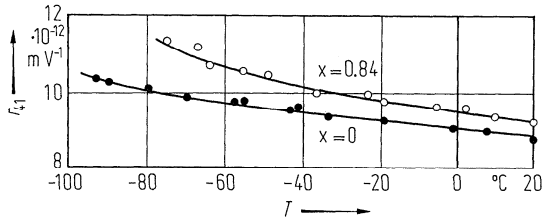

Fig. 33A-1-189. $KH_{2(1-x)}D_{2x}PO_4$. r_{41} vs. T [75Vlo]. Parameter: x. $\lambda = 633$ nm.

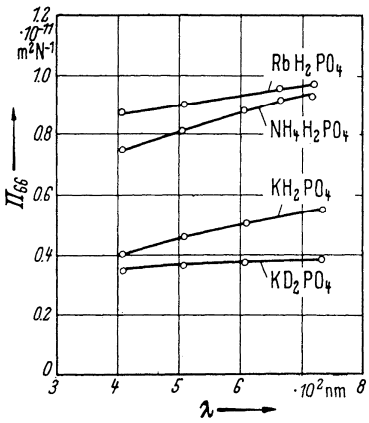

Fig. 33A-1-190. KH_2PO_4 (KDP), KD_2PO_4 (DKDP), RbH_2PO_4 (RDP), $NH_4H_2PO_4$ (ADP). Π_{66} vs. λ [66Vas]. Π_{66}: piezooptic constant.

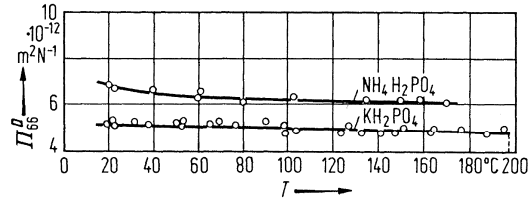

Fig. 33A-1-191. KH_2PO_4 (KDP), $NH_4H_2PO_4$ (ADP). $\Pi_{66}^{\boldsymbol{D}}$ vs. T [71Vlo]. $\Pi_{66}^{\boldsymbol{D}}$: piezooptic constant for **T** at constant ***D***. $\lambda = 450$ nm.

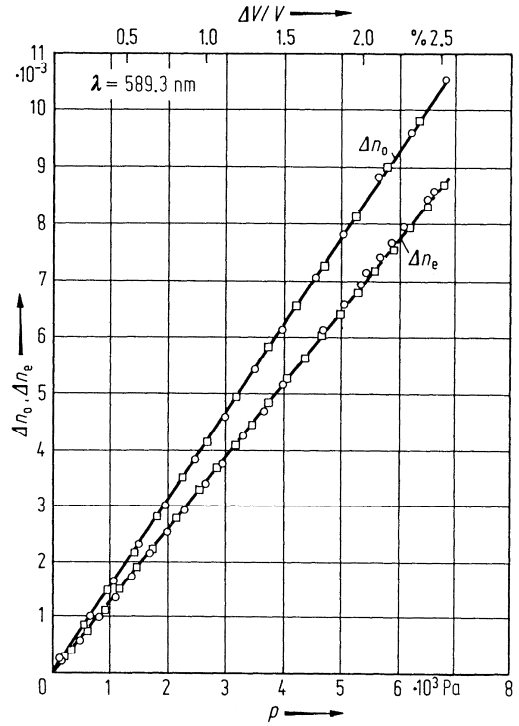

Fig. 33A-1-192. KH_2PO_4 (KDP). Δn_o, Δn_e vs. p [68Dav]. $\Delta n_o = n_o(p) - n_o(0)$, $\Delta n_e = n_e(p) - n_e(0)$. $T = 22$ °C.

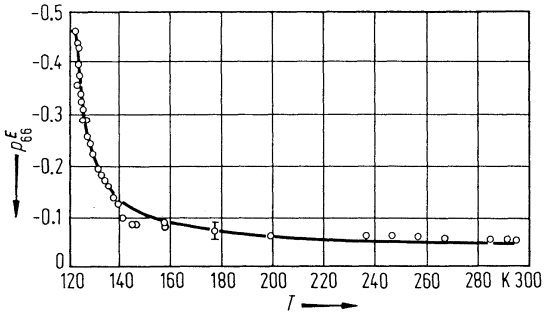

Fig. 33A-1-193. KH_2PO_4 (KDP). $p_{66}^{\boldsymbol{E}}$ vs. T [69Bro]. $p_{66}^{\boldsymbol{E}}$: piezooptic constant for **S** at constant $\boldsymbol{E}$, obtained from Brillouin scattering spectra. $\lambda = 633$ nm.

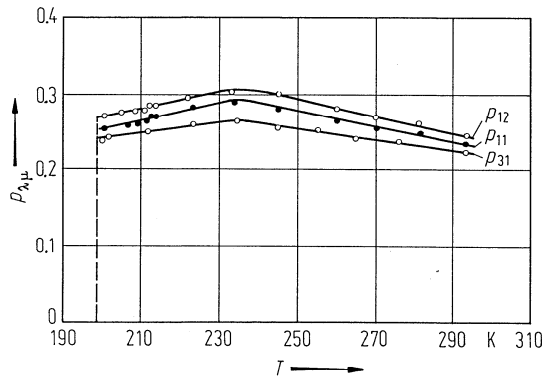

Fig. 33A-1-194. KD_2PO_4 (DKDP). $p_{\lambda\mu}$ vs. T [87Str]. $p_{\lambda\mu}$: piezooptic constant for **S**. $\lambda = 632.8$ nm.

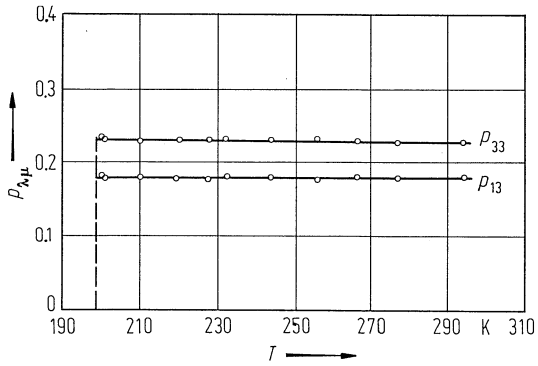

Fig. 33A-1-195. KD_2PO_4(DKDP). $p_{\lambda\mu}$ vs. T [87Str]. $p_{\lambda\mu}$: piezooptic constant for **S**. $\lambda = 632.8$ nm.

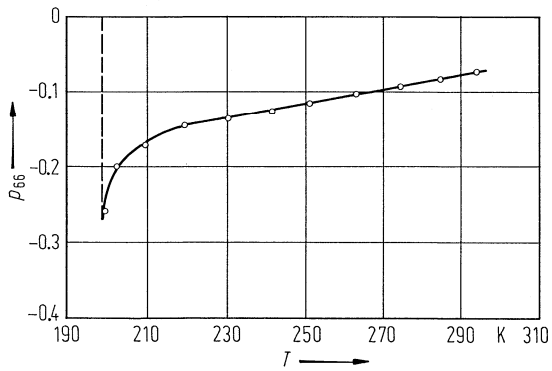

Fig. 33A-1-196. KD_2PO_4 (DKDP). p_{66} vs. T [87Str]. λ = 632.8 nm.

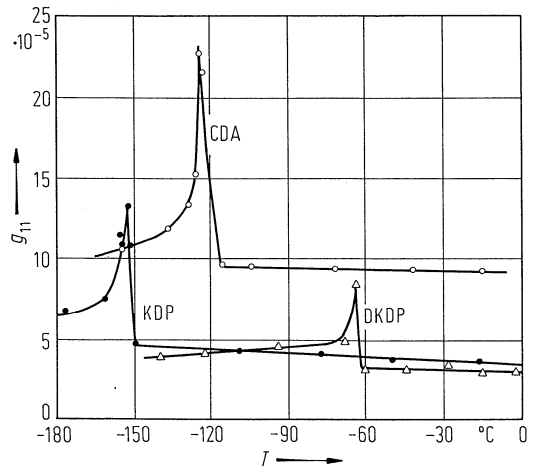

Fig. 33A-1-197. KH_2PO_4 (KDP), $KH_{2(1-x)}D_{2x}PO_4$ (x = 0.89), CsH_2AsO_4 (CDA). g_{11} vs. T [86Vlo]. g_{11}: gyration tensor component. λ = 632.8 nm.

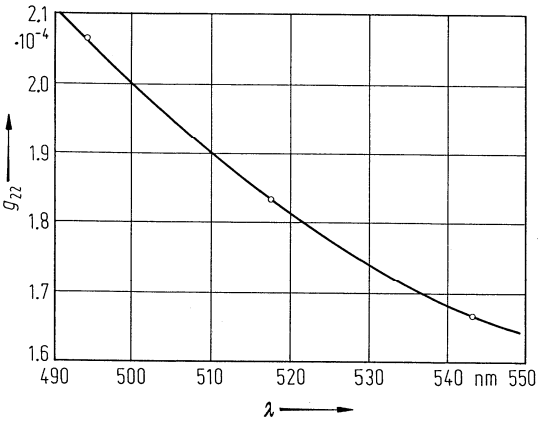

Fig. 33A-1-198. KD_2PO_4 (DKDP). g_{22} vs. λ [80Kos]. g_{22}: gyration tensor component. T = 20 °C.

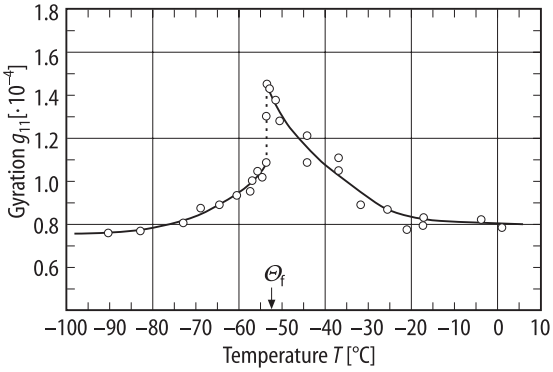

Fig. 33A-1-199. KD_2PO_4 (DKDP). g_{11} vs. T [89Tak]. g_{11}: gyration tensor component.

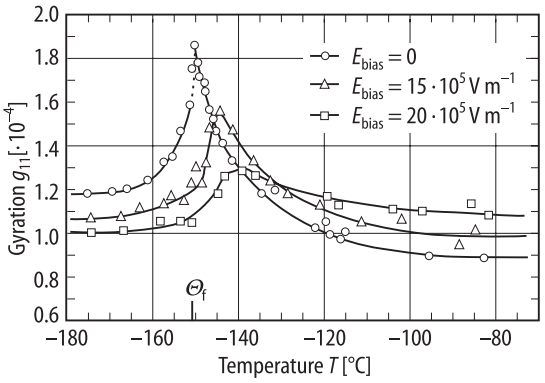

Fig. 33A-1-200. KH_2PO_4 (KDP). g_{11} vs. T [89Tak]. Parameter: E_{bias}. g_{11}: gyration tensor component.

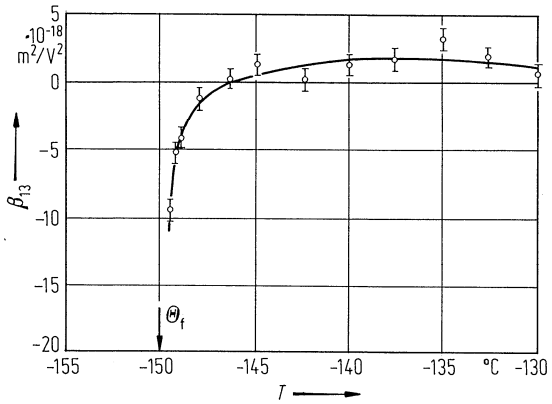

Fig. 33A-1-201. KH_2PO_4 (KDP). β_{13} vs. T [79Ues]. β_{13}: quadratic electrogyration coefficient for E. $\lambda = 535.9$ nm.

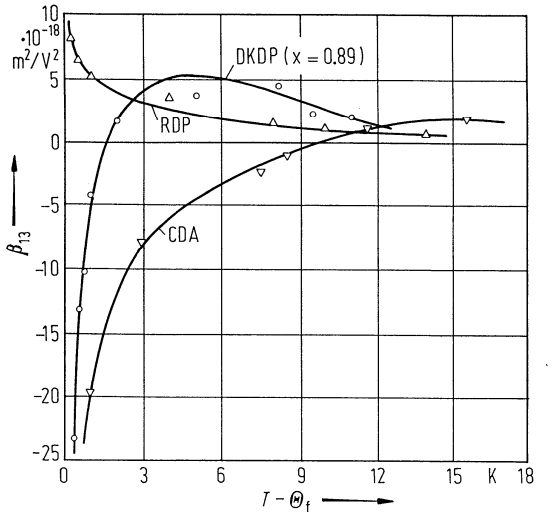

Fig. 33A-1-202. $KH_{2(1-x)}D_{2x}PO_4$ (x = 0.89), RbH_2PO_4 (RDP), CsH_2AsO_4 (CDA). β_{13} vs. $T - \Theta_f$ [86Vlo]. β_{13}: quadratic electrogyration coefficient for $\boldsymbol{E}$. $\lambda = 632.8$ nm.

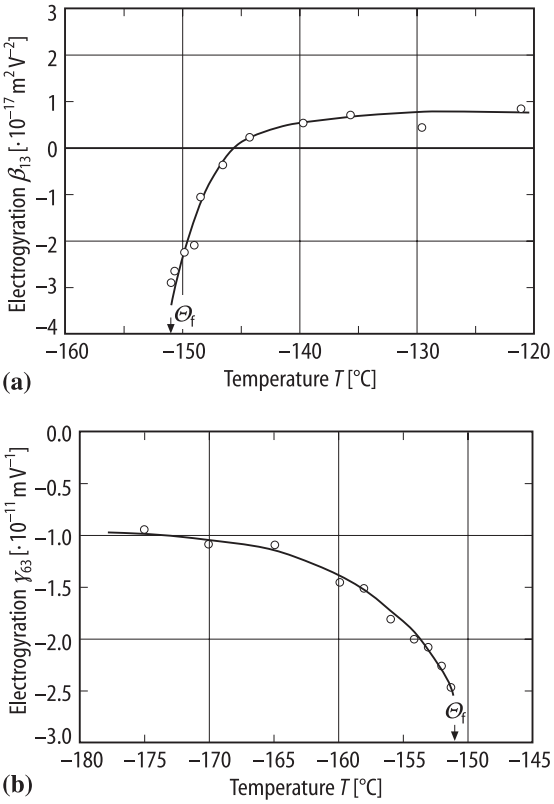

Fig. 33A-1-203. KH_2PO_4 (KDP). (**a**) β_{13}, (**b**) γ_{63} vs. T [89Tak]. β_{13}: quadratic electrogyration coefficient. γ_{63}: linear electrogyration coefficient.

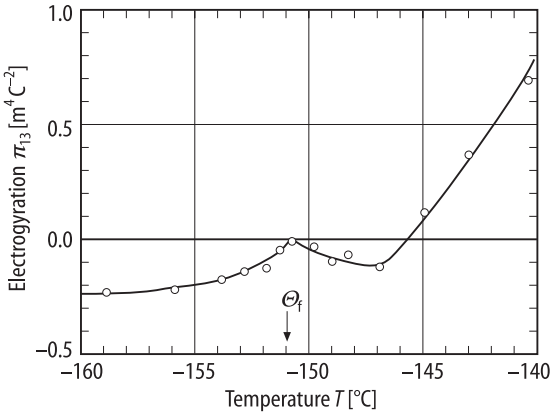

Fig. 33A-1-204. KH_2PO_4 (KDP). π_{13} vs. T [89Tak]. π_{13}: quadratic electrogyration coefficient for P.

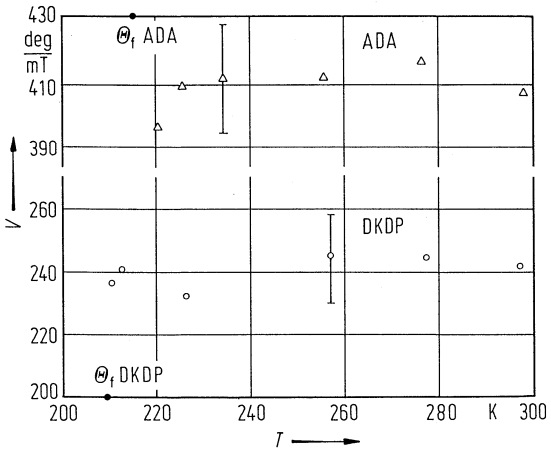

Fig. 33A-1-205. KD_2PO_4 (DKDP), $NH_4H_2AsO_4$ (ADA). V vs. T [81Kor]. V: Verdet constant. $\lambda = 632.8$ nm.

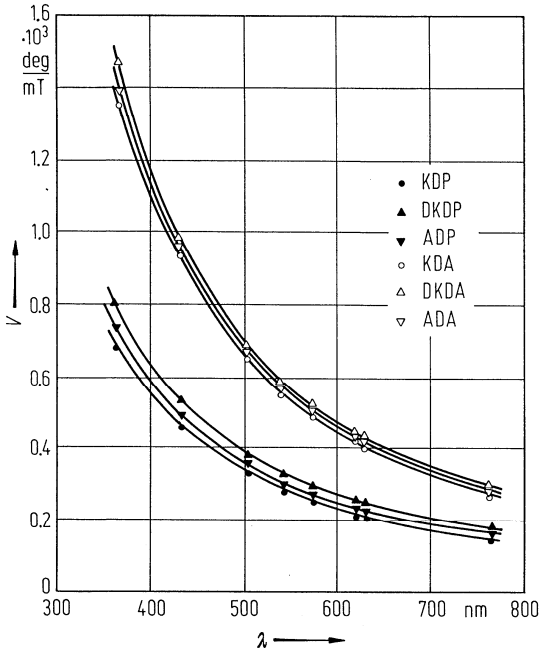

Fig. 33A-1-206. KH_2PO_4 (KDP), KD_2PO_4 (DKDP), $NH_4H_2PO_4$ (ADP), KH_2AsO_4 (KDA), KD_2AsO_4 (DKDA), $NH_4H_2AsO_4$ (ADA). V vs. λ [81Kor]. V: Verdet constant. T = 298 K.

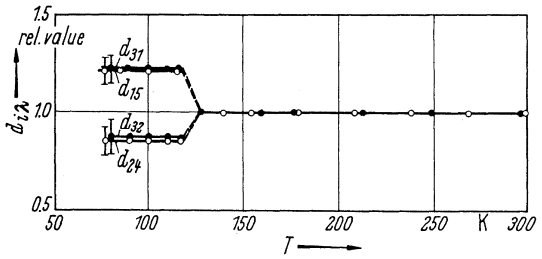

Fig. 33A-1-207. KH_2PO_4 (KDP). $d_{i\lambda}$ vs. T [64Van2]. $d_{i\lambda}$: nonlinear optical susceptibility for SHG (relative value).

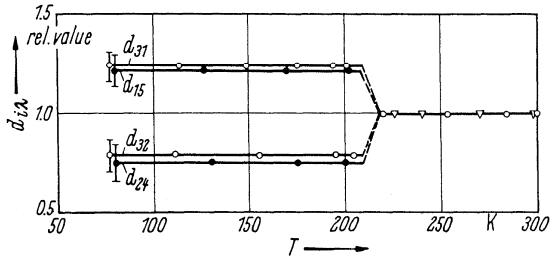

Fig. 33A-1-208. KD_2PO_4 (DKDP). $d_{i\lambda}$ vs. T [64Van2]. $d_{i\lambda}$: nonlinear optical susceptibility for SHG (relative value).

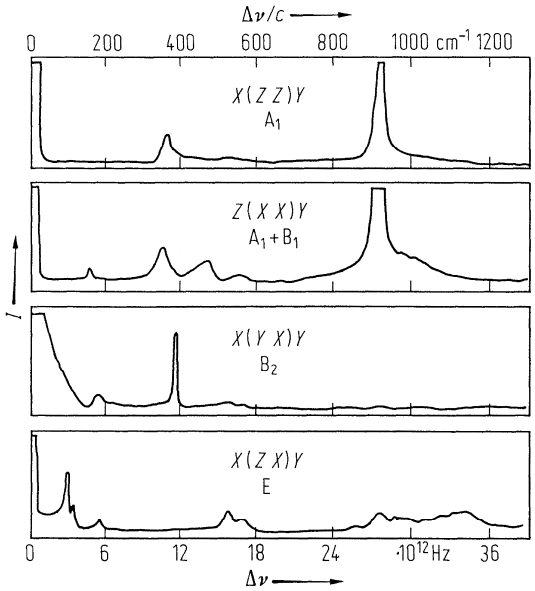

Fig. 33A-1-209. KH_2PO_4 (KDP). I vs. $\Delta\nu$ at RT [70Wil]. I: Raman scattering intensity. Scattering geometry and the associated symmetry of phonons are given in the figure.

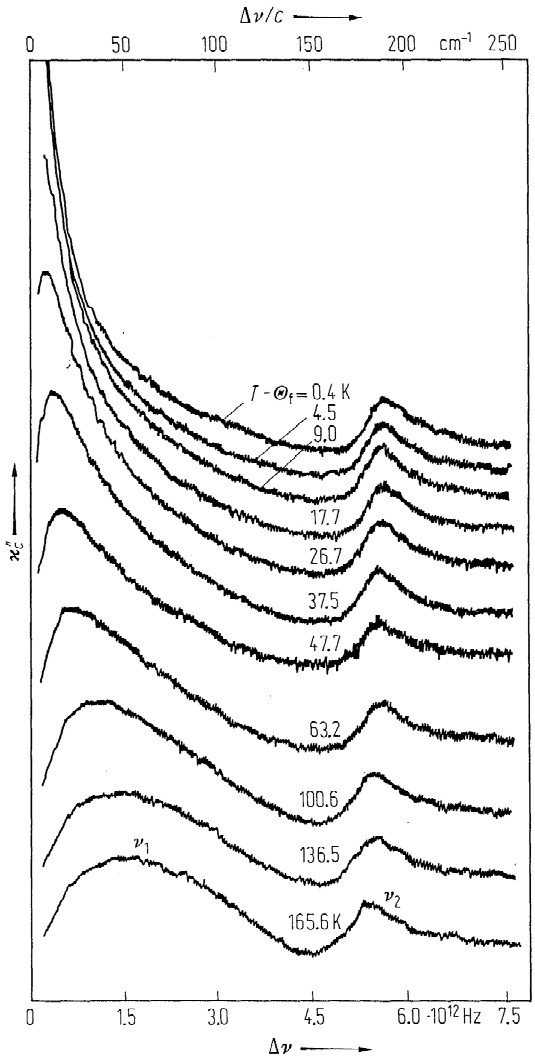

Fig. 33A-1-210. KH_2PO_4 (KDP). κ_c'' vs. $\Delta\nu$ [79Tak]. Parameter: $T - \Theta_f$. $\Delta\nu$: frequency shift of Raman spectrum. κ_c'' was obtained by dividing the Raman scattering intensity by the thermal factor $[1 - \exp(-h\Delta\nu/kT)]^{-1}$. Scattering geometry is $X(YX)Y$ which gives the spectrum of B_2-symmetry phonons.

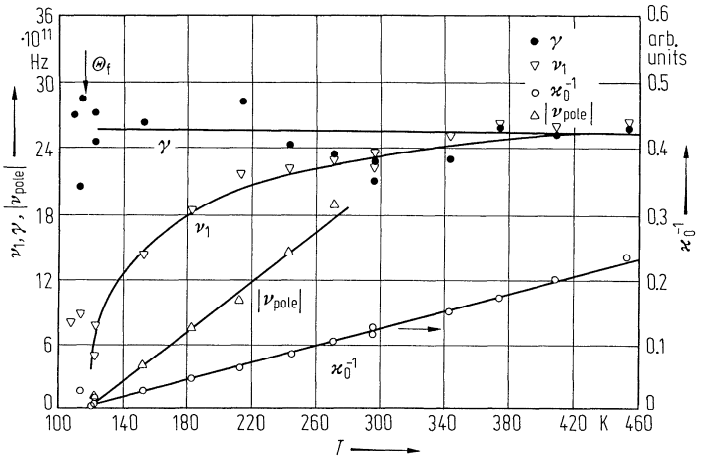

Fig. 33A-1-211. KH_2PO_4 (KDP). ν_1, γ, $|\nu_{pole}|$, κ_0^{-1} vs. T [68Kam]. ν_1, γ: the characteristic frequency and the damping factor of the soft B_2-mode obtained from the Raman spectra. $|\nu_{pole}|$: the distance of the pole of $\kappa(\nu)$ from the origin.

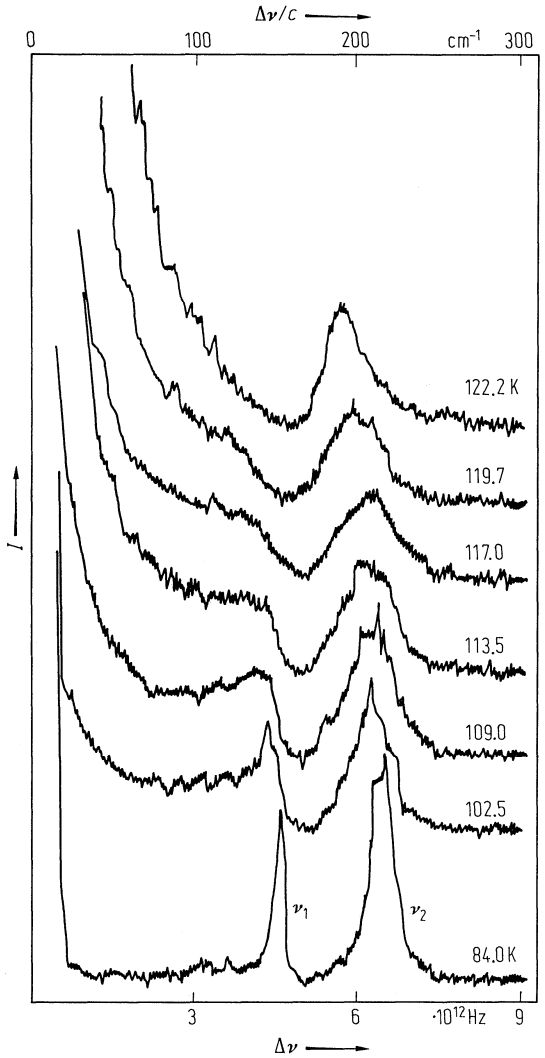

Fig. 33A-1-212. KH_2PO_4 (KDP). I vs. $\Delta\nu$ in the ferroelectric phase [72Sco]. Parameter: T. Scattering geometry is $X(YX)Y$. X, Y, Z: tetragonal axes. See also [71Shi, 73Bli].

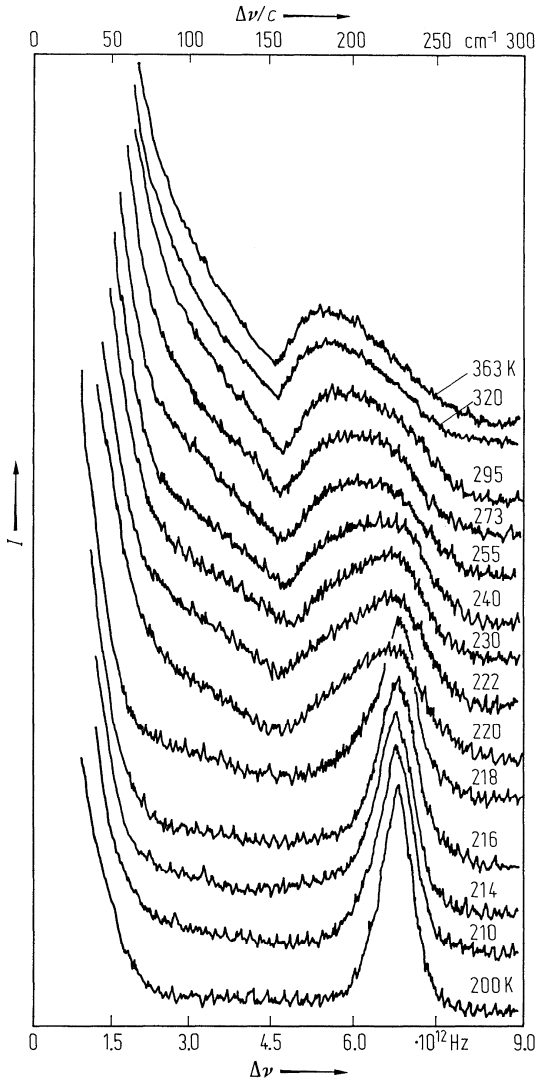

Fig. 33A-1-213. KD_2PO_4 (DKDP). I vs. $\Delta\nu$ [74Kaw]. Parameter: T. I: Raman scattering intensity for the scattering geometry of $X(YX)Y$.

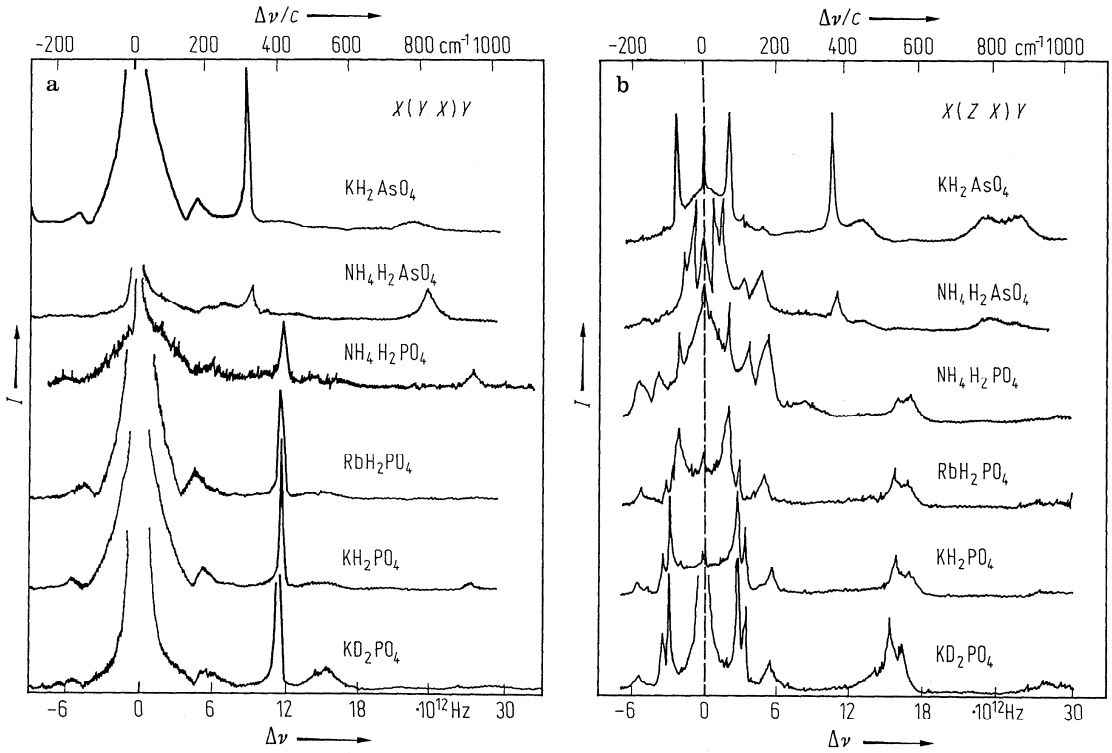

Fig. 33A-1-214. KDP family. I vs. $\Delta\nu$ [71Ham]. I: Raman scattering intensity. (**a**) B_2 modes measured with the scattering geometry $X(YX)Y$. (**b**) E modes measured with $X(ZX)Y$.

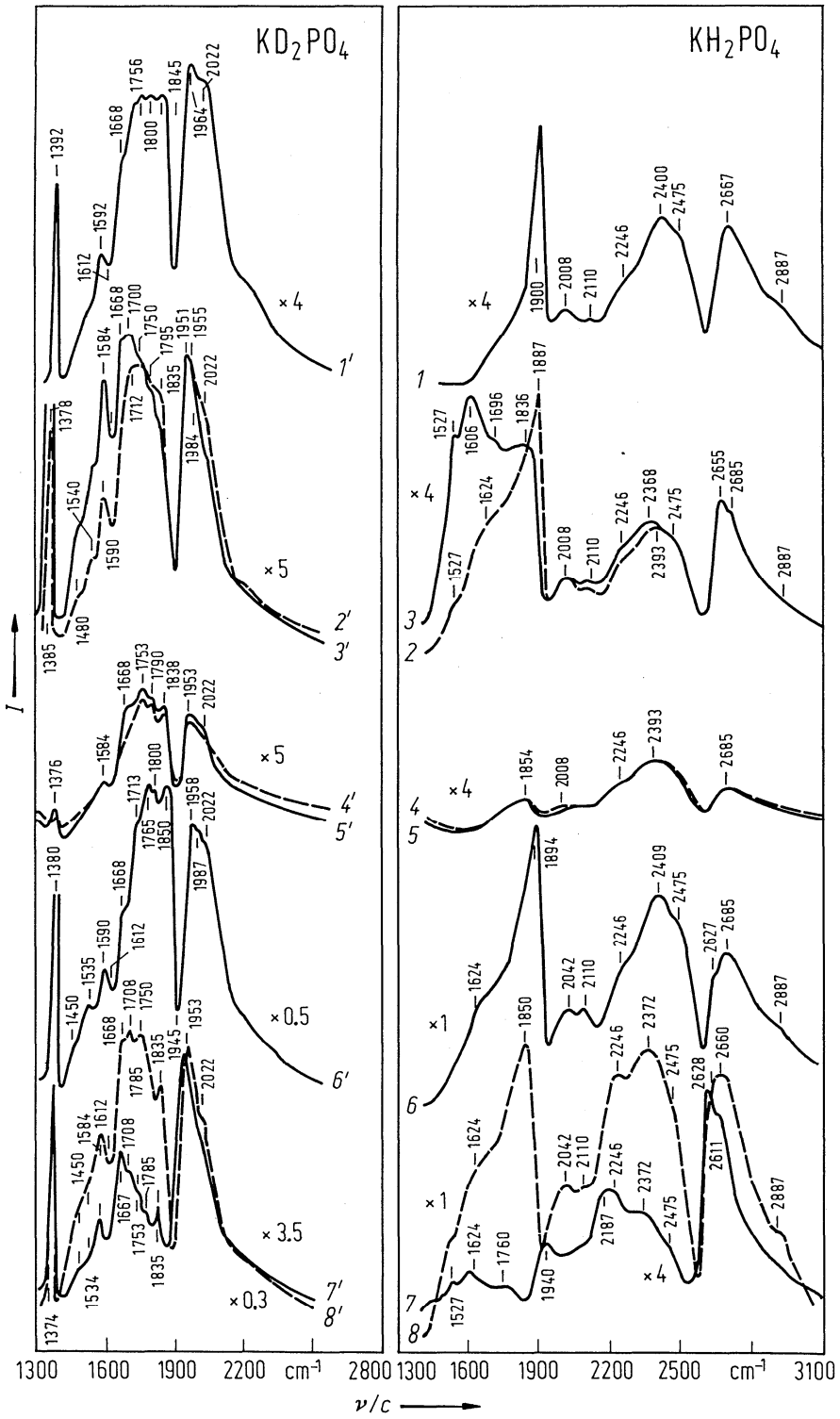

Fig. 33A-1-215. KH_2PO_4 (KDP), KD_2PO_4 (DKDP). *I* vs. *ν/c* [84Dav]. *I*: intensity of Raman spectra at 7 K of single domain samples. Scattering geometries: *1*, *1′*: *X*(*YZ*)*Y*, *2*, *2′*: *Z*(*Y′X*)*X′*, *3*, *3′*: *Z*(*Y′Z*)*X′*, *4*, *4′*: *Z*(*X′Z*)*X′*, *5*, *5′*: *Z*(*X′Z*)*Y′*, *6*, *6′*: *Z*(*Y′X′*)*Y′*, *7*, *7′*: *X′*(*ZZ*)*Y*, *8*, *8′*: *Z*(*X′X′*)*Y′*. *X*, *Y*, *Z*: paraelectric axes; *X′*, *Y′*, *Z′*: ferroelectric axes.

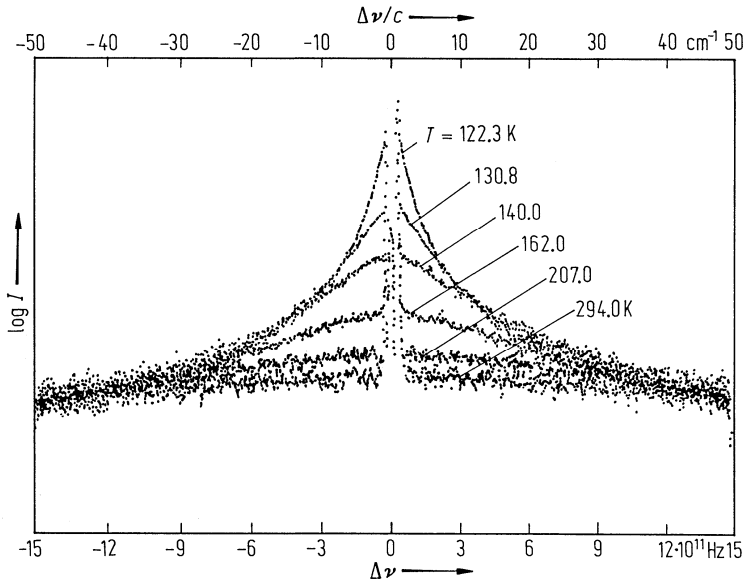

Fig. 33A-1-216. KH_2PO_4 (KDP). log I vs. $\Delta\nu$ [82Tom]. Parameter: T. $\Delta\nu$: frequency shift of Raman spectra.

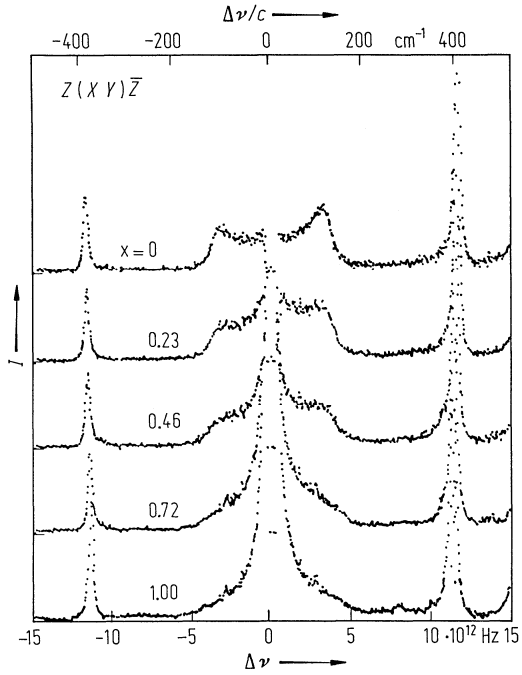

Fig. 33A-1-217. $KH_{2(1-x)}D_{2x}PO_4$. I vs. $\Delta\nu$ at 296 K [83Tom]. Parameter: x. $\Delta\nu$: Raman shift of LO mode measured in the geometry $Z(XY)\bar{Z}$.

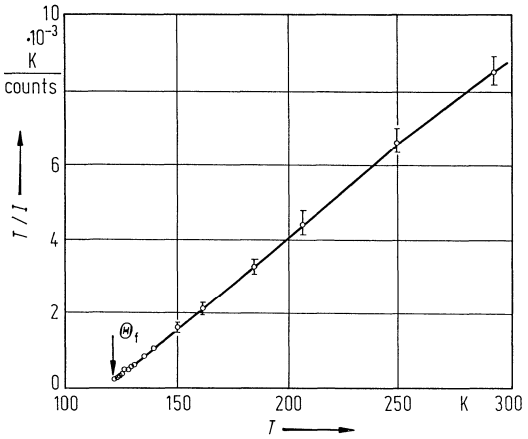

Fig. 33A-1-218. KH_2PO_4 (KDP). T/I vs. T [82Tom]. I: integrated Raman scattering intensity below 50 cm^{-1}. Scattering geometry: $X(YX)Y$.

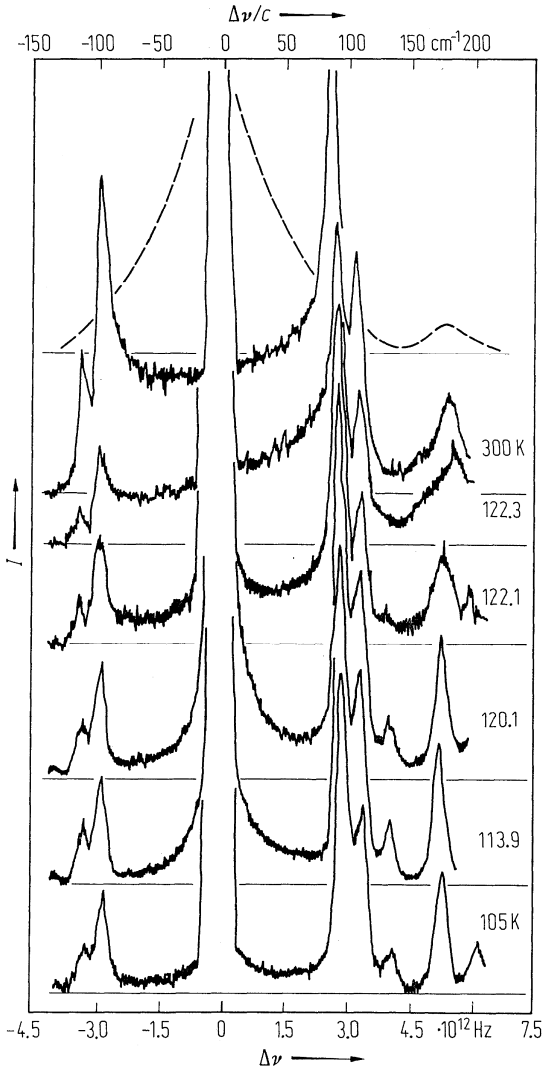

Fig. 33A-1-219. KH_2PO_4 (KDP). I vs. $\Delta\nu$ [75Tak]. I: Raman scattering intensity of E-modes measured in the scattering geometry of $X(YZ)Y$. Parameter: T. The dashed line at the top is the spectrum of B_2-modes at 300 K.

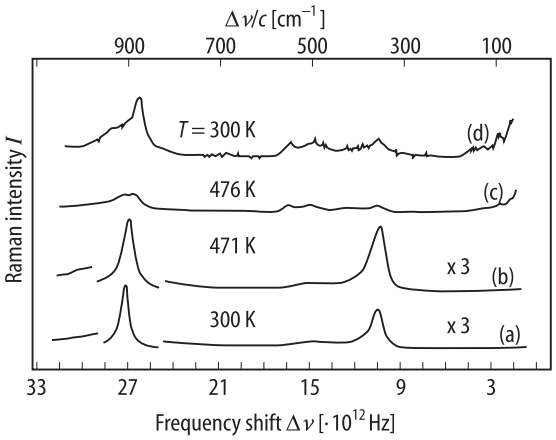

Fig. 33A-1-220. KH_2PO_4 (tetragonal, monoclinic). I vs. $\Delta\nu$ [88Ser]. Parameter: T. I: Raman scattering intensity. (a), (b) single crystals in the tetragonal phase; (c), (d) powder samples in the monoclinic phase.

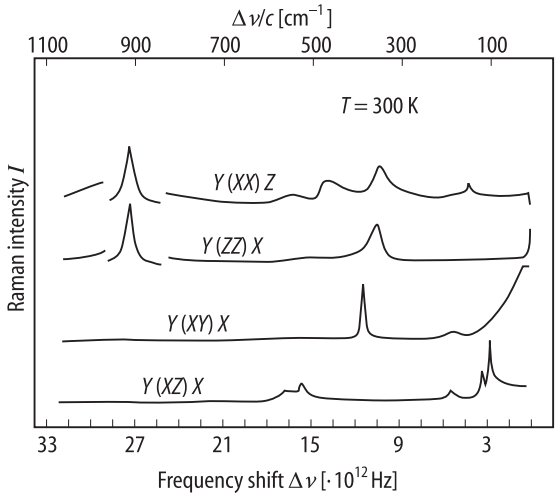

Fig. 33A-1-221. KH_2PO_4 (KDP). I vs. $\Delta\nu$ for several different scattering geometries [88Ser]. I: Raman scattering intensity. T = RT.

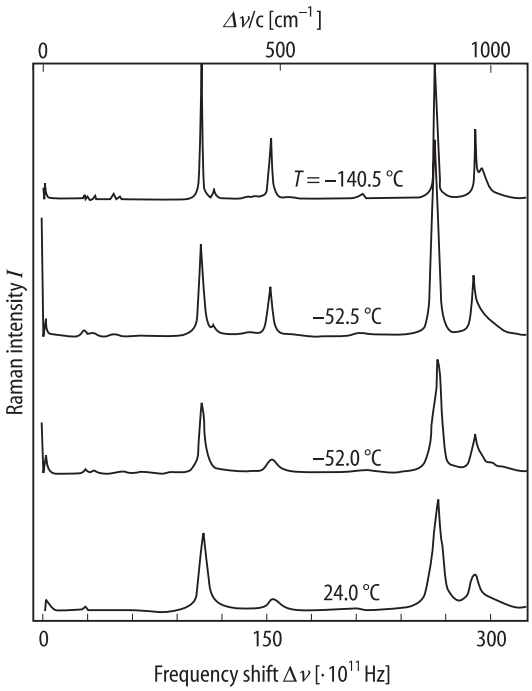

Fig. 33A-1-222. KD_2PO_4 (DKDP). I vs. $\Delta\nu$ in $X(ZZ)Y$ geometry [90Kas]. Parameter: T. I: Raman scattering intensity.

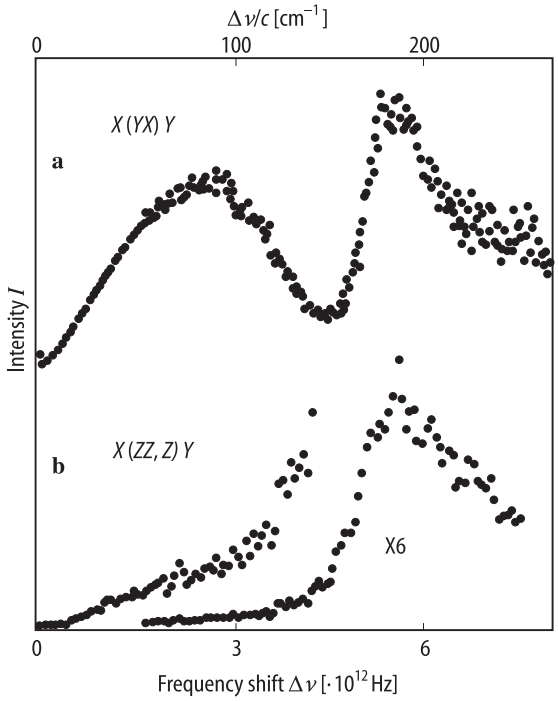

Fig. 33A-1-223. KH_2PO_4 (KDP). I vs. $\Delta\nu$ [89Shi]. I: intensity of $\omega\chi''(\omega)$ spectra obtained at RT. (a) Raman scattering, (b) hyper-Raman scattering.

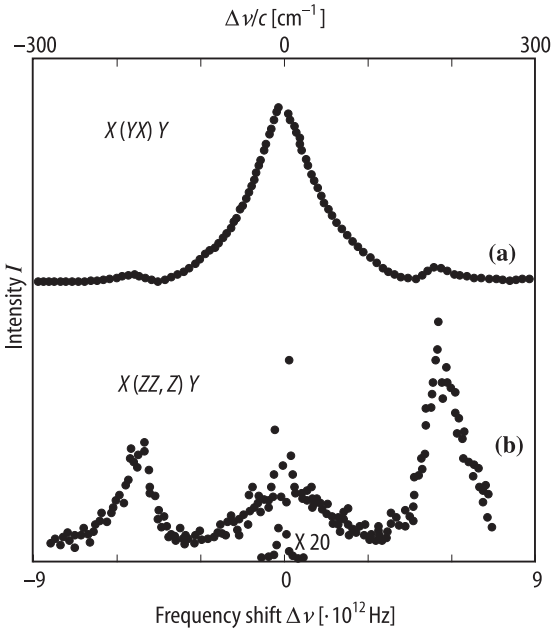

Fig. 33A-1-224. KH_2PO_4 (KDP). I vs. $\Delta\nu$ [89Shi]. I: intensity of $X(YX)Y$ Raman scattering (a), and $X(ZZ,Z)Y$ hyper-Raman scattering (b). T = RT.

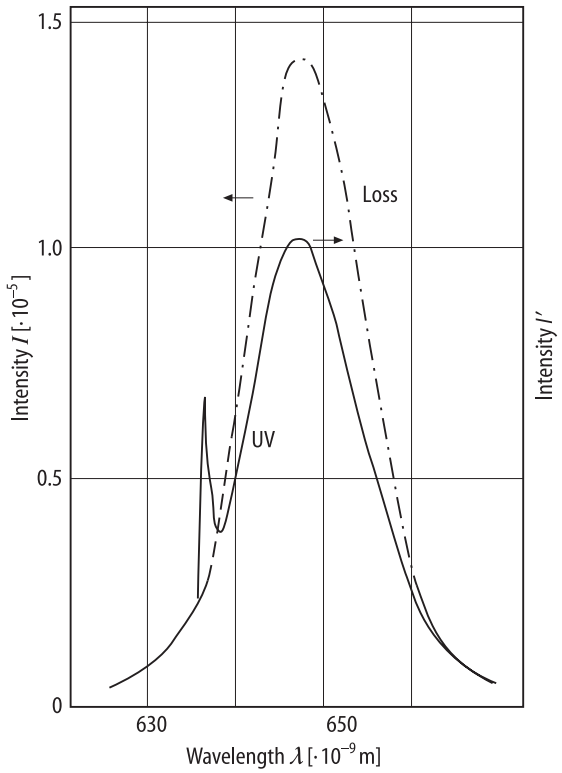

Fig. 33A-1-225. KH_2PO_4 (KDP). I, I' vs. λ [90Jon]. I: fractional probe laser loss of inverse Raman spectrum in a KDP frequency-doubling crystal. $\lambda_1 \approx 600$ nm. λ_2 being scanned over the wavelength range indicated. I': intensity of UV radiation. Sharp spike at 637 nm is the ν_1 transition of the PO_4^- ion.

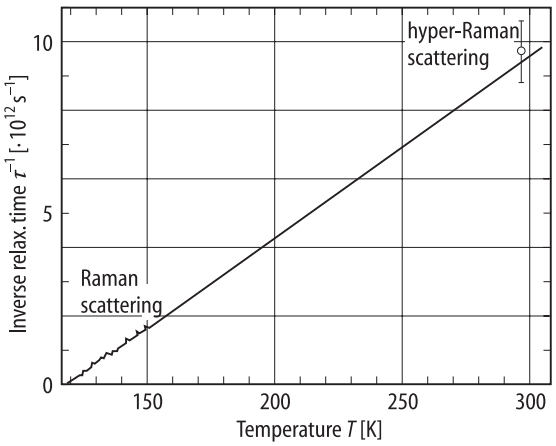

Fig. 33A-1-226. KH_2PO_4 (KDP). τ^{-1} vs. T [89Shi]. τ: relaxation time obtained by Raman and hyper-Raman scattering. Full circle: Raman scattering; open circle: hyper-Raman scattering at RT. The solid line gives a relation $\tau^{-1} = (T - T_0)/(\tau_0 T_0)$, where $\tau_0 = 1.57 \cdot 10^{-13}$ s and $T_0 = 118.7$ K.

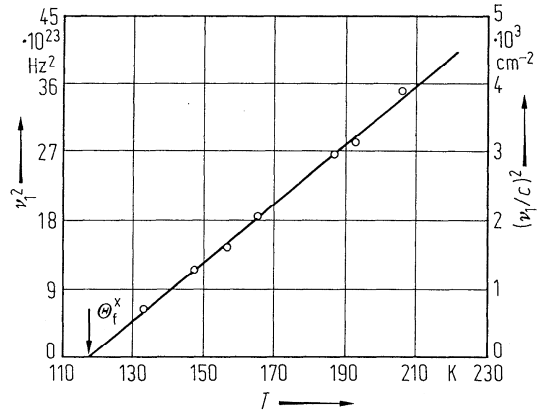

Fig. 33A-1-227. KH_2PO_4 (KDP). ν_1^2 vs. T [74Lag]. ν_1: frequency of the lowest B_2 mode calculated from the coupled mode analysis with an imaginary coupling constant. Θ_f^x: "clamped" Curie temperature.

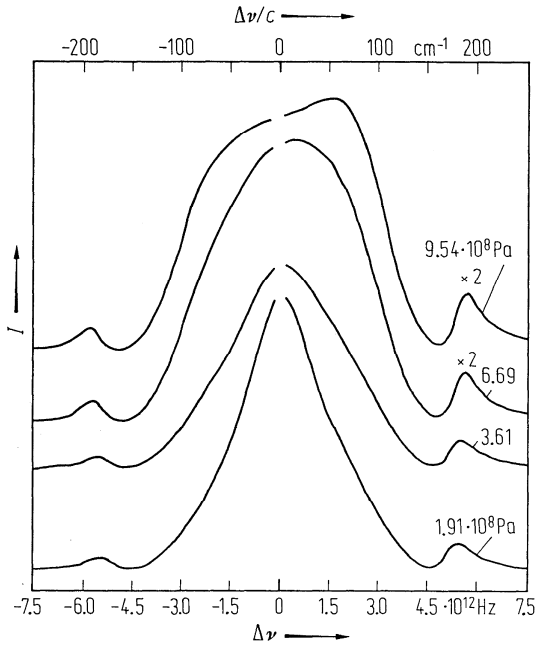

Fig. 33A-1-228. KH_2PO_4 (KDP). I vs. $\Delta\nu$ [75Pee]. Parameter: hydrostatic pressure p. I: Raman scattering intensity for the scattering geometry of $X(YX)Y$. $T = 296$ K.

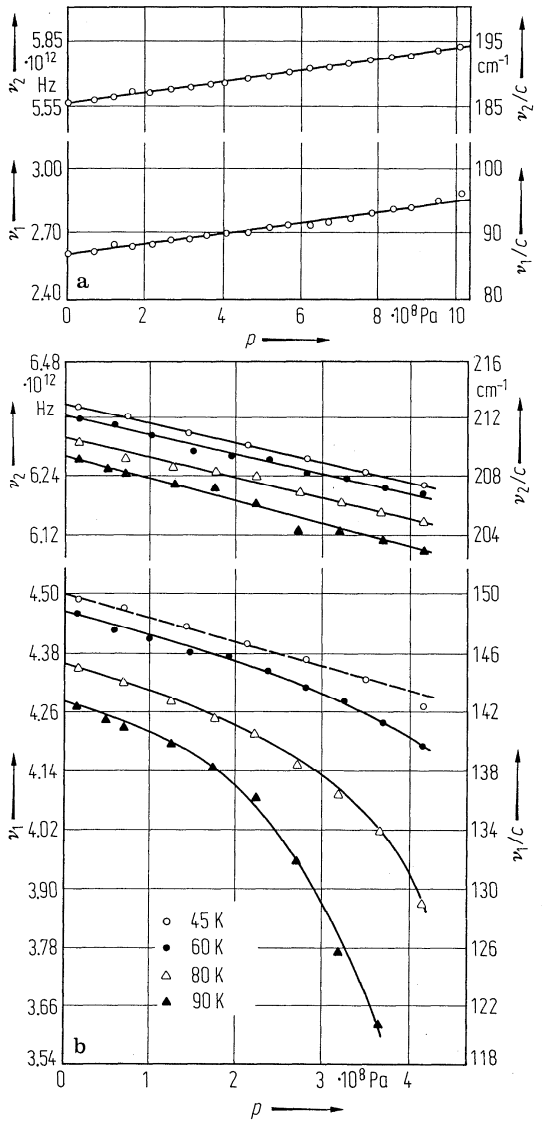

Fig. 33A-1-229. KH_2PO_4 (KDP). ν_1, ν_2 vs. p [75Pee]. ν_1, ν_2: frequencies of the two low-lying B_2-modes shown in Fig. 33A-1-210, Fig. 33A-1-212. (**a**) $T = 297$ K, (**b**) $T < \Theta_f$.

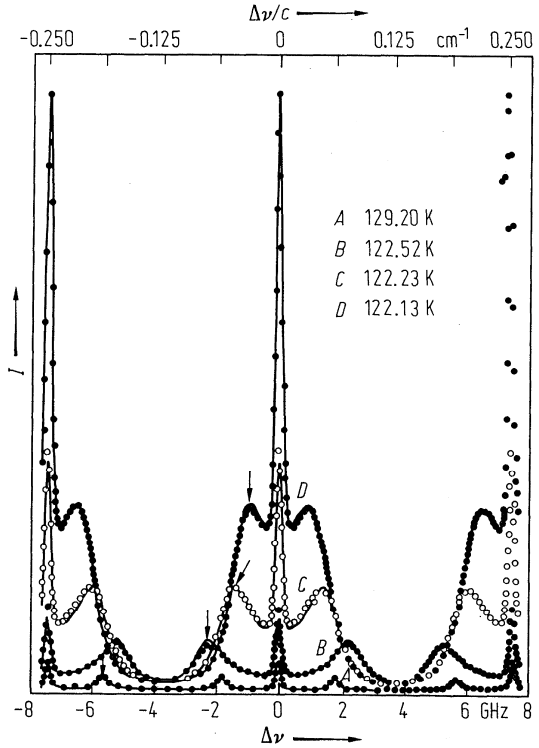

Fig. 33A-1-230. KH_2PO_4 (KDP). I vs. $\Delta\nu$ [74Lag]. Parameter: T. I: intensity of Brillouin spectrum and central peak. $\Delta\nu$: frequency shift of the scattered light. Arrows indicate positions of the anti-Stokes Brillouin peaks of the order centered at zero.

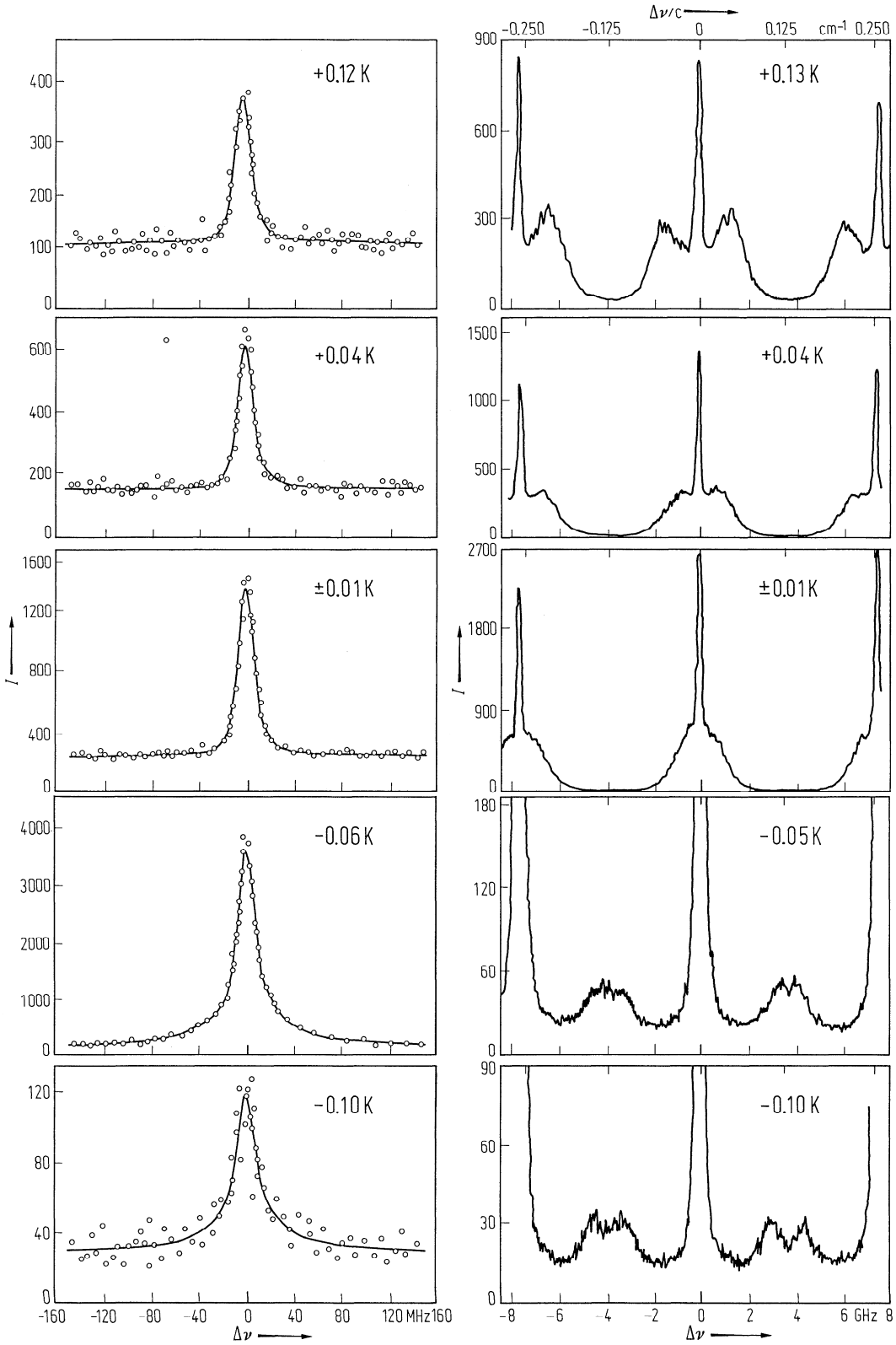

Fig. 33A-1-231. KH_2PO_4 (KDP). I vs. $\Delta\nu$ [77Mer]. Parameter: $T - \Theta_f$. $\Delta\nu$: frequency shift of the Brillouin scattering light. I in arb. units.

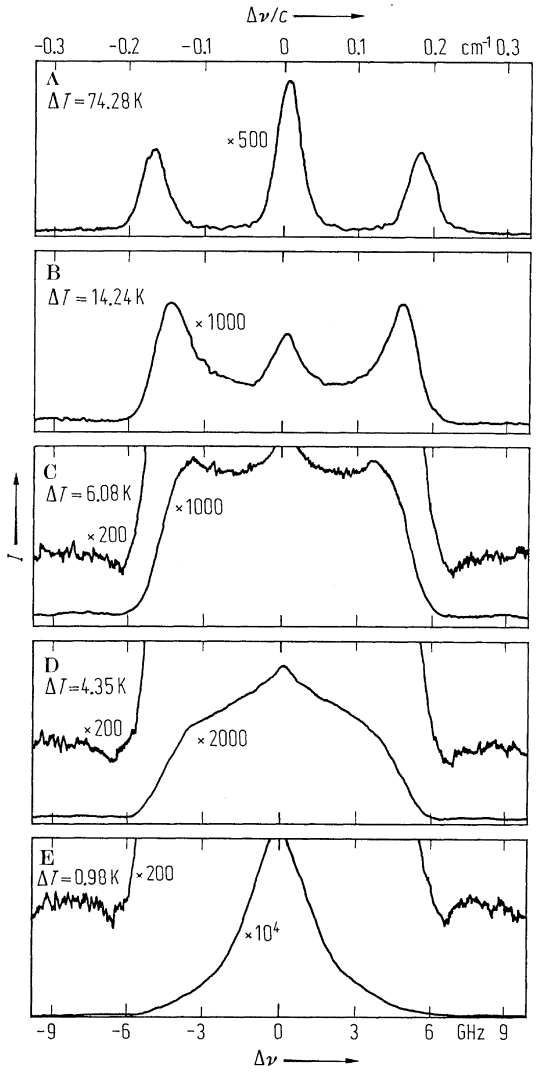

Fig. 33A-1-232. KD_2PO_4 (DKDP). I vs. $\Delta\nu$ [73Ree]. Parameter: $\Delta T = T - \Theta_f$. Θ_f = 220.678 K. I: intensity of the scattered light. Scattering geometry: $XZ(-XZ,Y)-XZ$. Note the change of the vertical scale (counting rate) denoted inside the figures.

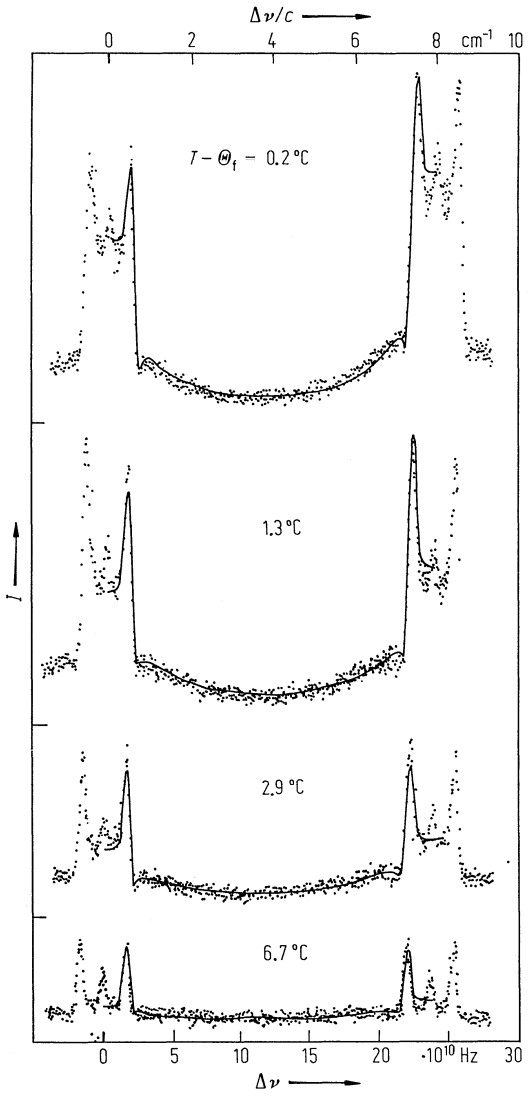

Fig. 33A-1-233. KH_2PO_4 (KDP). I vs. $\Delta\nu$ [81Kas1]. Parameter: $T - \Theta_f$. I: intensity of central mode in $X(YX)Y$ scattering geometry. $\Delta\nu$: Brillouin scattering frequency shift. $\lambda = 488$ nm.

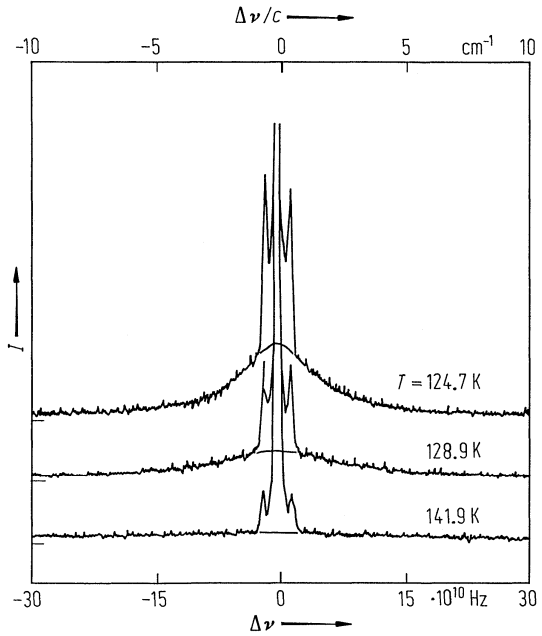

Fig. 33A-1-234. KH_2PO_4 (KDP). I vs. $\Delta\nu$ [84Sak]. Parameter: T. I: intensity of the low-frequency spectra in $X(YX)Y$ scattering geometry. $\Delta\nu$: Brillouin scattering frequency shift.

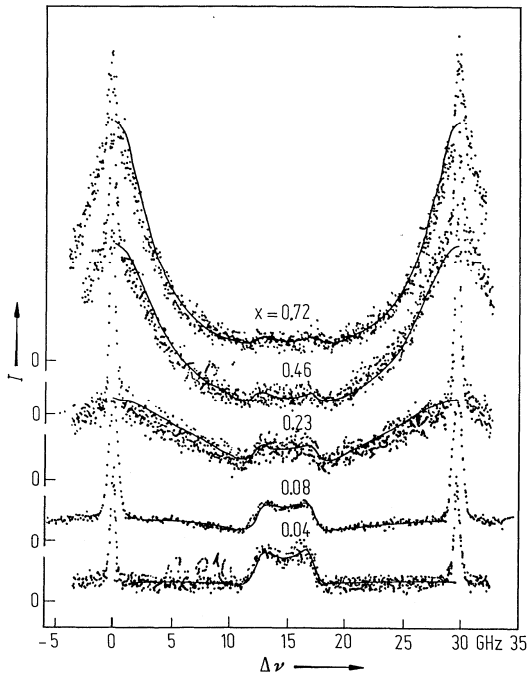

Fig. 33A-1-235. $KH_{2(1-x)}D_{2x}PO_4$. I vs. $\Delta\nu$ [81Kas2]. Parameter: x. I: intensity of Brillouin spectra in $X(YX)Y$ geometry at $T - \Theta_f = 0.2$ K. $\lambda = 488$ nm.

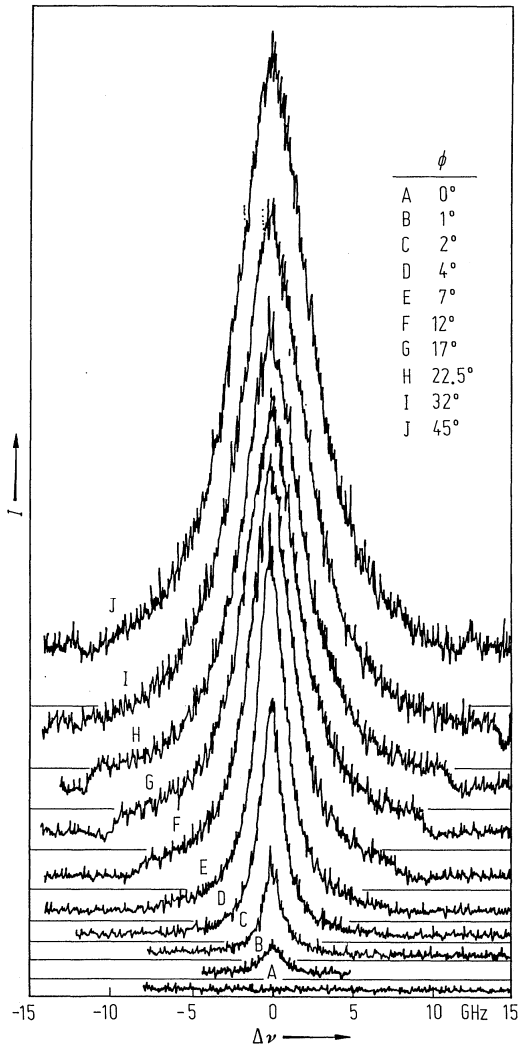

Fig. 33A-1-236. KD_2PO_4 (DKDP). I vs. $\Delta\nu$ [81Tan1]. Parameter: ϕ. I: spectral intensity of HH-scattering configuration and the right angle scattering in the XY plane at $T = \Theta_f + 0.05$ K. ϕ: angle between scattering wave vector $\boldsymbol{q}$ and a axis in the ab-scattering plane.

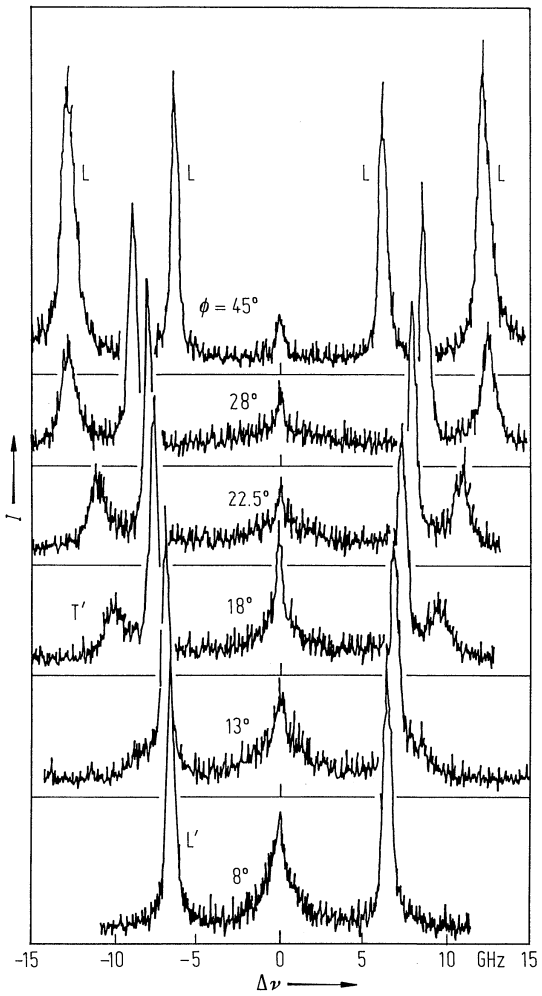

Fig. 33A-1-237. KD_2PO_4 (DKDP). I vs. $\Delta\nu$ [81Tan2]. Parameter: ϕ. I: intensity of the VV-scattering spectra in the *ab* plane measured at Θ_t + 0.05 K. $\Delta\nu$: Brillouin scattering frequency shift. ϕ: angle between q and the a axis. Scattcring angle is 90°. L: pure longitudinal mode. T′: quasi-transverse mode. L′: quasi-longitudinal mode. λ = 488 nm. The spectrum of ϕ = 0° is superimposed on the spectrum of ϕ = 45° between two inner peaks.

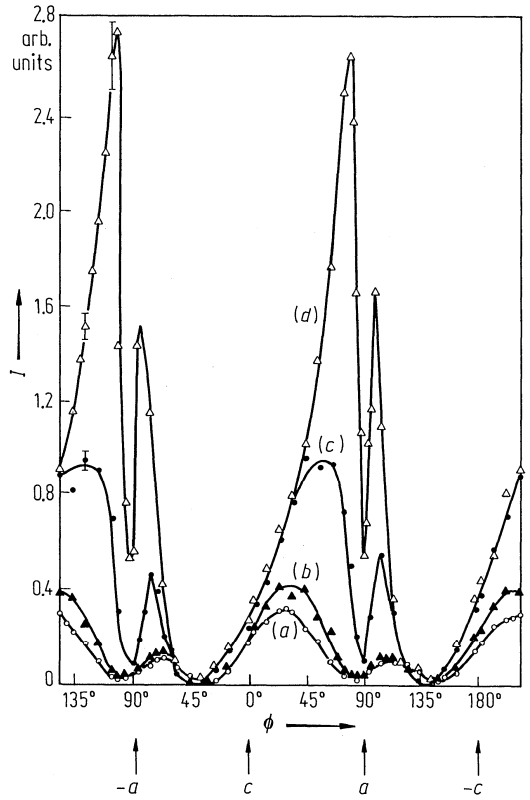

Fig. 33A-1-238. KD_2PO_4 (DKDP). I vs. ϕ [79Saw2]. Parameter: $\Delta T = T - \Theta_f$. I: scattering intensity of the narrow central component in the VH-scattering in the *ac*-scattering plane. ϕ: angle between the *c* axis and scattering vector. (*a*) ΔT = 51.3 K, (*b*) 31.4 K, (*c*) 6.1 K, (*d*) 1.3 K.

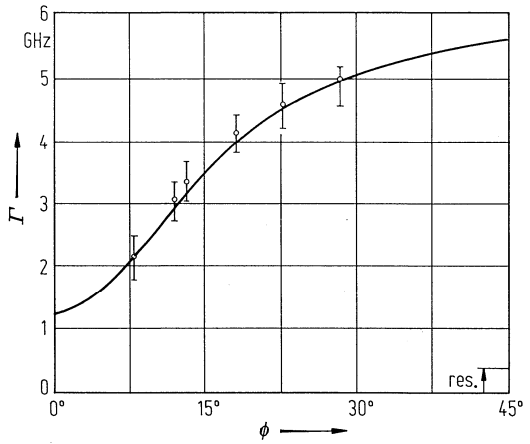

Fig. 33A-1-239. KD_2PO_4 (DKDP). Γ vs. ϕ [81Tan2]. Γ: full line width of a central peak observed with VV-scattering in the (001) plane. ϕ: angle between the scattering wave vector and the *a* axis in (001) plane. res.: instrumental line width.

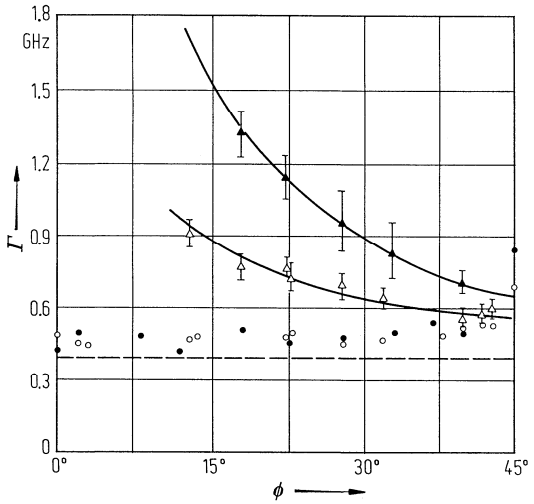

Fig. 33A-1-240. KD_2PO_4 (DKDP). Γ vs. ϕ [82Tan]. Γ: full width of quasi-transverse and longitudinal phonons propagating in the *ab*-plane. ϕ: angle between the scattering wave vector and the *a* axis. Open triangle, full triangle: quasi-transverse phonon; open circle, full circle: quasi-longitudinal phonon. Open triangle, open circle: $T = -34.8$ °C; full triangle, full circle: $T = -52.5$ °C. Scattering angle: $\pi/2$. Broken line: instrumental width.

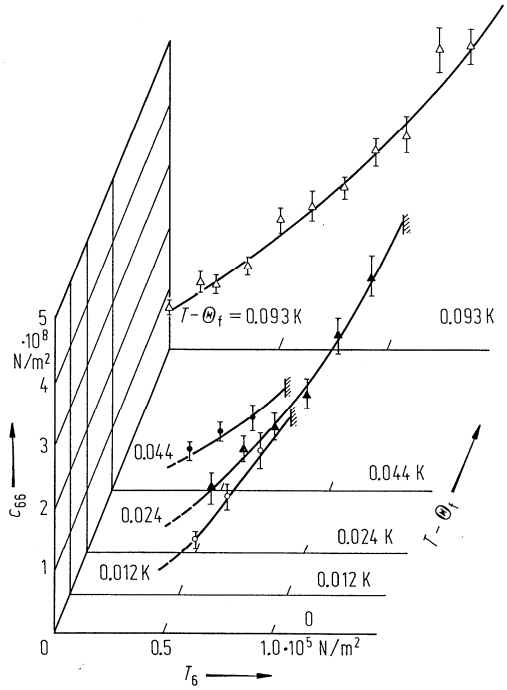

Fig. 33A-1-241. KH_2PO_4 (KDP). c_{66} vs. T_6 [85Tak2]. Parameter: $T - \Theta_f$. T_6: stress tensor component.

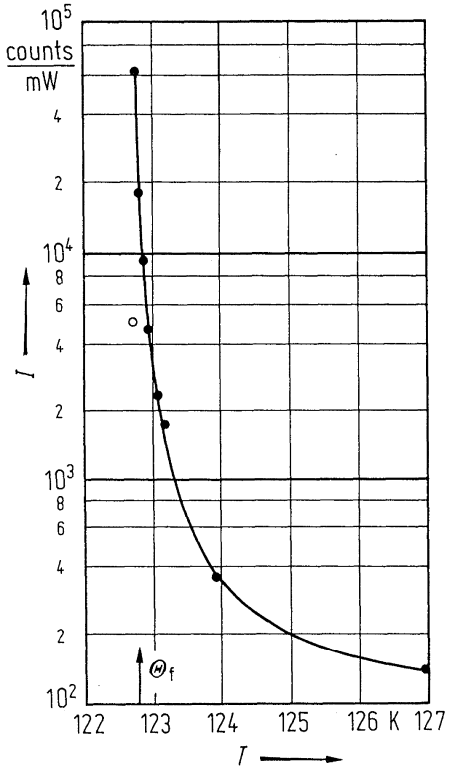

Fig. 33A-1-242. KH_2PO_4 (KDP). I vs. T [77Dur]. I: Rayleigh scattering intensity. Open circle: result in the ferroelectric phase.

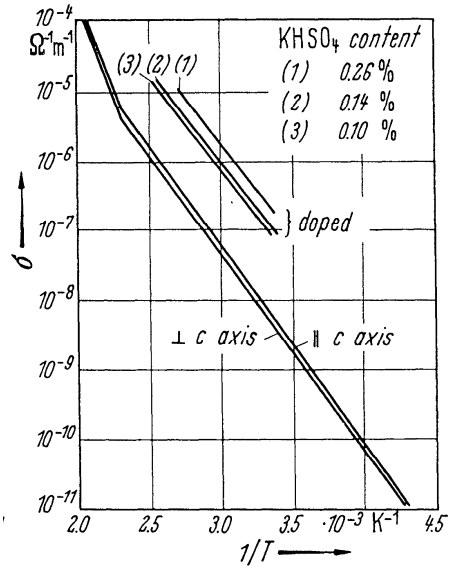

Fig. 33A-1-243. KH_2PO_4 (KDP). σ vs. $1/T$ for pure and doped specimens [67OKe2].

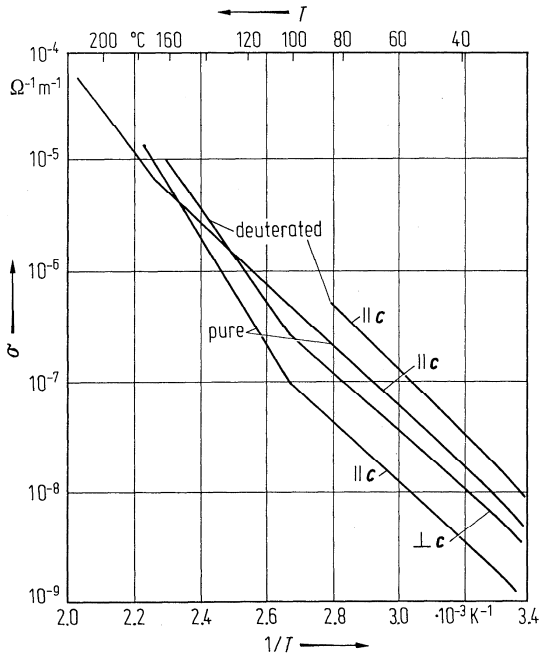

Fig. 33A-1-244. KH_2PO_4 (KDP), KD_2PO_4 (DKDP). σ vs. $1/T$ along or perpendicular to [001] [73Har, 67OKe2].

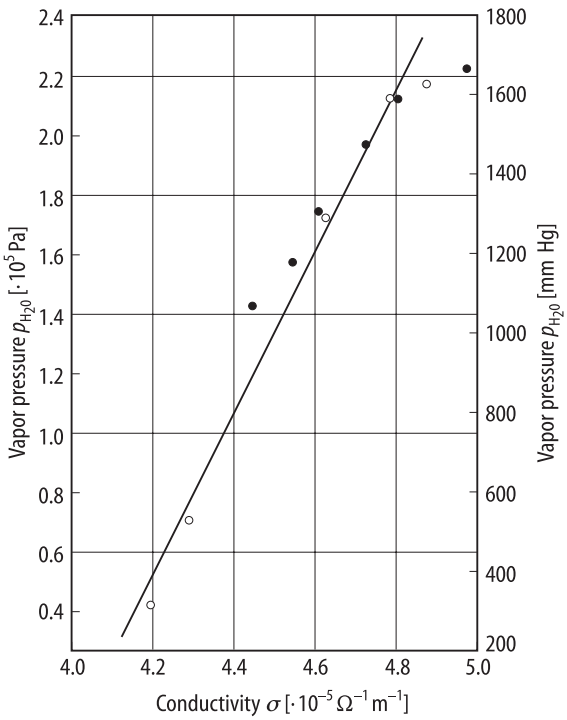

Fig. 33A-1-245. KH_2PO_4 (KDP). p_{H_2O} vs. σ [67OKe2]. p_{H_2O} : water vapor pressure. Open circles: increasing pressure, full circles: decreasing pressure.

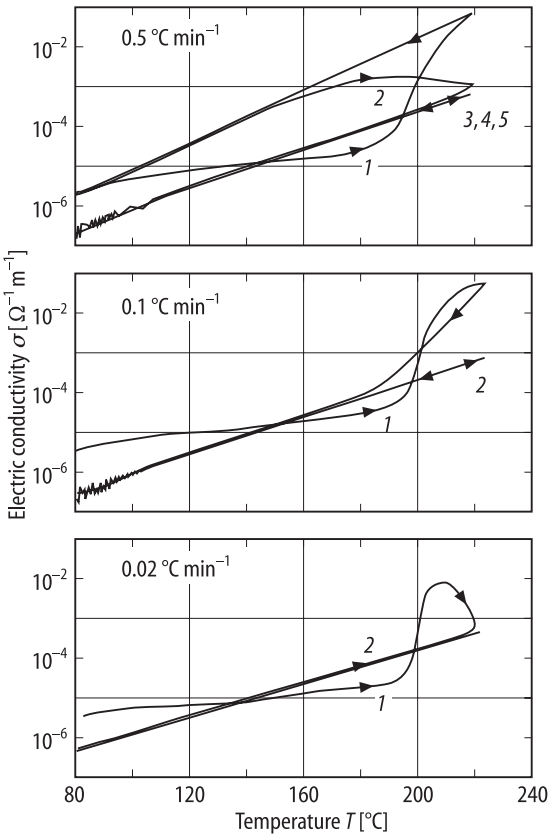

Fig. 33A-1-246. KH_2PO_4 (KDP, powder). σ vs. T [94Cho]. Data for three different heating rates are indicated. Numerals by the data indicate heating cycles.

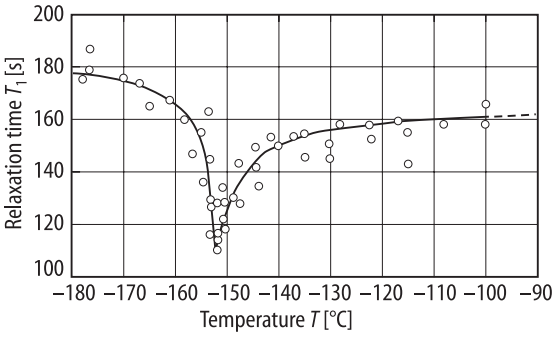

Fig. 33A-1-247. KH_2PO_4 (KDP). T_1 vs. T [74Lah]. T_1: proton spin-lattice relaxation time. f = 15.3 MHz. $\boldsymbol{H} \perp \boldsymbol{c}$ axis.

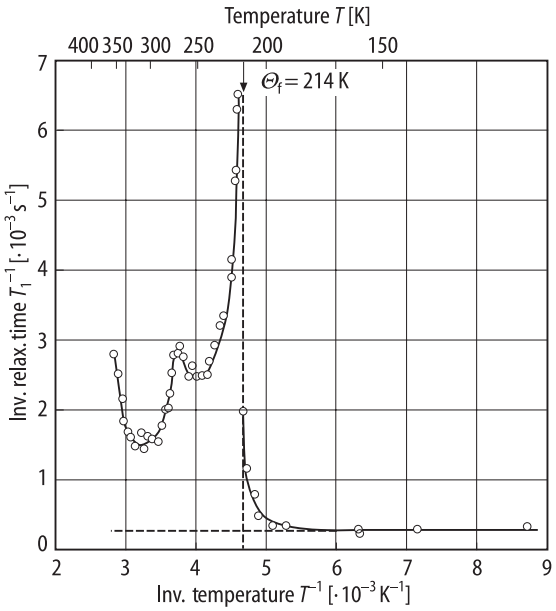

Fig. 33A-1-248. KD_2PO_4 (DKDP). T_1^{-1} vs. T^{-1} [76Sla]. T_1: deuteron spin-latttce relaxation time. $\boldsymbol{H} \perp \boldsymbol{c}$, θ_z = 55°. f = 10.6 MHz. For θ_z, see Fig. 33A-1-249.

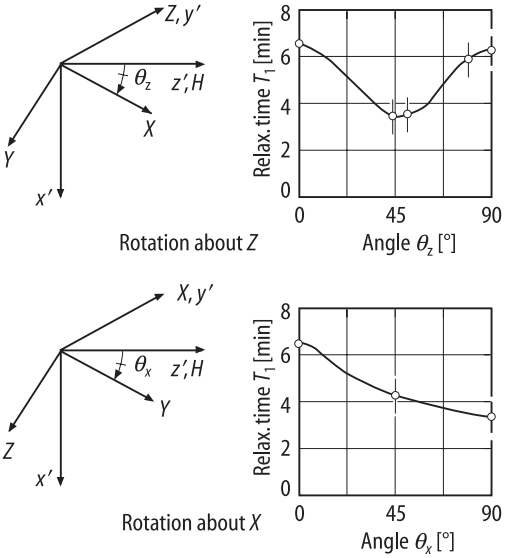

Fig. 33A-1-249. KD_2PO_4 (DKDP). Orientation dependence of spin-lattice relaxation time, T_1 at RT [59Bjo]. f = 8 MHz. (x' y' z'): laboratory fixed coordinates, (X Y Z): crystal fixed coordinates. $\boldsymbol{H} \parallel \boldsymbol{z'}$.

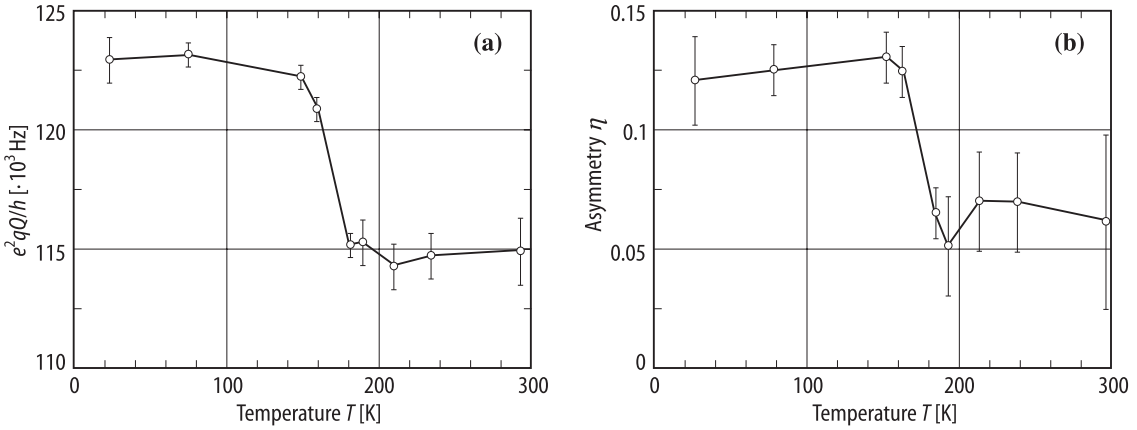

Fig. 33A-1-250. $KH_{2(1-x)}D_{2x}PO_4$ (x = 0.5). (**a**) e^2qQ/h, (**b**) η vs. T from nuclear quadrupole double resonance spectrum of deuteron [83Bre]. η: asymmetry parameter.

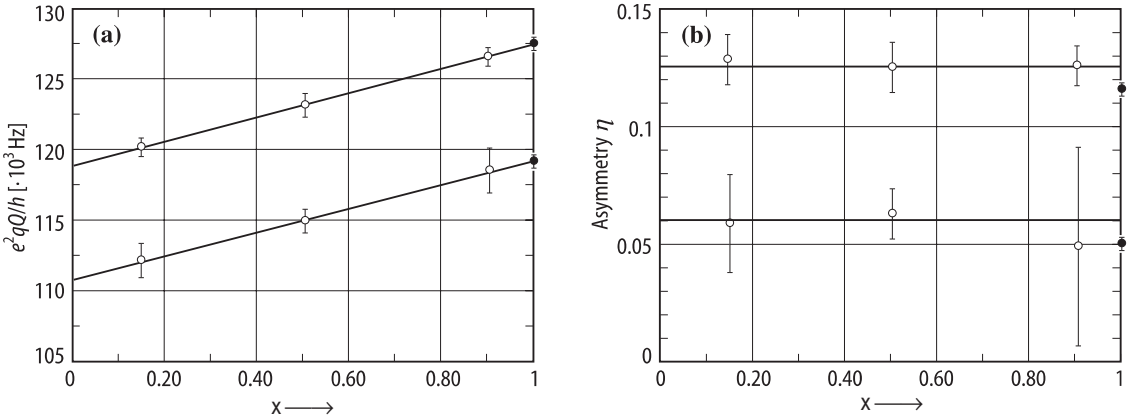

Fig. 33A-1-251. $KH_{2(1-x)}D_{2x}PO_4$. (**a**) e^2qQ/h, (**b**) η vs. x from nuclear quadrupole double resonance spectrum of deuteron [83Bre]. η: asymmetry parameter. Upper line: $T < \Theta_f$. Lower line: $T > \Theta_f$. Full circle: data from [67Bjo].

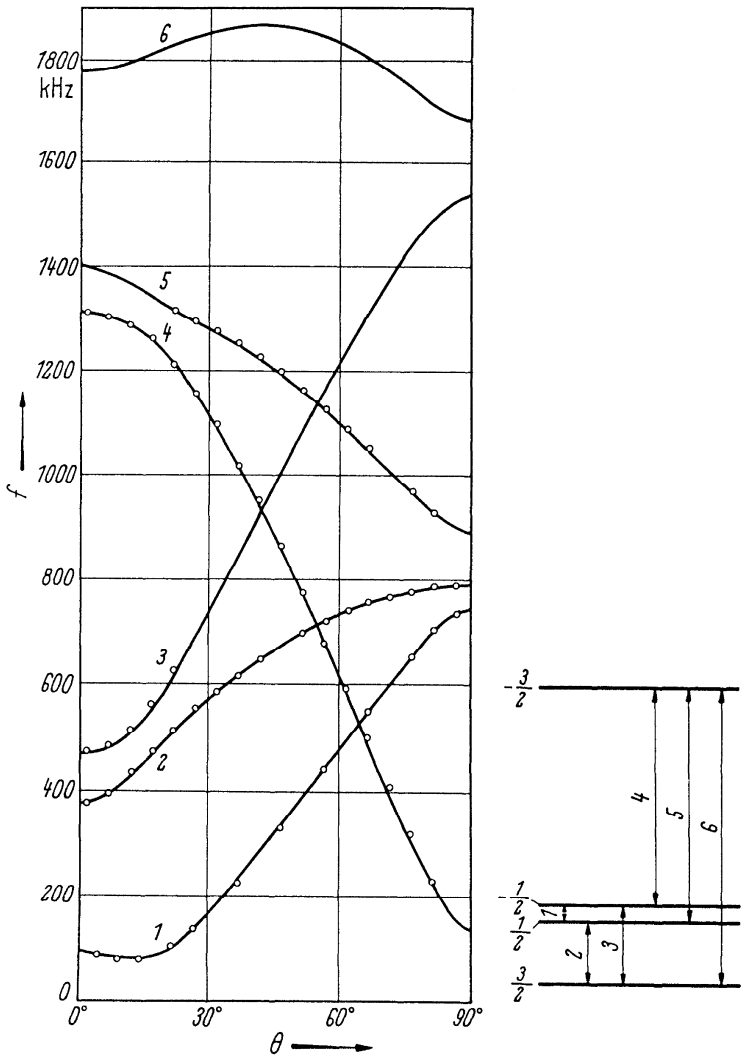

Fig. 33A-1-252. KH_2PO_4 (KDP). f vs. θ [67Kun]. f: NMR resonance frequency of ^{39}K. θ: angle between $\boldsymbol{H}$ and the c axis in the b–c plane. Solid curves are calculated values. e^2qQ/h = 1.68(1) MHz. The major principal axes of the electric field gradient tensor coincides with the c axis. Corresponding transitions are schematically shown on the right-hand side.

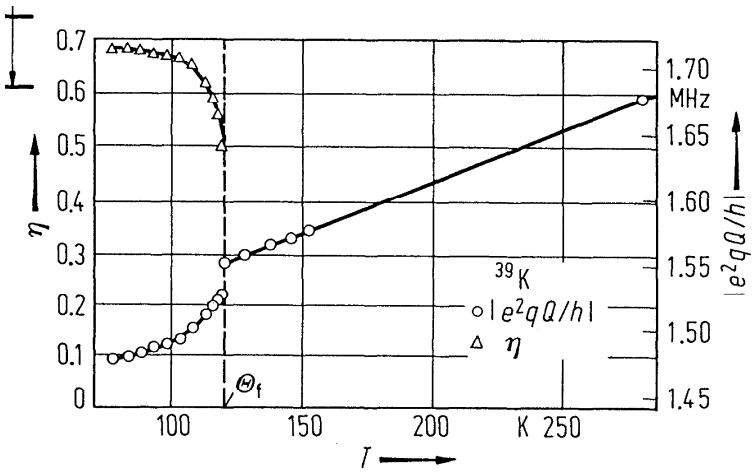

Fig. 33A-1-253. KH_2PO_4 (KDP). $|e^2qQ/h|$, η vs. T of ^{39}K [70Kun]. η: asymmetry parameter.

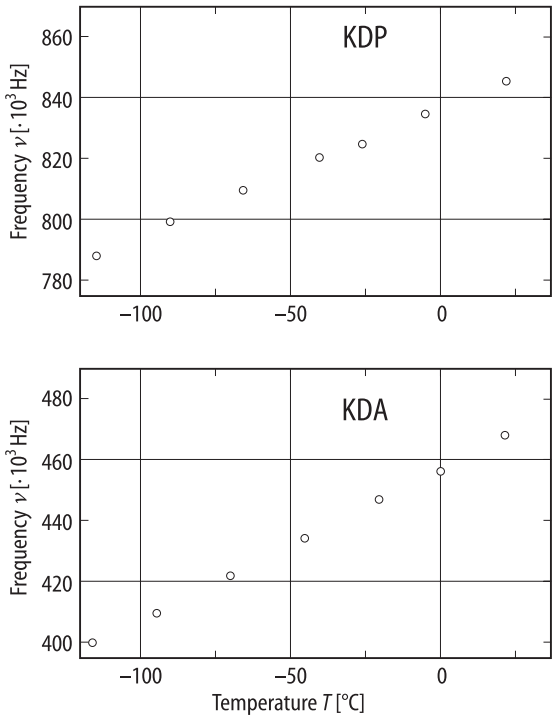

Fig. 33A-1-254. KH_2PO_4 (KDP), KH_2AsO_4 (KDA). ν vs. T [94Sel]. ν: ^{39}K NQR frequency.

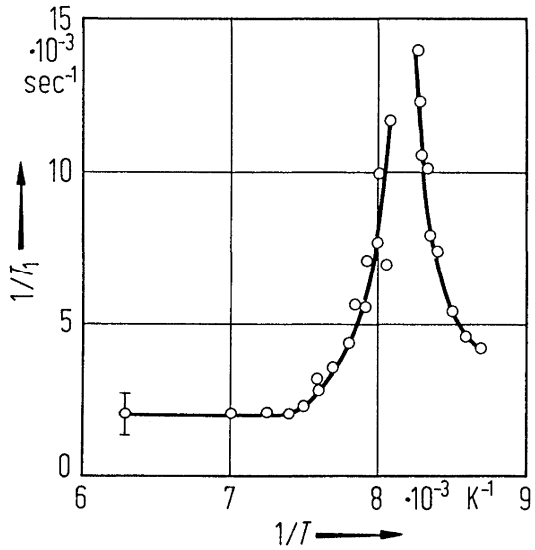

Fig. 33A-1-255. KH_2PO_4 (KDP). $1/T_1$ vs. $1/T$ [68Bli2]. T_1: ^{31}P spin lattice relaxation time. f = 8.0 MHz. $\boldsymbol{H} \perp \boldsymbol{c}$ axis.

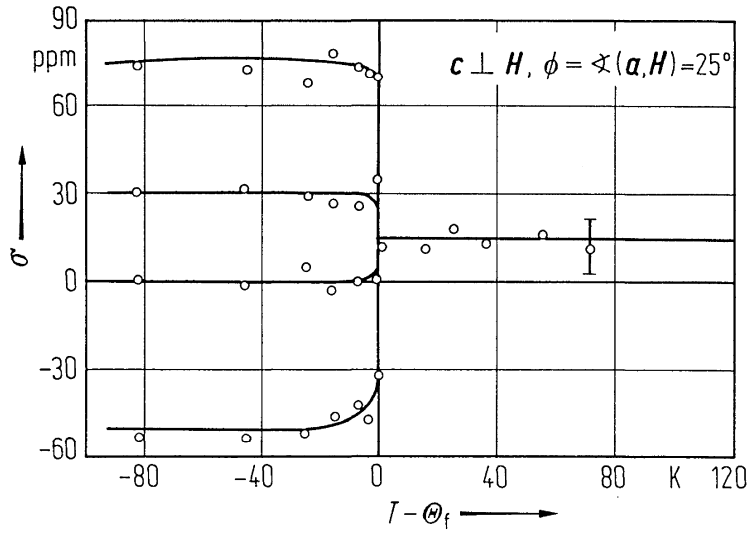

Fig. 33A-1-256. KD_2PO_4 (DKDP). σ vs. $T - \Theta_f$ [77Bli]. σ: chemical shift of ^{31}P in units of ppm.

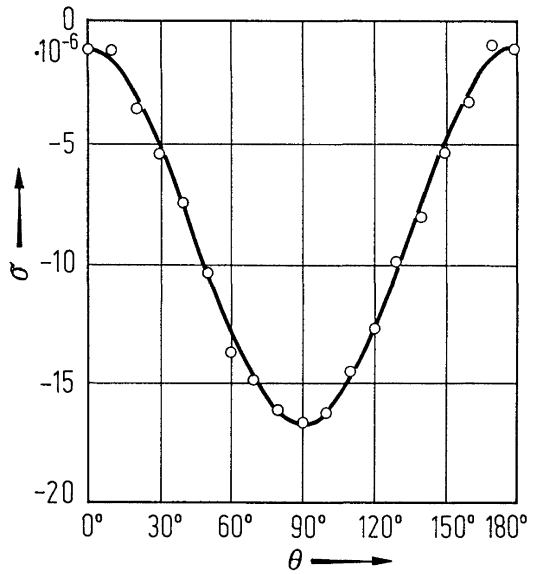

Fig. 33A-1-257. KH_2PO_4 (KDP). σ vs. θ [72Ter]. σ: ^{31}P chemical shift. θ: angle between ***H*** and *c* axis.

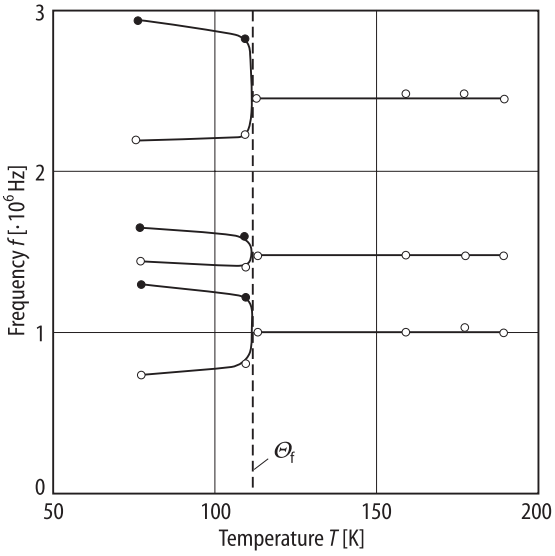

Fig. 33A-1-258. KH_2PO_4 (KDP). f vs. T [74Bli]. f: ^{17}O NQR resonance frequency. Open circle, full circle: two chemically nonequivalent ^{17}O sites.

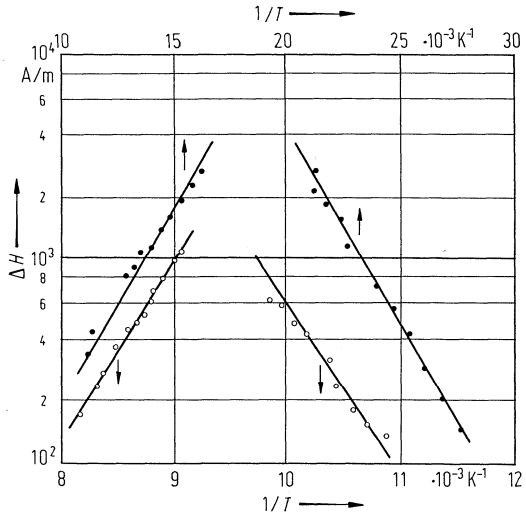

Fig. 33A-1-259. KH_2PO_4:Tl^{2+}, RbH_2PO_4:Tl^{2+}. ΔH vs. T^{-1} [86Gri]. ΔH: Tl^{2+} ESR line width. Full circle: KH_2PO_4, open circle: RbH_2PO_4.

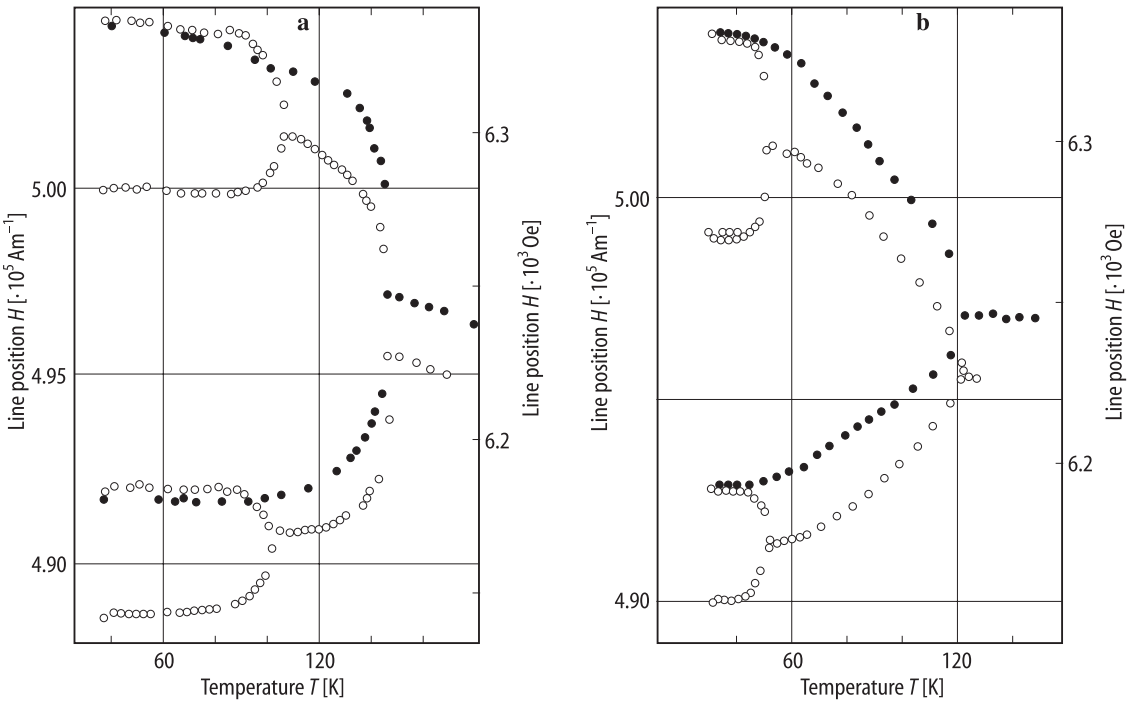

Fig. 33A-1-260. KH_2PO_4:Tl^{2+}, RbH_2PO_4:Tl^{2+}. H vs. T [83Bog]. H: position of ESR lines due to a weak-field transition of Tl^{2+} ions. (**a**) RbH_2PO_4. (**b**) KH_2PO_4. Full circle: $\boldsymbol{H} \parallel \boldsymbol{a}$ + 45° in the *ab* plane; open circle: $\boldsymbol{H}$ inclined at an angle of 20° to the *c* axis.

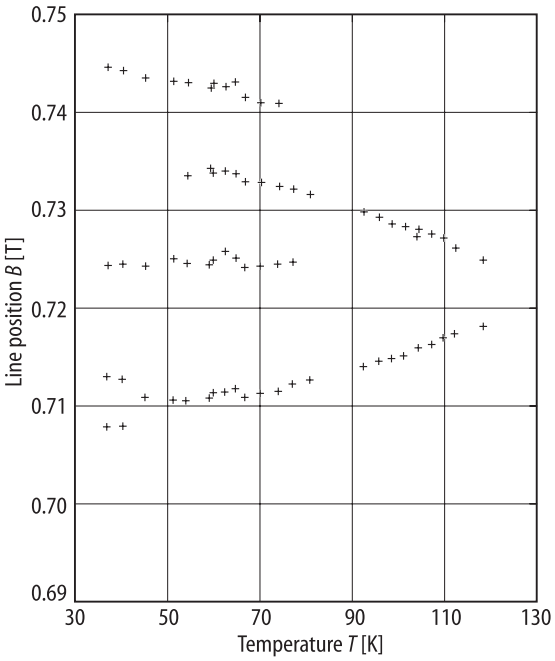

Fig. 33A-1-261. KH_2PO_4:Tl^{2+}. *B* vs. *T* [87Alv]. *B*: line position of Tl^{2+} ESR. The magnetic field lies in the *ac* plane at an angle $\theta = 67.5°$ from *c*.

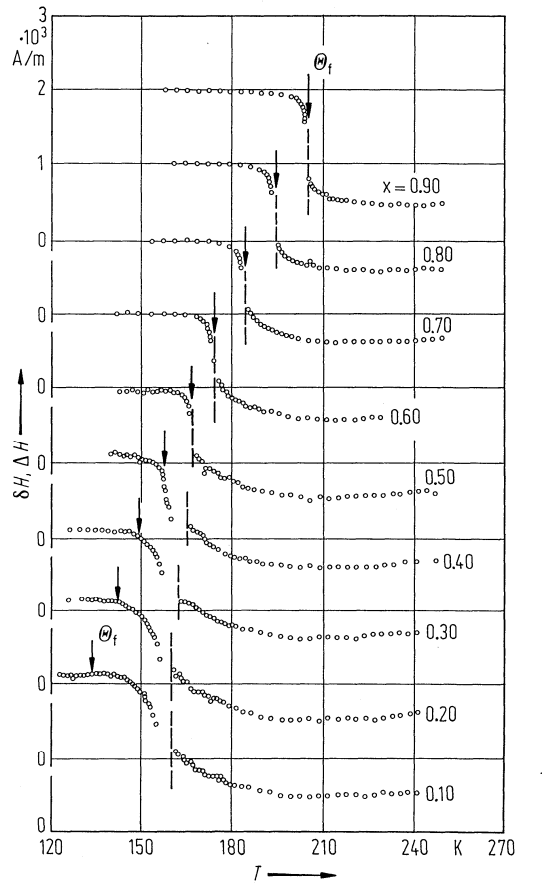

Fig. 33A-1-262. $KH_{2(1-x)}D_{2x}PO_4$: SeO_4^{3-}. ΔH, δH vs. T of SeO_4^{3-} ESR [84Mat]. Parameter: x. ΔH: line separation (left hand side of broken line); δH: line width (right hand side of broken line).

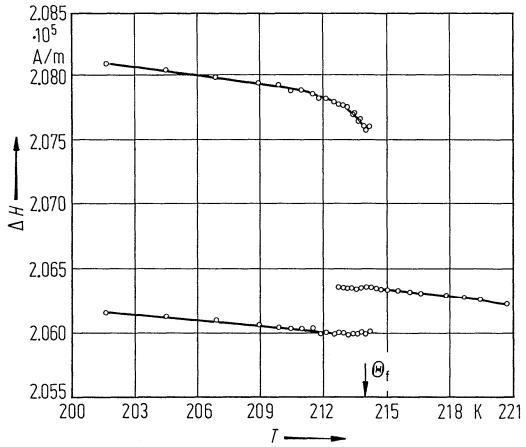

Fig. 33A-1-263. KD_2PO_4: SeO_4^{3-}. ΔH vs. T [82Huk]. ΔH: splitting of the lower component of ^{77}Se hyperfine structure of SeO_4^{3-}.

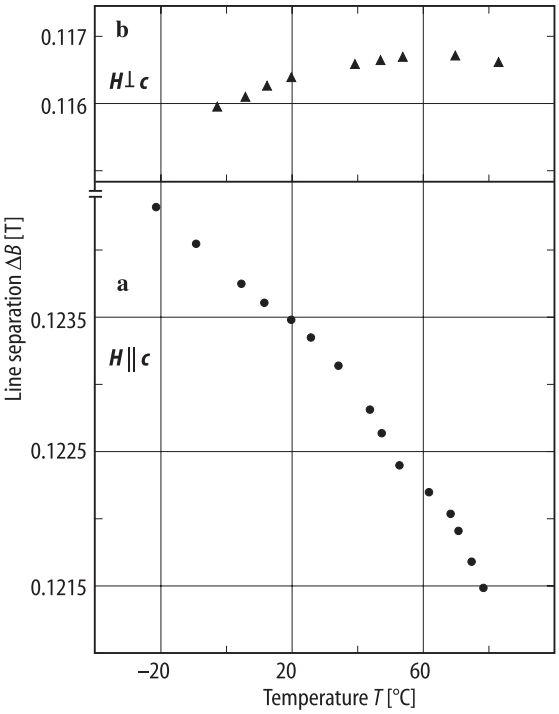

Fig. 33A-1-264. KH_2PO_4: SeO_4^{3-}. ΔB vs. T [87Owe]. ΔB: separation between highest and lowest field line of the ESR of SeO_4^{3-}. (a) $\boldsymbol{H} \parallel \boldsymbol{c}$, (b) $\boldsymbol{H} \perp \boldsymbol{c}$.

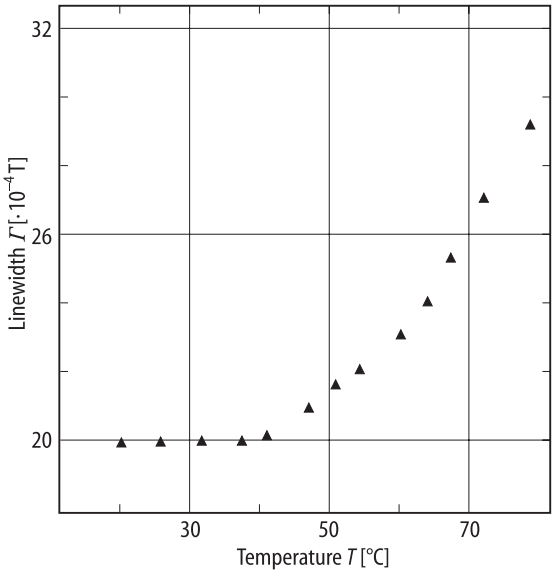

Fig. 33A-1-265. KH_2PO_4: SeO_4^{3-}. Γ vs. T [87Owe]. Γ: linewidth of the high field ESR of SeO_4^{3-} radical for $\boldsymbol{H} \parallel \boldsymbol{c}$.

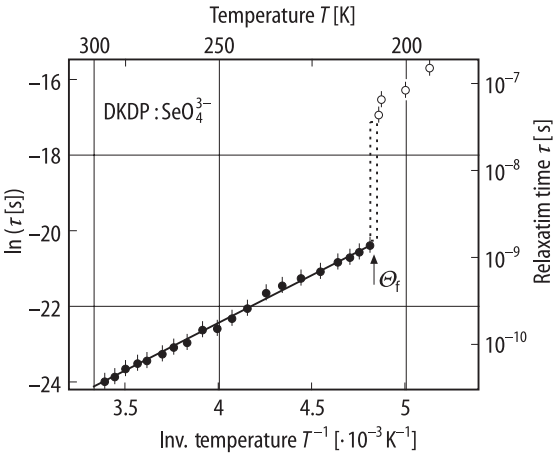

Fig. 33A-1-266. KD_2PO_4: SeO_4^{3-}. $\ln\tau$ vs. T^{-1} [89Dal1]. τ: correlation time determined from ESR of SeO_4^{3-} linewidth in the unit of s.

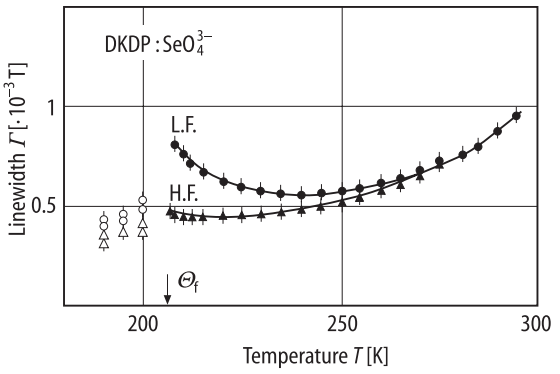

Fig. 33A-1-267. KD_2PO_4: SeO_4^{3-}. Γ vs. T [89Dal1]. Γ: peak-to-peak linewidth for ^{77}Se hyperfine component of SeO_4^{3-} ESR line. Open triangle, full triangle: high field components; open circle, full circle: low-field components; open triangle, open circle: slow motion regime; full triangle, full circle: fast motion regime.

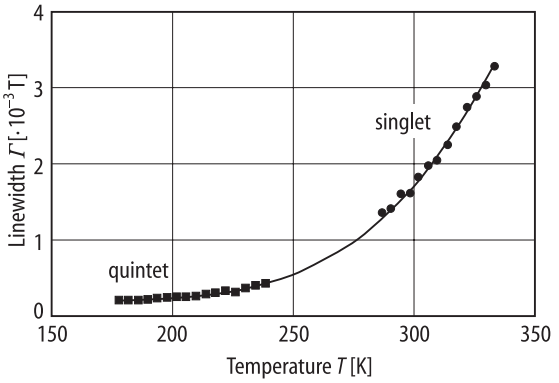

Fig. 33A-1-268. KH_2PO_4: SeO_4^{3-}. Γ vs. T [90Rak]. Γ: peak-to-peak linewidth of ESR line for SeO_4^{3-}. $\boldsymbol{H} \parallel \boldsymbol{c}$. Full square: single component of proton super-hyperfine quintet; full circle: whole signal.

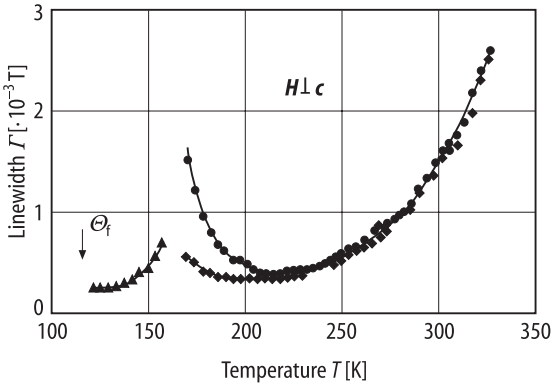

Fig. 33A-1-269. KH_2PO_4: SeO_4^{3-}. Γ vs. T [90Rak]. Γ: peak-to-peak linewidth of ESR line of SeO_4^{3-}. $\boldsymbol{H} \perp \boldsymbol{c}$. Full triangle: low field component of slow motion regime; full diamond: high field component of fast motion regime; full circle: low field component of fast motion regime.

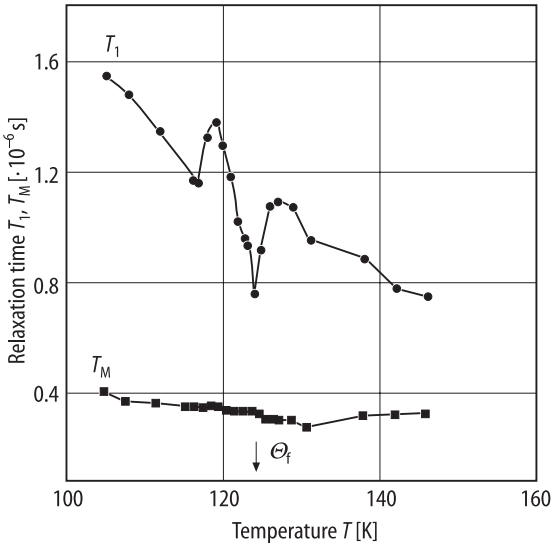

Fig. 33A-1-270. KH_2PO_4: SeO_4^{3-}. T_1, T_M vs. T [92Rak2]. T_1: spin-lattice relaxation time. T_M: spin-phase memory time. Electron spin echo techniques were utilized.

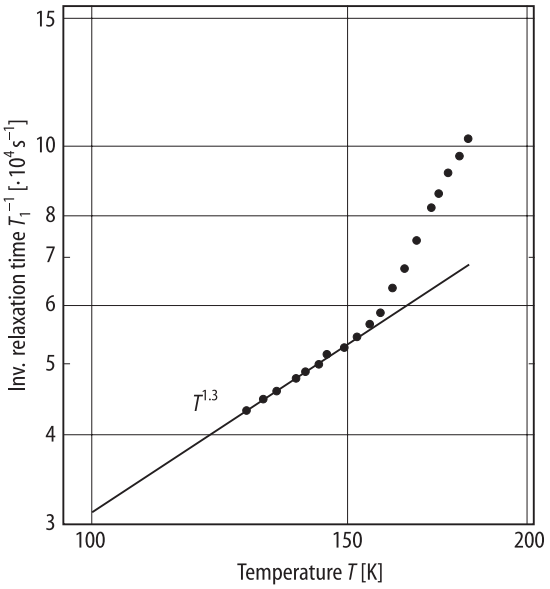

Fig. 33A-1-271. $KH_{2(1-x)}D_{2x}PO_4$: SeO_4^{3-} (x = 0.73). T_1^{-1} vs. T [94Rak2]. T_1: spin-lattice relaxation time determined from double-modulation electron spin resonance linewidth. The solid line represents the best fit to data in the low-temperature region.

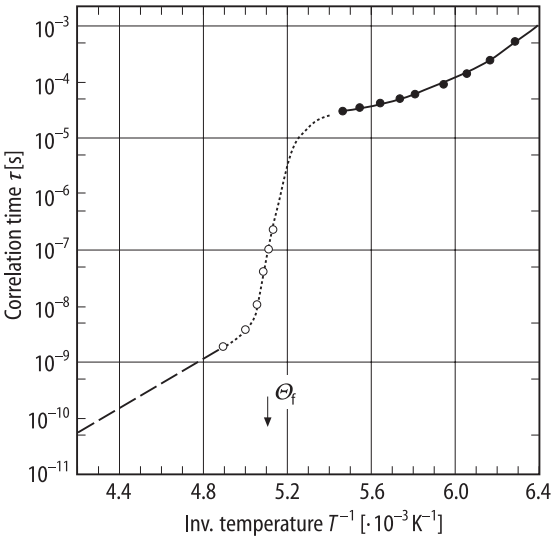

Fig. 33A-1-272. $KH_{2(1-x)}D_{2x}PO_4$: SeO_4^{3-} (x = 0.73). τ vs. T^{-1} [94Rak2]. τ: correlation time determined from ENDOR (open circle) and double-modulated ESR (full circle). Broken line: data from [89Dal1, 90Rak]. Solid line: Vogel-Fulcher relationship. Dotted line is a guide to eye.

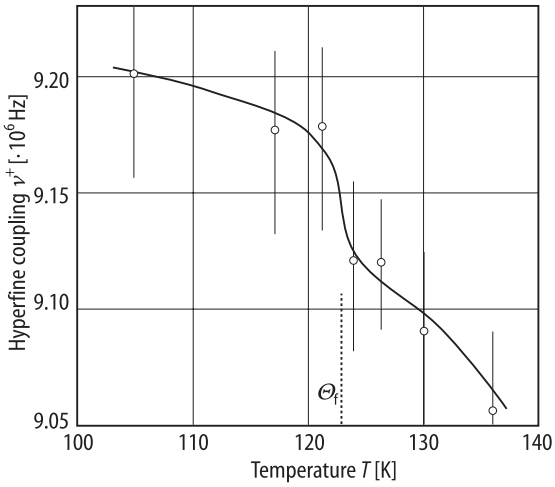

Fig. 33A-1-273. KH_2PO_4: AsO_4^{4-}. ν^+ vs. T [89Dal2]. ν^+: ENDOR determined ^{31}P hyperfine coupling constant.

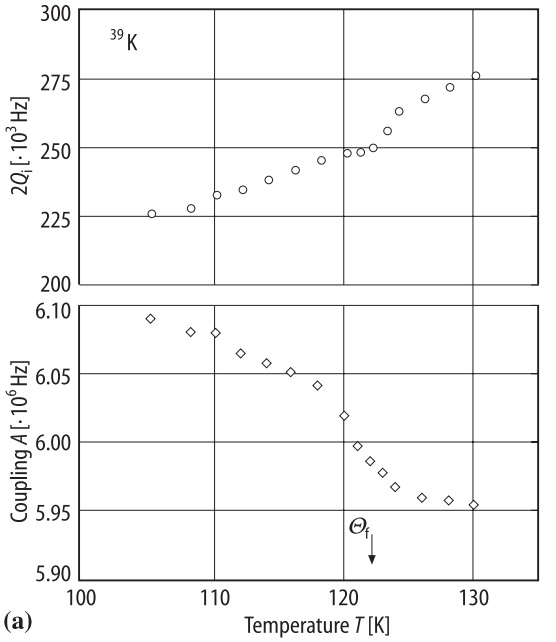

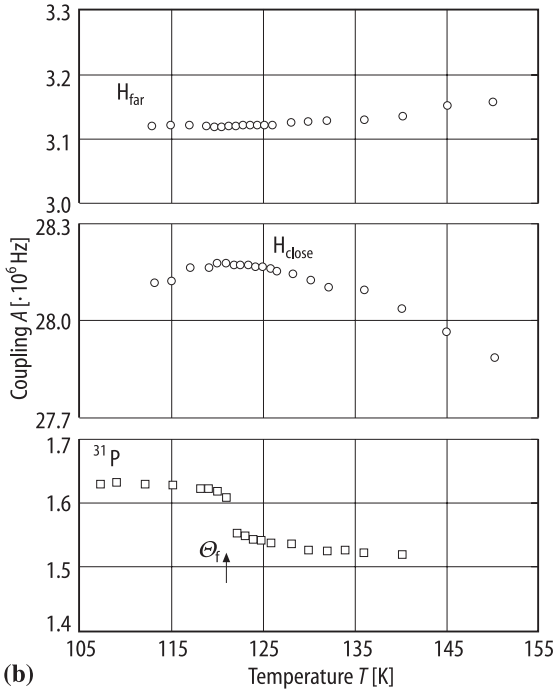

Fig. 33A-1-274. KH_2PO_4: AsO_4^{4-}. A, $2Q_i$ vs. T obtained by ENDOR measurements on the AsO_4^{-} radical as a spin probe [91Rak]. A: hyperfine coupling constant. Q_i: quadrupole coupling constant. (**a**) Q_i and A of ^{39}K. (**b**) A of ^{31}P and ^{1}H close to (H_{close}) and far from (H_{far}) AsO_4^{4-}.

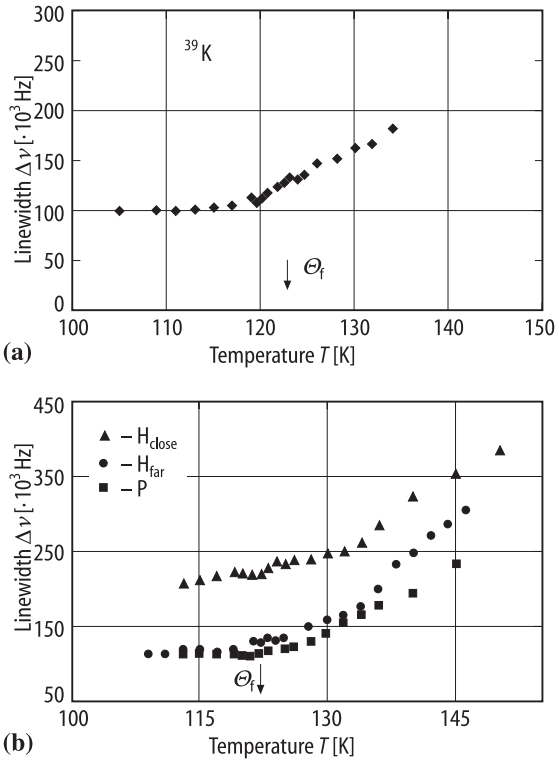

Fig. 33A-1-275. KH_2PO_4: AsO_4^{4-}. $\Delta\nu$ vs. T [91Rak]. $\Delta\nu$: ENDOR linewidth of AsO_4^{4-} center. (**a**) ^{39}K. (**b**) ^{31}P and ^{1}H close to (H_{close}) and far from (H_{far}) AsO_4^{4-}.

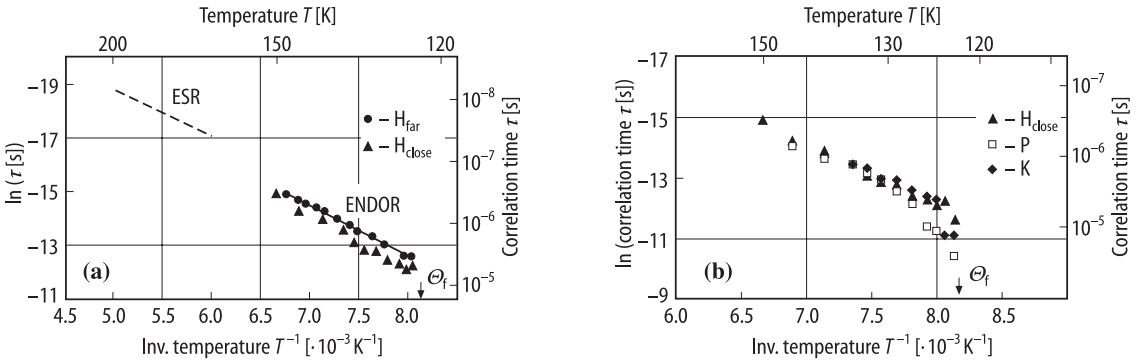

Fig. 33A-1-276. KH_2PO_4: AsO_4^{4-}. τ, $\ln\tau$ vs. T^{-1} [91Rak]. τ: correlation time (in units of s) obtained from ENDOR of AsO_4^{-} radical as a spin radical. (**a**) ^{1}H. Broken line: ESR data from [67Bli]. (**b**) ^{31}P, ^{39}K, close ^{1}H.

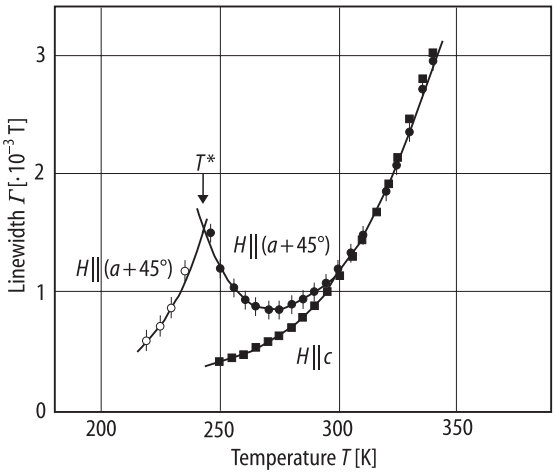

Fig. 33A-1-277. KD_2PO_4: CrO_4^{3-}. Γ vs. T [89Dal1]. Γ: peak-to-peak linewidth of ESR for CrO_4^{3-}. Open circle, full circle: $\boldsymbol{H}$ || ($\boldsymbol{a}$ + 45°); full square: $\boldsymbol{H}$ || $\boldsymbol{c}$. T*: coalescence temperature. Open circle: data in the slow motion regime.

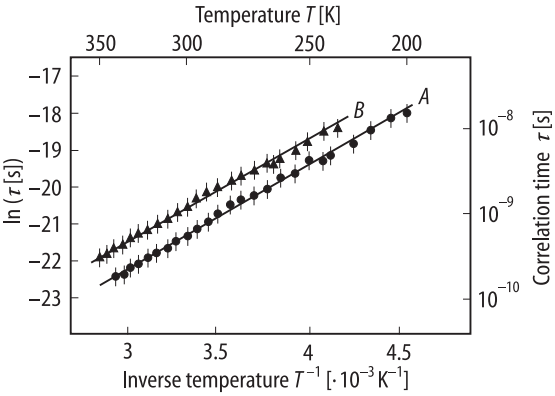

Fig. 33A-1-278. KD_2PO_4 : CrO_4^{3-}, KD_2AsO_4 : CrO_4^{3-}. τ, ln τ vs. T^{-1} [89Dal1]. τ: correlation time (in units of s) obtained from CrO_4^{3-} ESR linewidth. A: KD_2PO_4, B: KD_2AsO_4.

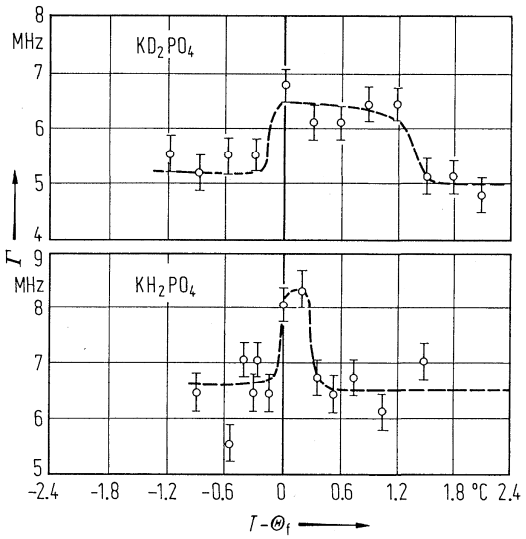

Fig. 33A-1-279. KH_2PO_4 : ^{57}Co, KD_2PO_4 : ^{57}Co. Γ vs. T [70Bru]. Γ: line width of the central ^{57}Co Mössbauer line.

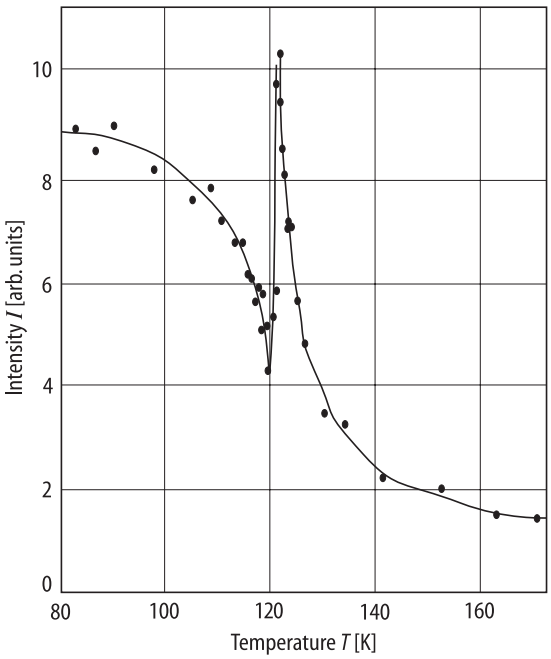

Fig. 33A-1-280. KH_2PO_4 (KDP). I vs. T at (0.9, 0, 7) in the reciprocal space [86And]. I: X-ray diffuse scattering intensity.

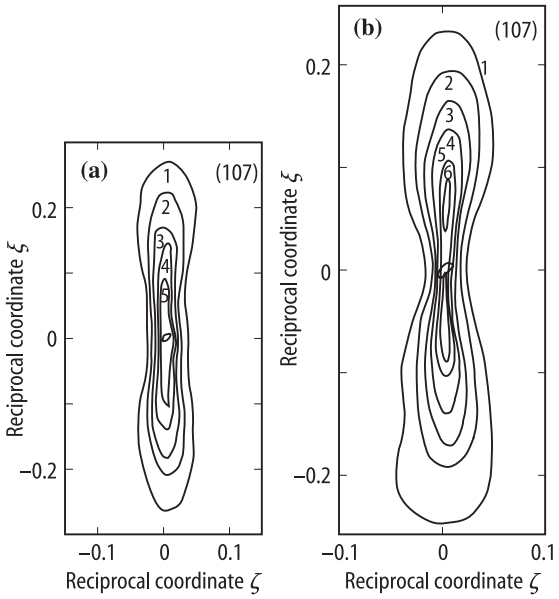

Fig. 33A-1-281. KH_2PO_4 (KDP), KD_2PO_4 (DKDP). Contour maps of X-ray diffuse scattering intensity around (1 0 7) in the (ξ 0 ζ) zone of reciprocal space [86And]. $T = \Theta_f + 2$ K. (**a**) KH_2PO_4, (**b**) KD_2PO_4.

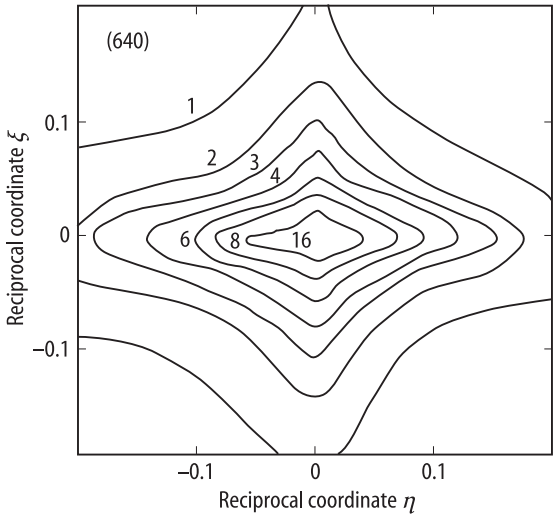

Fig. 33A-1-282. KH_2PO_4 (KDP). A contour map of X-ray diffuse scattering intensity around (6 4 0) in the (ξ η 0) zone of reciprocal space [86And]. $T = \Theta_f + 2$ K.

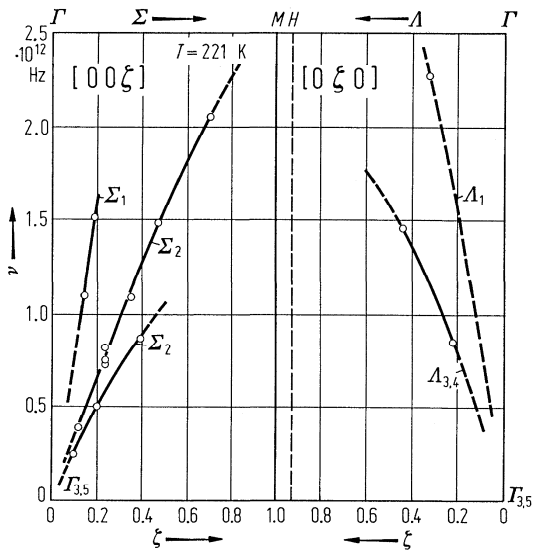

Fig. 33A-1-283. KD_2PO_4 (DKDP). ν vs. ζ [70Ska]. ν: phonon frequency, ζ: reduced wave vector coordinate.

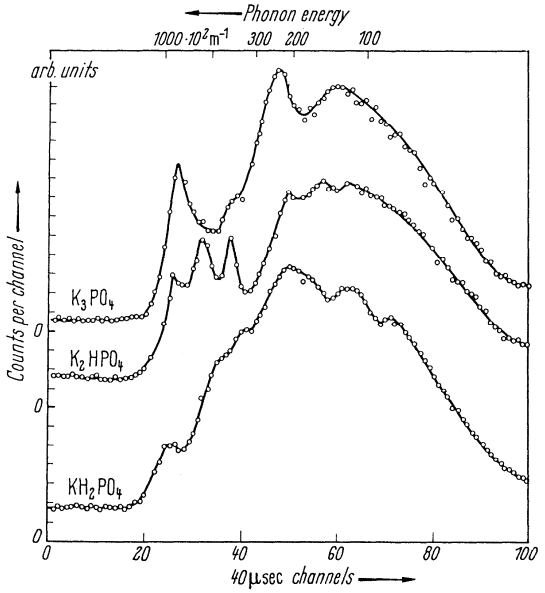

Fig. 33A-1-284. KH_2PO_4 (KDP, polycrystal). Time of flight spectra of inelastically scattered slow neutrons of 0.0005 eV at RT [59Pep]. E: phonon energy in units of 10^2 m^{-1}. The data of K_2HPO_4 and K_3PO_4 are shown for comparison.

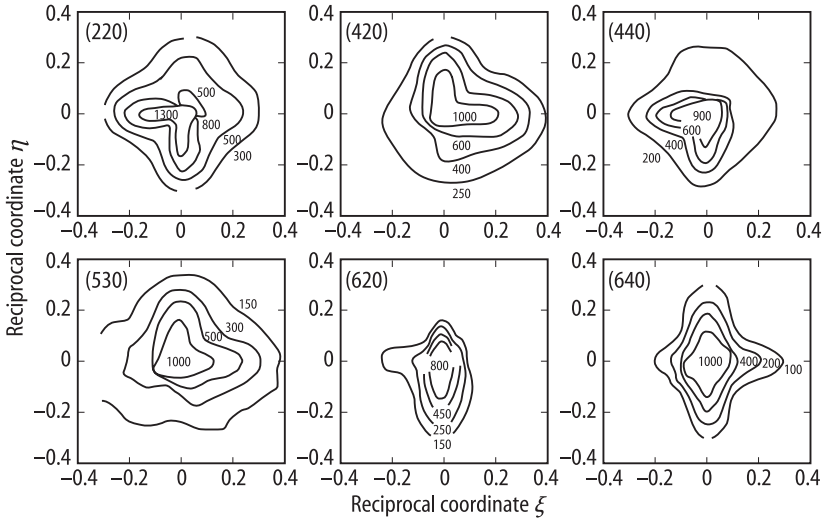

Fig. 33A-1-285. KD_2PO_4 (DKDP). Contour maps of neutron scattering intensity [rel. units] around the reciprocal lattice points in ($\xi\ \eta\ 0$) zone [80Hos]. $T = \Theta_f + 5$ K.

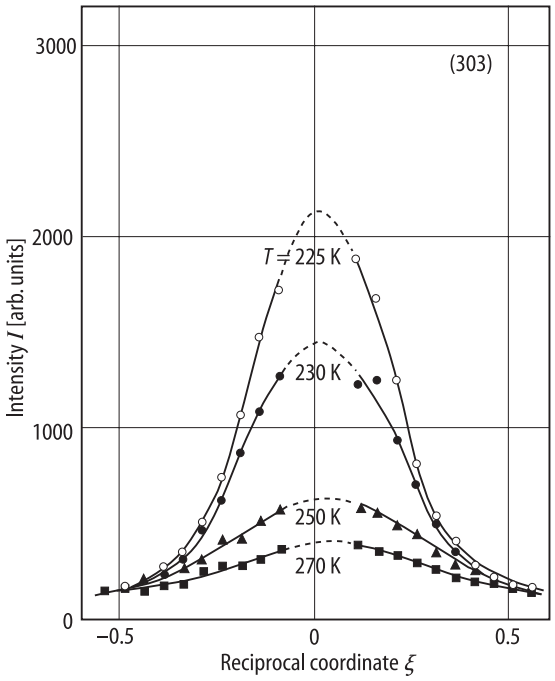

Fig. 33A-1-286. KD_2PO_4 (DKDP). I vs. ξ near (303) [70Ska]. Parameter: T. I: intensity of the neutron diffuse scattering from overdamped Σ_2 phonon measured in the [010] zone.

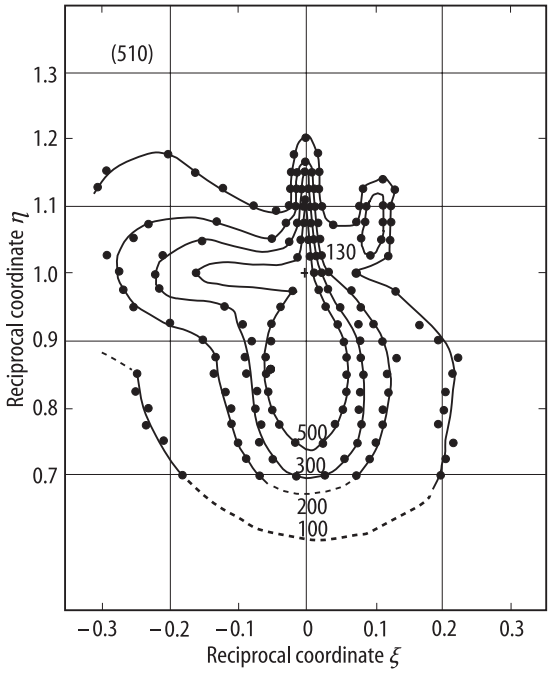

Fig. 33A-1-287. KD_2PO_4 (DKDP). A contour map of neutron diffuse scattering intensity in the (ξ η 0) zone near (510) [70Ska]. T = 225 K.

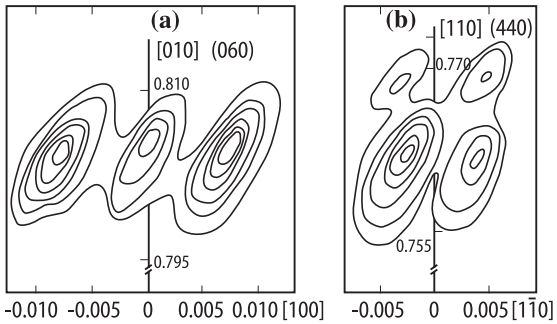

Fig. 33A-1-288. KD_2PO_4 (DKDP). Neutron scattering intensity distributions by domain structure near (**a**) (060) and (**b**) (440) reciprocal lattice points [80Bal]. T = 80 K. Contours are in steps of 50.

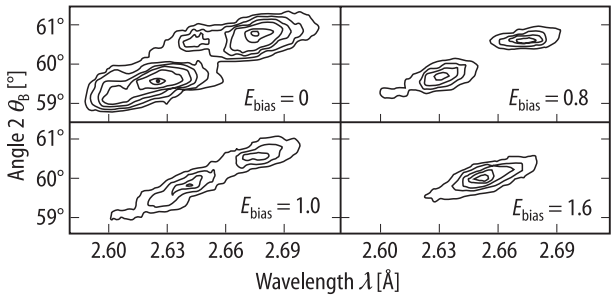

Fig. 33A-1-289. KD_2PO_4 (DKDP). Intensity distributions of neutron scattering by domain structure near (440) reciprocal lattice point [80Bal]. Parameter: E_{bias} [$\cdot 10^5$ V m^{-1}]. λ: incident neutron wavelength. T = 210 K. Contours are in steps of 50 for $E_{bias} \neq 0$. For $E_{bias} = 0$ the contours 10, 30, 50, 100, 150 and 200 are shown.

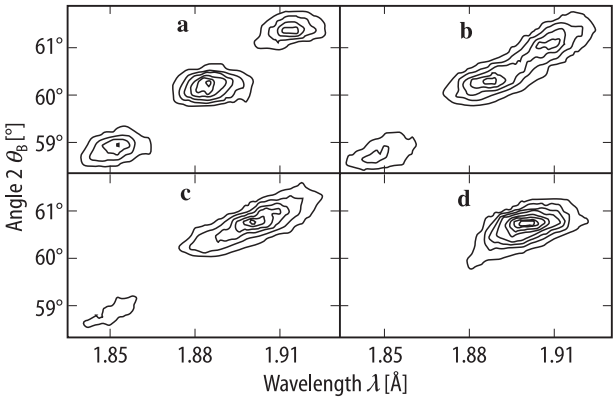

Fig. 33A-1-290. KD_2PO_4 (DKDP). Intensity distributions of neutron scattering by domain structure near (060) reciprocal lattice point [80Bal]. Parameter: E_{bias}. λ: incident neutron wavelength. T = 210 K. Contours are in steps of 50. (**a**) E_{bias} = 0; (**b**) $0.8 \cdot 10^5$ V m^{-1}; (**c**) $1.0 \cdot 10^5$ V m^{-1}; (**d**) $1.4 \cdot 10^5$ V m^{-1}.

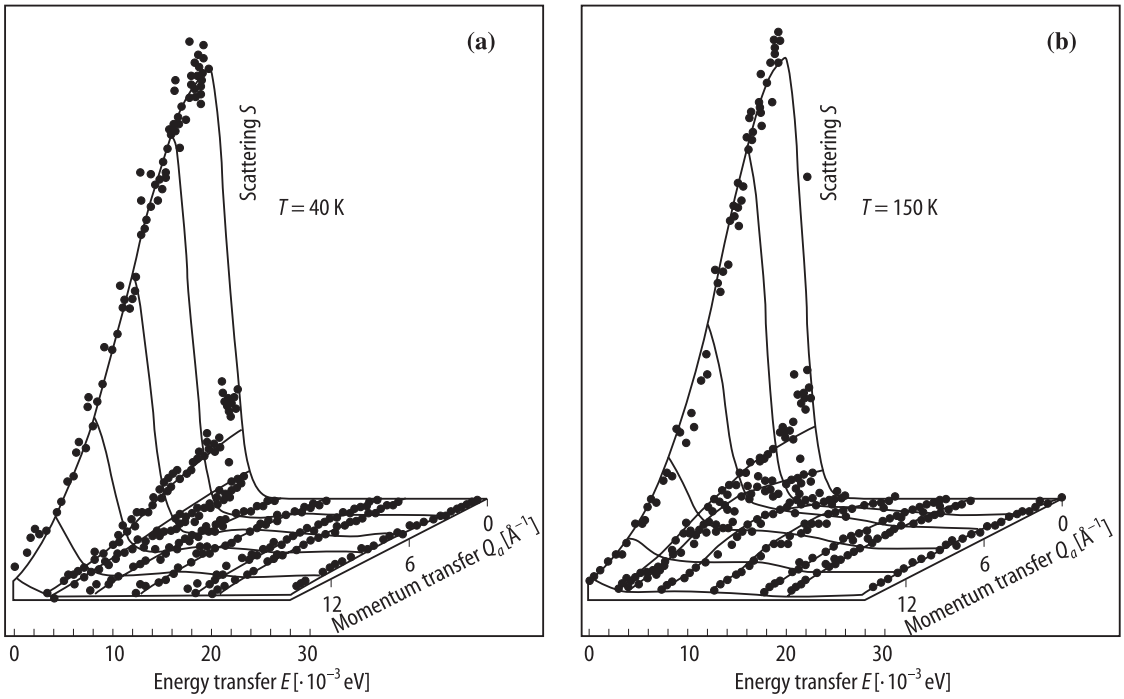

Fig. 33A-1-291. KH_2PO_4 (KDP). S vs. Q_a, E [94Ike]. S: incoherent neutron scattering function. Q_a: component of momentum transfer along the a^* axis. E: energy transfer. (**a**) T = 40 K; (**b**) T = 150 K.

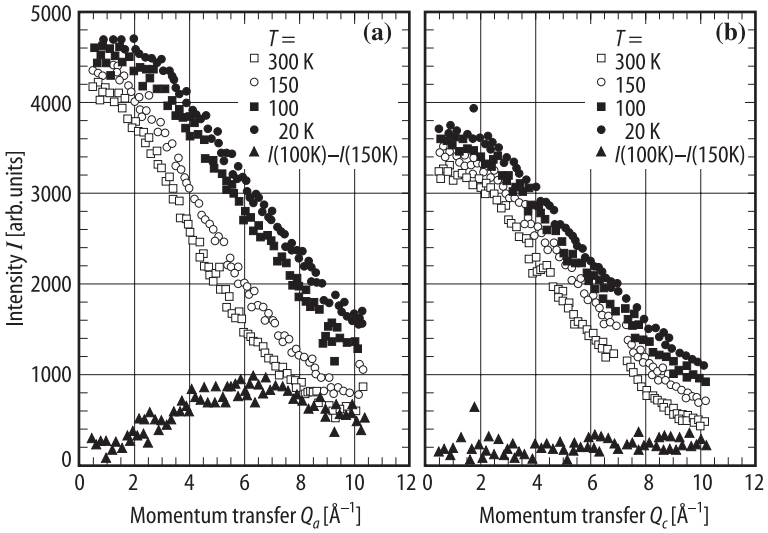

Fig. 33A-1-292. KH_2PO_4 (KDP). (**a**) I vs. Q_a, (**b**) I vs. Q_c [94Ike]. Parameter: T. I: neutron incoherent elastic scattering intensity. Q_a, Q_c: components of momentum transfer along the a^* and the c^* axes, respectively.

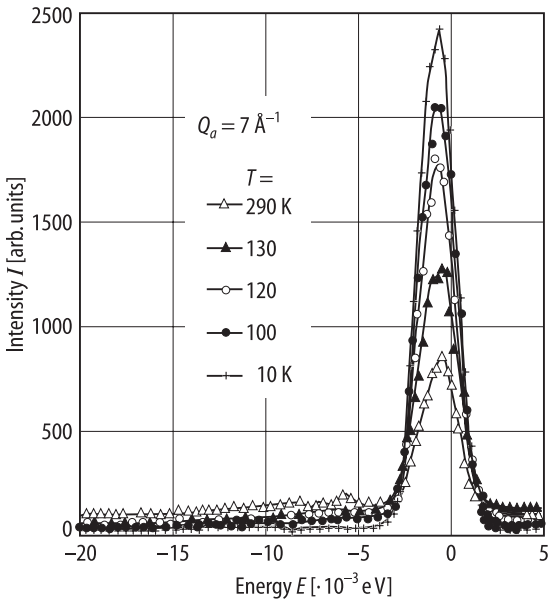

Fig. 33A-1-293. KH_2PO_4 (KDP). I vs. E [94Ike]. Parameter: T. I: intensity of neutron incoherent scattering. E: energy transfer. Q_a: component of momentum transfer along the a^* axis.

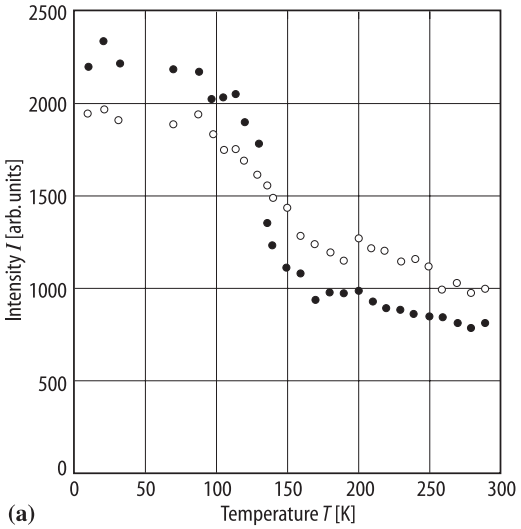

(a)

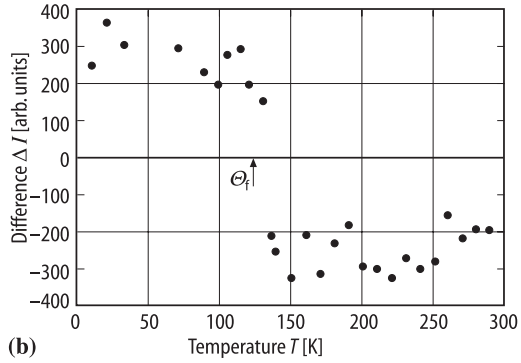

(b)

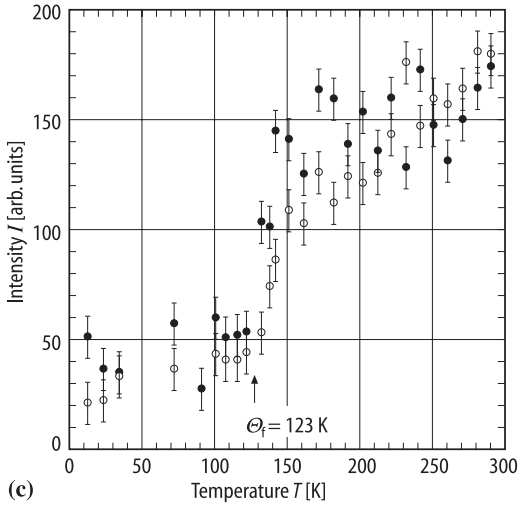

(c)

Fig. 33A-1-294. KH_2PO_4 (KDP). I, ΔI vs. T [94Ike]. I: intensity of neutron incoherent scattering. ΔI: difference between I for $\boldsymbol{Q} \parallel \boldsymbol{a}^*$ and $\boldsymbol{Q} \parallel \boldsymbol{c}^*$, where Q is the momentum transfer. (**a**), (**b**) elastic scattering with $Q = 7$ Å^{-1}; (**c**) quasielastic scattering with $E = 5$ meV and $Q = 7$ Å^{-1}, where E is transfer energy. Open circle: $\boldsymbol{Q} \parallel \boldsymbol{c}^*$; full circle: $\boldsymbol{Q} \parallel \boldsymbol{a}^*$ in (**a**) and (**c**).

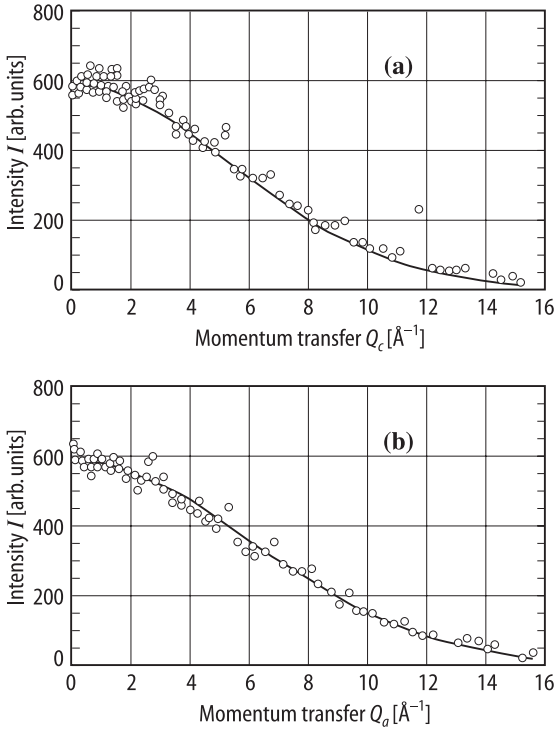

Fig. 33A-1-295. KH_2PO_4 (KDP). I vs. (**a**) Q_c, (**b**) Q_a [94Ike]. T = 40 K. I: incoherent neutron elastic scattering intensity. Q_a, Q_c: momentum transfers parallel to a^*, c^*, respectively. Full lines: calculated curves using Gaussian scattering functions.

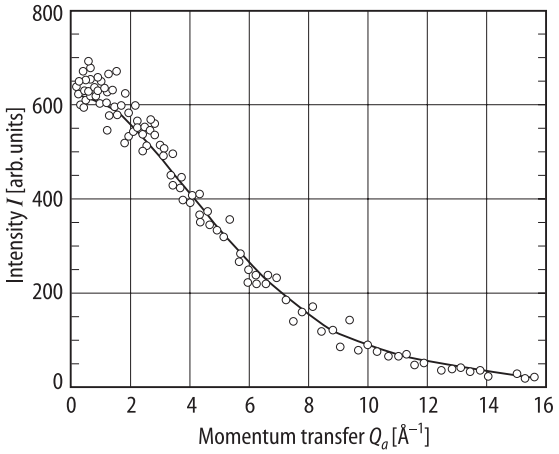

Fig. 33A-1-296. KH_2PO_4 (KDP). I vs. Q_a [94Ike]. T = 150 K. I: incoherent neutron elastic scattering intensity. Q_a: component of momentum transfer along the a^* direction. Full line: calculated curve using a modified Gaussian scattering function.

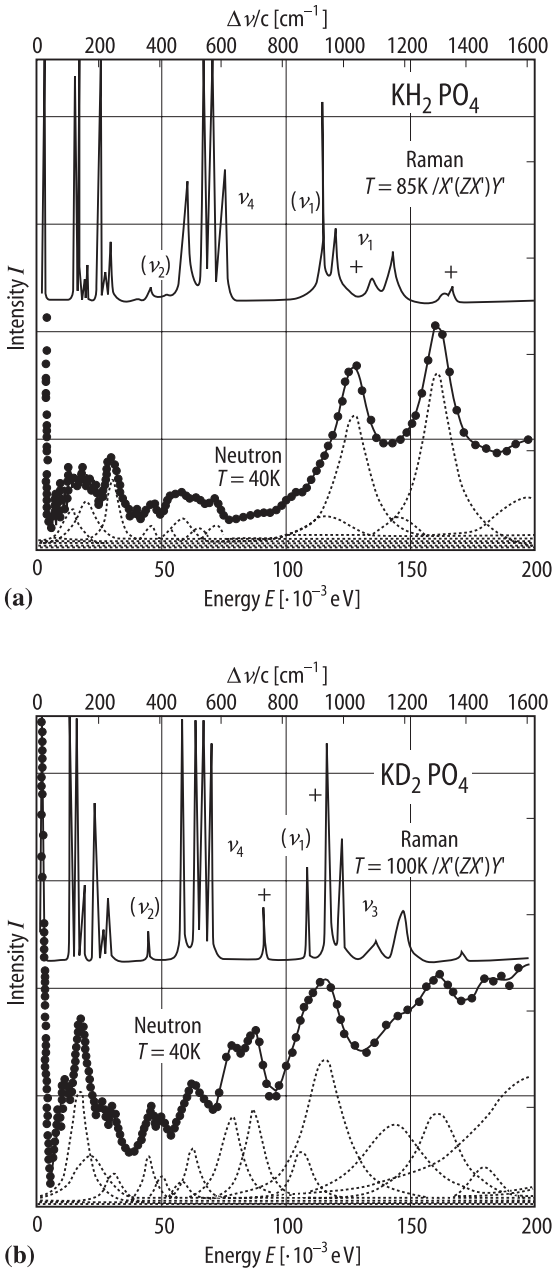

Fig. 33A-1-297. KH_2PO_4 (KDP), KD_2PO_4 (DKDP). I vs. E [93Miz]. I: intensity of Raman scattering or incoherent neutron scattering. E: energy transfer of neutron scattering. $\Delta\nu$: Raman frequency shift. (**a**) KH_2PO_4; T = 85 K for Raman scattering and T = 40 K for neutron scattering. (**b**) KD_2PO_4; T = 100 K for Raman scattering and T = 40 K for neutron scattering. Dotted curves: Lorentzian modes; solid curves for neutron spectra were calculated by means of these Lorentzian modes. +: hydrogen mode for KH_2PO_4 and deuterium mode in KD_2PO_4.

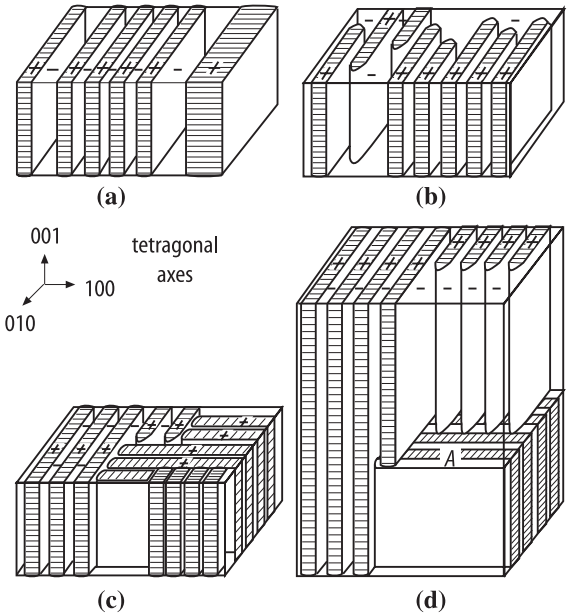

Fig. 33A-1-298. KH_2PO_4 (KDP). Four examples of domain structure [87Bor]. (**a**), (**b**) with only one direction for the walls; (**c**) with two possible directions of permissible walls; (**d**) with a charged boundary *A* between domain packs.

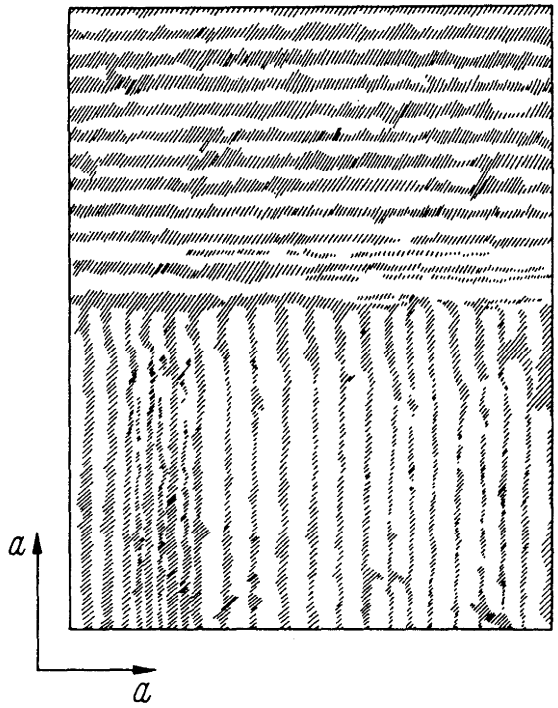

Fig. 33A-1-299. KH_2PO_4 (KDP). Frost pattern which shows a complicated domain structure [63Tos]. Arrows indicate the *a* axes at RT.

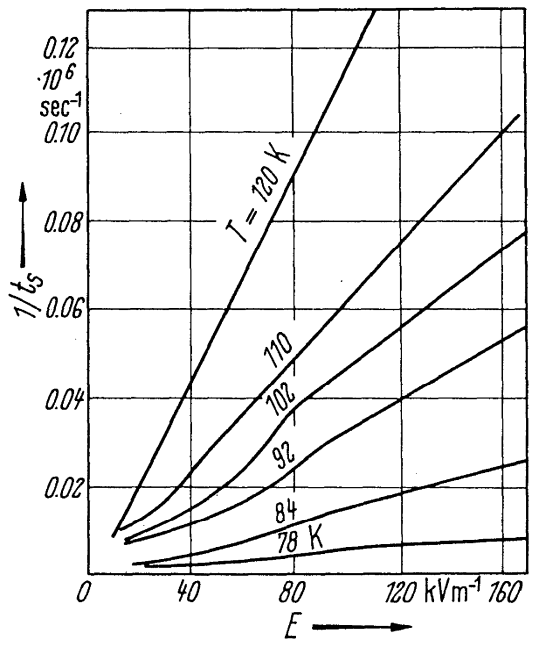

Fig. 33A-1-300. KH_2PO_4 (KDP). $1/t_s$ vs. E [66Guy]. Parameter: T. t_s: switching time. E: applied field.

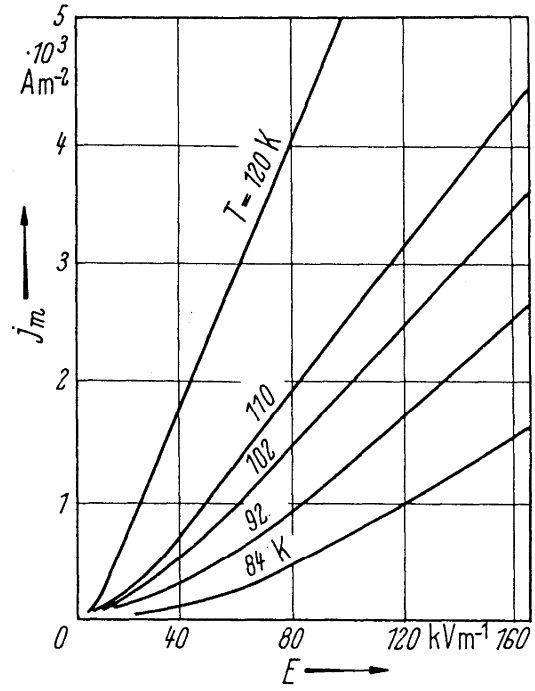

Fig. 33A-1-301. KH_2PO_4 (KDP). j_m vs. E [66Guy]. Parameter: T. j_m: maximum switching current density.